TAILORING OPTICAL FIBERS FOR CELL TRANSFECTION

Nan Ma

A Thesis Submitted for the Degree of PhD
at the
University of St. Andrews

2012

TAILORING OPTICAL FIBERS FOR CELL TRANSFECTION

Nan Ma

This thesis is submitted for the degree of PhD
at the
University of St Andrews

February 2012

Dedicated to

My parents
&
Jing,

With Love

谢谢

Tailoring Optical Fibers for Cell Transfection

Nan Ma

This thesis is submitted for the degree of PhD
at the
University of St Andrews

February 2012

Abstract

Optical transfection is a promising technique for the delivery of foreign genetic material into cells by transiently changing the permeability of the cell membrane. Of the different optical light sources that have been used, femtosecond laser based transfection has been one of the most effective methods for optical transfection which is generally implemented using a free-space bulk optical setup. Here in this thesis, a few novel fabrication methods are devised to obtain easy and inexpensive fabrication of microlensed optical fibers, which can be used to replace traditional optical setup and perform femtosecond optical transfection. These fabrication methods offer the flexibility to fabricate a microlens which can focus femtosecond laser pulses at 800 nm to a small focal spot whilst keeping a relatively large working distance. In conventional optical transfection methods the foreign genetic material to be transfected is homogenously mixed in the medium. This thesis reports the first realization of an integrated optical transfection system which can achieve transfection along with localized drug delivery by combining lensed fiber based optical transfection system with a micro-capillary based microfluidic system. Finally, based on an imaging fiber (coherent optical fiber bundle), the first endoscope-like integrated system for optical transfection with subcellular resolution epifluorescence imaging was built. The transfection efficiency of these fiber based systems is comparable to that of a standard free-space transfection system. Also the use of integrated system for localized gene delivery resulted in a reduction of the required amount of genetic material for transfection. The miniaturized, integrated design opens a range of exciting experimental possibilities, such as the dosing of tissue slices to study neuron activities, targeted drug delivery, and in particular for using endoscope-like integrated systems for targeted *in vivo* optical microsurgery.

Declarations

1. Candidate's declarations:

I, Nan Ma, hereby certify that this thesis, which is approximately 51,000 words in length, has been written by me, that it is the record of work carried out by me and that it has not been submitted in any previous application for a higher degree.

I was admitted as a research student in August, 2007 and as a candidate for the degree of Doctor of Philosophy in June, 2012; the higher study for which this is a record was carried out in the University of St Andrews between 2007 and 2011.

Date …… Signature of candidate ……

2. Supervisor's declaration:

I hereby certify that the candidate has fulfilled the conditions of the Resolution and Regulations appropriate for the degree of Doctor of Philosophy in the University of St Andrews and that the candidate is qualified to submit this thesis in application for that degree.

Date …… Signature of supervisor ……

3. Permission for electronic publication:

In submitting this thesis to the University of St Andrews I understand that I am giving permission for it to be made available for use in accordance with the regulations of the University Library for the time being in force, subject

to any copyright vested in the work not being affected thereby. I also understand that the title and the abstract will be published, and that a copy of the work may be made and supplied to any bona fide library or research worker, that my thesis will be electronically accessible for personal or research use unless exempt by award of an embargo as requested below, and that the library has the right to migrate my thesis into new electronic forms as required to ensure continued access to the thesis. I have obtained any third-party copyright permissions that may be required in order to allow such access and migration, or have requested the appropriate embargo below.

Access to printed copy and electronic publication of thesis through the University of St Andrews.

Date …… Signature of candidate ……

Signature of supervisor ……

Acknowledgements

I would like to express my appreciation to my supervisors, Professor Kishan Dholakia and Professor Frank Gunn-Moore, for this great opportunity to work in their group, for their guidance, encouragement and many valuable advices on the execution of my interesting multidisciplinary projects.

I would also like to thank my colleagues and friends from the group. Eddie Tan and Xanthi Tsampoula helped me to start my PHD on the dangerous fiber project and guided me through the very beginning of my PHD. Thanks Leilani Torres who helped me on the fiber photoporation work and various other issues. The first fluorescent cell, after so many days and nights working in the lab, that we successfully transfected, will be remembered forever. And Patience Mthunzi, for helping me on cell culture and answering all my biological questions. It's a pity, although with a lot of support from Kelvin Agboh and Maciej Antkowiak, the tissue transfection is still not working. I'd very much like to thank Praveen Ashok and Rob Marchington, for their help on the lensed fiber fabrication. Without this break point, I could never finish my PHD. And of course Dave Stevenson, thanks for sitting behind me all these years and being a reference book, not to mention numerous ideas and great Google Sketchup you introduced to me. Thanks Heather, Rob, Maciej and Leilani, and of course my supervisors, especially Frank, for the proof reading of my awkwardly written thesis.

On a personal note, I'd like to thank my parents for their support, encouragement, belief and unconditional love all my life. And also a very big thanks to my dearest wife, my forever love, Jing, who endured with me and has been supportive, encouraging and taking care of me throughout my PHD. Jing always have faith in me, even when I was lost. Without her, I would never have been able even to imagine where I am now. It is therefore, with great pleasure that I dedicate this dissertation to them.

Publications

Peer Reviewed Publications

[1] X. Tsampoula, K. Taguchi, T. Cizmar, V. Garces-Chavez, N. Ma, S. Mohanty, K. Mohanty, F. Gunn-Moore, and K. Dholakia, "Fibre based cellular transfection," Optics Express **16**, 17007-17013 (2008).

[2] N. Ma, P. C. Ashok, D. J. Stevenson, F. J. Gunn-Moore, and K. Dholakia, "Integrated optical transfection system using a microlens fiber combined with microfluidic gene delivery," Biomed. Opt. Express **1**, 694-705 (2010).

[3] N. Ma, F. Gunn-Moore, and K. Dholakia, "Optical transfection using an endoscope-like system," J Biomed Opt **16**, 028002-028007 (2011).

Conference Proceedings

[4] N. Ma, P. C. Ashok, F. J. Gunn-Moore, and K. Dholakia, "Fabrication of polymer microlens at the apex of optical fiber," in *Photonics 2010* (Guwahati, India, 2010).

Patents

[5] Microlensed fiber-based photoporation (Europe Patent Application PCT/GB2011/000881)

Attended International Conference

[6] Optics Within Life Sciences (OWLS) 11th. Quebec, Canada 2010. Oral and poster presentations.

List of Abbreviations

1D	1 dimensional
2D	2 dimensional
3D	3 dimensional
AFM	Atomic force microscope
CAD	Computer aided design
CARS	Coherent anti-Stokes Raman scattering
CCD	Charge coupled device
CFP	Cyan fluorescent protein
CHO-K1	Chinese hamster ovary
CSF	Coreless silica fiber
CW	Continuous wave
DCF	Double-clad photonic crystal fiber
DEAE-dextran	Diethylaminoethyl-dextran
DM	Dichroic mirror
DNA	Deoxyribonucleic acid
DsRed	*Discoideum sp*, red fluorescent protein
EGFP	Enhanced green fluorescent protein
FCS	Fetal calf serum
FFB	Fluorescence filter block
FFT	Fast Fourier transform
FIB	Focused ion beam
GFP	Green fluorescent protein
GRIN	Gradient refractive index
GVD	Group velocity dispersion
HEK-293	Human embryonic kidney
HF	Hydrofluoric acid
LMA	Large mode area

LMA-PCF	Large mode area photonic crystal fiber
MEM	Modified eagles medium
MitoDsRed	DsRed fused with a mitochondrial targeting sequence
MMF	Multimode fiber
mRNA	Messenger RNA
NA	Numerical aperture
ND	Neutral density; filter
NH_4F	Ammonium fluoride
NIR	Near infrared
OCT	Optical coherence tomography
PBF	Photonic bandgap fiber
PCF	Photonic crystal fiber
PtK2	Rat-kangaroo kidney epithelial
RNA	Ribonucleic acid
ROS	Reactive oxygen species
RT-PCR	Real-time polymerase chain reaction
SEM	Scanning electron microscopy or Scanning electron microscope
siRNA	Small interfering ribonucleic acid
SLM	Spatial light modulator
SMF	Single mode fiber
SNOM	Scanning near-field optical microscopy
SPM	Self-phase modulation
UV	Ultra-violet
YFP	Yellow fluorescent protein

Contents

Chapter 1:

1. Introduction to Cell Transfection Methods

As early as 1917, Albert Einstein set the theoretical foundations for the formulation of the laser in his paper "*On the Quantum Theory of Radiation".* Fifty years after this on 16 May 1960, the first working laser was built. Nowadays, the applications of lasers are evident in our daily life. Lasers have been applied to surgery, national defence, printing and they are continually gaining more importance in various research fields, such as spectroscopy, laser annealing, interferometry, optical trapping and microscopy [1, 2].

Laser delivery with optical fibers is a key development. As an example, Charles Kao recently won the Nobel Prize in Physics in 2009 for his ground-breaking achievements concerning the transmission of light in fibers for optical communication. Optical fibers have become a major conduit for communication within our society: it has been used to transfer images, videos and music, globally in a fraction of a second. They have also been extensively applied to the medical field and are becoming an indispensable tool in this area.

Following the domination of the 20th century by physics and the 19th century by chemistry, many specialists predicted that this century would be the century of biology. Although, it has been approximately 5 decades since the discovery of the structure and function of Deoxyribonucleic Acid (DNA), which was probably the most significant biological discovery and medical advancement of the 20th century, it was only until June 2000, that the first draft of the human genetic code was completed. The use of genetically personalized medicine has been to date fairly limited and the all-purpose stem cell has not yet been produced. Nevertheless, substantial advancement in genetics has been achieved: researchers have discovered hundreds of genes that contribute, alongside with environmental factors, to multi-causal disorders such as diabetes, cancer

and heart disease. These new understanding of disease mechanisms may lead to new diagnostic tools and treatments in the near future. Genetic material transfer is very important in current research for molecular and cellular biology, and in particular in many applications involved in biotechnology. Today, many gene transfection methods that were developed for the transfection of cultured cell lines, are now entering *in vivo* and clinical trials for gene therapy and DNA vaccines.

This thesis will present a multidisciplinary approach, which combines the knowledge from three different fields: lasers, optical fibers and gene transfer. With regard to the later, there are many traditional transfection technologies that can be used to deliver foreign genetic material into biological cells. A promising and relatively new method called optical transfection, uses lasers to temporarily change the permeability of a cell's membrane in order to achieve the same goal. Following the active trend of miniaturization in the biophotonics field, optical fibers are used throughout this work for the laser delivery and imaging of cells.

After a brief introductory chapter, which summarizes the basic principles of gene transfer and contemporary non-viral gene transfection technologies, Chapter 2 will introduce the development of an optical transfection technique using a femtosecond laser. Chapter 3 will review the different lensed fiber fabrication techniques. Chapter 4 will discuss the first fiber based optical transfection work, which involved using an axicon tipped single mode optical fiber for femtosecond laser delivery and focusing and in Chapter 5, a novel lensed fiber fabrication method will be presented, followed by an optical transfection experiment using an integrated system combining a liquid delivery module. Chapter 6 will demonstrate an upgraded version of the integrated system in Chapter 5, with which the laser delivery, focusing and fluorescence imaging of biological cells can all be realized through one system, without the need of an extra objective lens. Chapter 7 will explore the feasibility of using a gradient refractive index (GRIN) lens based imaging probe, with an increased working distance and smaller focus spot, for optical transfection.

1.1. Basic Principles of Gene Transfer

1.1.1 Introduction

The techniques of DNA delivery into biological cells have been widely studied and applied in basic research and biology [3-5]. This indispensable tool can be used to study gene function and regulation, and also the production of small amounts of recombinant proteins for analysis and verification. Normally, gene transfer is used to express delivered genetic material into the recipient cells and offer the possibility to observe a specific protein's function. Genetic material transfer can also be used to disable certain protein functions by interfering or inactivating certain endogenous genes using small interfering Ribonucleic Acid (siRNA). The application of gene transfer techniques ranges from using biological cells to produce recombinant antibodies and vaccines, the production of genetically modified animals, to gene therapy of the human body.

There have been various different names provided for different types of DNA delivery mechanisms. The term transfection is generally accepted as a way to describe the introduction of any sort of genetic material DNA/RNA into a eukaryotic cell. The transfection of animal cells thus encompasses all physical and chemical means of nucleic acid delivery, which will be discussed in this chapter.

Regardless of the different transfection methods, successful gene transfer into animal cells must achieve three objectives. First, the exogenous genetic material must pass through the cell membrane. This is a passive process, independent of the genetic material. Secondly, once it traverses through the cell membrane, the genetic material must be released in the cell and transported to a specific sub-cellular site for expression or activation. In most transfection methods, genetic material is delivered to the cytoplasm. DNA must then be transported to the nucleus. However, this intrinsic DNA trafficking system is still poorly understood. On the other hand, RNA does not necessitate translocation to the nucleus and

is directly involved in cytoplasmic processes. Lastly, the exogenous genetic material must be expressed and/or interact with the host genome.

There are often various transfection methods available to researchers and therefore it is necessary to have the means to compare each method and measure the relative transfection efficiency. Also, it is essential to examine the activities of transfected genes. Some traditional methods, such as real-time polymerase chain reaction (RT-PCR) and northern blot hybridization have been developed to detect expression of genes at the Messenger RNA (mRNA) level [6]. However, these methods can be laborious and time-consuming, and where multiple genes have been transfected these traditional methods may have difficulty in distinguishing multiple gene products.

To avoid these problems, reporter genes can be used which encode a product that can be easily detected and ideally quantified using a simple, inexpensive and rapid assay. GFP (green fluorescent protein) and its derivatives is one of the most commonly used in reporter genes [7]. GFP was originally discovered in the jelly fish *Aequorea victoria*; many other fluorescent proteins are also naturally occurring from different coral reef species. These proteins are fluorescent, can be long lasting and observed under blue or Ultra-violet (UV) light. Therefore genes that encode these fluorescent proteins can be used to identify easily successfully transfected cells using a fluorescence microscope. Protein expression and its subsequent changes can therefore be monitored in real time. These sensitive genes can be used in living cells and animals and are available in a variety of spectral excitation and emission wavelengths. For some systems, the fluorescent signal from GFP is not strong enough; however, modified GFP proteins (through specific mutations) with improved emission at a wide-range of wavelengths [GFP, CFP (cyan fluorescent protein) and YFP (yellow fluorescent protein)] have been created.

Another fluorescent protein that was again first isolated from coral reefs, is called DsRed (*Discoideum sp*, red fluorescent protein). The

crystal structure exhibits a similar topology to GFP, but additional chemical modifications accounts for different spectra properties [7]. The reporter gene used throughout this thesis is a mammalian expression vector that encodes a fusion of DsRed with a mitochondrial targeting sequence (MitoDsRed), thereby specifically expressing DsRed only in the cell's mitochondria. In genetic engineering, a vector is also called a plasmid, which is double-stranded DNA, and in many cases, circular, and can replicate independently of the chromosomal DNA within a suitable host [8]. Therefore, once a small amount of MitoDsRed plasmid enters the cell's nucleus, it can multiply and subsequently express high levels of this red fluorescent protein.

1.2. Gene Transfer to Animal Cells Using Chemical and Physical Methods

1.2.1 Introduction

In this section, the focus will be on gene transfer methods using chemical and physical means to carry the exogenous genetic material across the cell membrane. Chemical methods normally involve mixing specific chemicals and genetic material together to form synthetic complexes, which can either enter the cell through endocytosis or fuse with the cell membrane. The genetic material is then released into the cell cytoplasm. Without the need to form synthetic complexes, physical transfection methods can directly change the permeability of the cell membrane and allow the genetic material to enter the cell, and in some cases directly enter the nucleus. Techniques such as Nucleofector [9], utilize the advantages of both methods and combine them to greatly enhance the transfection efficiency.

The first boundary for transfection is the cell membrane, which is hydrophobic and negatively charged. DNA is hydrophilic but also

negatively charged. Therefore, in chemical methods of transfection, in order to allow passage of DNA to cross the cell membrane, a fusogenic capsule or complex that carries a net positive charge are used to enclose the DNA molecules. Following the fusing with the cell membrane, the DNA encapsulated in the fusogenic particles, is released into the cytoplasm and subsequently enters the nucleus via an intrinsic transport pathway, which is still poorly understood. However, after entering the cell through an endocytic process, the complexes are transported into endosomes and can be degraded by lysosomes. Therefore, the complexes must escape from the endosome into cytosol before being degraded. Certain reagents such as chloroquine can be further added to the transfection protocol to disrupt endosomes and the endosomal transport pathway to release DNA. After which, the DNA can either simply diffuse into the cytoplasm directly, or after the positively charged complex is neutralized by intracellular lipids and other molecules. Only free DNA can be used for gene expression or interaction with the host cell's genome.

The major difference between physical and chemical methods is that, in physical methods, the DNA is delivered to the cytoplasm or nucleus directly without having to consider the nature of the cell plasma membrane or endosomal pathways. In this fashion, DNA molecules may also suffer less damage from chemical agents. There are very few similarities between the different physical methods and they are driven by their respective physical principles. However, all of them require expensive apparatus and need experienced experts to operate them. In the next few sections, the most common chemical and physical transfection methods will be briefly described.

1.2.2 Chemical Transfection Methods

1.2.2.1. Calcium phosphate

Calcium phosphate has been widely used in the chemical transfection of animal cells [3]. The basic protocol for this method is that DNA in a buffered phosphate solution and calcium chloride are mixed together to generate a DNA-calcium phosphate co-precipitate, which forms on the cells and enter the cells through endocytosis. Applying this process on cells grown on a monolayer can provide a high transfection efficiency. However, some cells are sensitive to the density of the co-precipitate and also delicate primary cells often give poor results. In addition, a major drawback of this method is that the size of the formed particles depends on various factors including the method of mixing the reagents. Therefore the results are not consistent and are difficult to reproduce. Nevertheless, this inexpensive method is still easy, reliable, and suitable for many cultured cell lines, and it can be used to provide both transient and stable transfection.

1.2.2.2. DEAE-dextran

DEAE-dextran (diethylaminoethyl-dextran) was a popular method for chemical transfection before the advent of lipofection reagents in the 1990s [3]. This soluble polycationic carbohydrate forms complexes with DNA through electrostatic forces. The complexes have a net positive charge and so interact with the negatively charged cell membrane and then enter the cell through endocytosis (Fig. 1.1). The formed complexes are smaller than the calcium phosphate precipitates and this limits the maximum amount of DNA that can be used for each transfection experiment. This method is inexpensive, simple and efficient, and although the transfection efficiency is affected by different cell lines, this method has proven not to be good at creating stable transformations.

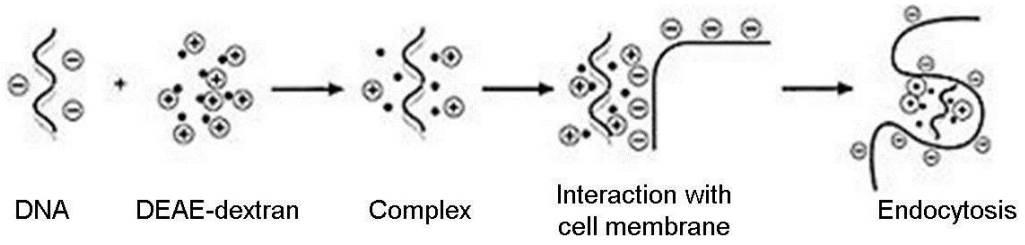

Fig. 1.1. *Transfection with DEAE-dextran. Negatively charged DNA and positively charged DEAE-dextran form a complex with a net positive charge. This complex then interacts with negatively charged cell membrane and promotes endocytosis. This graph is modified from Fig. 2.3, [3].*

1.2.2.3. Lipofection

There are two types of lipofection (lipid-mediated transfection), which are the most widely used chemical transfection methods for gene transfer into mammalian cells [3, 10]. In the first type, hydrophobic, unilaminar phospholipid vesicles called liposomes are first created from lipid molecules. The DNA is packaged inside the vesicles, which subsequently fuses with the cell membrane after being mixed with cells in the culture medium. DNA is then released to the cytoplasm directly (Fig. 1.2). Liposome-mediated transfection was the first non-viral *in vivo* DNA transfection technique, which was suitable for potential gene therapy studies.

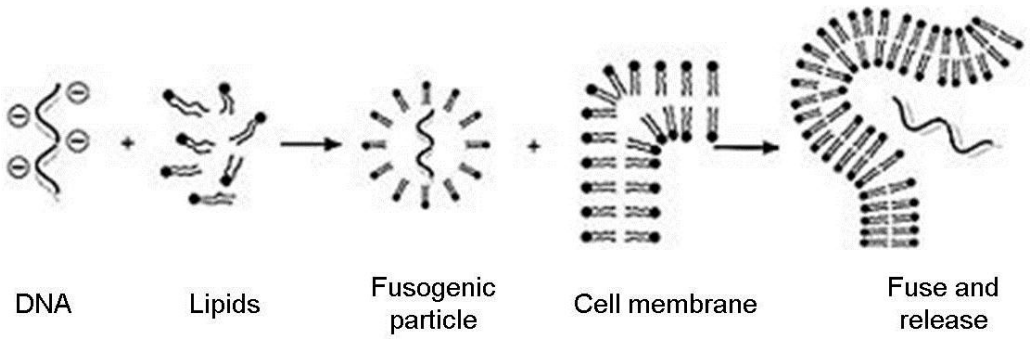

Fig. 1.2. *Transfection with liposomes. A fusogenic particle (liposome) is first created with DNA inside before fuses with the cell membrane, followed by the release of DNA into the cytoplasm. This graph is modified*

from Fig. 2.4, [3].

The second form is similar to the method using DEAE-dextran (Fig. 1.2). A complex called a lipoplex, is first created using cationic/neutral lipid mixtures and DNA. The lipoplex has a net positive charge and interacts with the negatively charged cell membrane, entering the cell through endocytosis. This method is extremely simple. Lipoplexes are first created by simply mixing a lipid preparation and the DNA in a serum-free medium which is then added to the cells. This transfection method can be very efficient for both transient and stable transfection. However, the lipids are generally difficult to make in the laboratory and therefore must be purchased.

1.2.3 Physical Transfection Methods

1.2.3.1. Electroporation

During electroporation, cells in buffered solution experience a pulsed electric field, from which a number of pores of ~100 nm in diameter are formed in the cell membrane and remain open for up to 30 minutes [3, 5, 11]. Free DNA molecules in the surrounding medium can then enter the cells through these pores which will self-heal. This method is applicable to many different cell lines, and especially those cells lines that cannot be transfected via chemical methods. This technique was initially designed for cells cultured in suspension; however, subsequent modifications have extended the application of electroporation to adherent cells growing on a polyethylene terephthalate or polyester membrane [12, 13].

This technique is very easy to implement. Normally, cells in a buffer solution are treated with a short high voltage electric pulse or pulse train. The amplitude, duration and the number of pulses applied to the cells is adjusted to achieve the optimum transfection efficiency. Although, electroporation is effective in delivering genetic materials into cells, their

viability after treatment is extremely poor, and so more cells are required as compared to other transfection methods.

Recently, a new type of electroporation called nucleofection was developed [14]. This new technique combines special designed transfection reagents and electroporation using a specifically designed electric field application for each cell line to promote the DNA delivery to the nucleus. Many traditional difficult-to-transfect cells, including primary neuron cells, have been transfected with this technique. Recently, needle electrodes have also been used in *in vivo* and *ex vivo* electroporation. Based on needle electrode, targeted single cell electroporation has been achieved [13, 15].

1.2.3.2. Microinjection

Fig. 1.3, shows a biological cell being held by a micropipette on the left while a micro-needle is inserted into the cell nucleus from the right. This technique is called microinjection and is used for the delivery of DNA into oocytes and embryos of animals for the creation of transgenic animals and artificial fertilization [16]. This technique also allows the injection of DNA either into the cytoplasm or nuclei of cells directly without concerns on the membrane boundaries and the inefficient endogenous DNA transporting pathways. Therefore, this technique has been traditionally used to transfect cells that are difficult to transfect by other methods. Although this technique is highly efficient for individual cells, this procedure is time consuming and has a low efficiency. The requirement of DNA purity is also extremely high, which means laborious preparation is needed. However, the automation of this technique can standardise the procedure, reducing human error and increasing the injection rates and reproducibility [17].

Fig. 1.3. *Microinjection technique. A cell is hold (sucked) by a micropipette on the left while a micro-needle is inserted and delivering DNA into the cell nucleus (Image from an unknown source on internet).*

1.2.3.3. Particle bombardment

Particle bombardment is also known as biolistics or microprojectile transfection [3, 5, 18]. This technique involves shooting micrometre sized gold or tungsten particles coated in DNA, into cells or tissues. By adjusting the force applied to the particles, the penetrating depth can be controlled. This technique is especially useful for the transfection of cells with a thick cell wall, such as with plant cells. For animal cells, this technique is particularly useful for transfection of whole organs, tissue slices and even living animals [19, 20]. The adjustment of the size, mass of the particles and the force of the bombardment are essential for finding a balance for penetration depth, transfection efficiency and tissue damage. The basic principle and setup of this technique is shown in Fig. 1.4, where DNA coated microprojectiles are spread onto a macrocarrier disc (Kapton disc); a membrane restraining the gas is ruptured by an electronically driven plunger and the disc is propelled toward the target tissue by the resulting shock-wave; the macrocarrier is stopped by a screen while the microprojectiles continue on to penetrate the tissue.

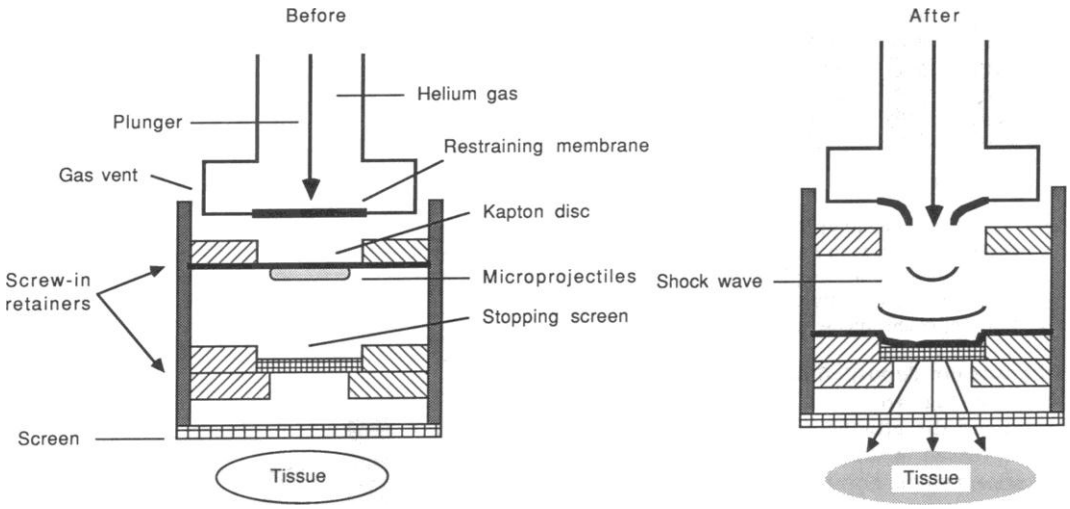

Fig. 1.4. *Basic features of a particle bombardment transfection system. DNA coated microprojectiles are spread onto a macrocarrier disc (Kapton disc). A membrane restraining the gas is ruptured by an electronically driven plunger and the disc is propelled toward the target tissue by the resulting shock wave. The macrocarrier is stopped by a screen while the microprojectiles continue on to penetrate the tissue. (Image from [19])*

1.2.3.4. Sonoporation

Applying high intensity ultrasound waves of specific frequencies to a dish of cells or tissue can also be used for the transfection of cells [21-24]. The mechanism of sonoporation relies on ultrasound generating bubbles which oscillate and collapse violently in the vicinity of the cell membrane. This phenomenon is known as cavitation, which produces a shock-wave causing the fluid to move against the cell membrane. The resulting shear force changes the permeability of the cell membrane by opening up specific holes. These self-healing holes remain open for several minutes and allow macromolecules to enter the cell. At certain ultrasound frequencies and exposure settings, this technique has no observable adverse effects when applied to the human body. However, it has been shown that this technique gives very low transfection efficiency on cultured cells, but as a result of its deep penetration capability, gene

therapy has already been achieved *in vivo* and is being actively studied for the use in *in vivo* targeted gene therapy [25, 26],

1.2.3.5. Laser induced transfection

Another *in vitro* transfection approach utilizes tightly focused laser to change the permeability of the cell membrane [27]. Lasers of different wavelengths [near infrared (NIR) [28] to UV [29]] and modes (continuous [29] and pulsed [28, 30, 31]) can be used to achieve the transfection through different mechanisms. So far, femtosecond laser mediated transfection has been regarded as the most promising and the most efficient optical transfection method, and so will be described in more detail in the next chapter.

1.3. Summary and Conclusion

Cell transfection is at the heart of this thesis and it can be achieved through various means. Before the presentation of optical fiber based optical transfection techniques, which will be shown in the next few chapters, it is necessary to understand what cell transfection is and familiarize with other cell transfection methods. This chapter first reviewed the basic principles of gene transfer, which include the brief introduction of the definition of cell transfection and three basic objectives for any successful transfections; the reporter genes that are commonly used to assess different transfection methods and measure the transfection efficiencies was also introduced. After that, most of the popular non-viral (chemical and physical) gene transfection technologies were introduced briefly. By comparison with these traditional gene transfection methods, it is easier to understand the strength and weakness of laser based optical transfection techniques. Although with low transfection throughput, optical transfection has proven to be a more attractive transfection method. This sterile, non-contact technique provides single cell selectivity with sub-

cellular resolution and can be easily combined with almost any classic microscopy, optical tweezers or microfluidic setups. The following chapter will explore the most effective optical transfection method: femtosecond laser mediated optical transfection.

Chapter 2:

2. Femtosecond Laser Mediated Optical Transfection

2.1. Introduction

Since the advent of the laser, it has not only been used to image biological cells [32], but also to manipulate them – ablating, moving, cutting and stretching using optical power [33-37]. In the previous chapter, the basic principles of gene transfection using various different chemical and physical transfection methods were introduced. Among these methods, a novel laser manipulation technique for the introduction of foreign material into biological cells, has been shown to have advantages over the others: Firstly, it is a physically non-contact and sterile process. The cells are normally manipulated by a focused laser beam delivered from a remote distance through an objective. Therefore the cells can be enclosed in an environment, such as a Petri dish or microfluidic chip without exposure to the air during transportation from the preparation bench to the transfection setup and throughout the whole experimental process. Secondly, laser mediated transfection can be easily integrated with almost any conventional imaging or microscopy setup. By coupling the laser beam for optical transfection into an imaging setup, the researcher can treat a particular area of a carefully chosen cell while watching the process in real time. Furthermore, this technique provides single cell selectivity with sub-cellular precision. With a sub-micron laser spot integrated with modern microscopy technologies, one chosen cell surrounded by many others can be transfected and leave the other cells unaffected. Thanks to the miniaturization trend in the biophotonics world, laser mediated transfection has the potential to be realized along with other imaging modalities and optical manipulation tools on a fiber based microendoscope, which will be discussed thoroughly in later chapters.

Laser mediated introduction of foreign material into biological cells

can be generally called optical injection. However, if the internalized substance is a nucleic acid, such as DNA, RNA or siRNA, then the process can also be called optical transfection [38]. Various laser sources of different wavelengths (NIR [28] to UV [29]) and modes [continuous wave (CW) [29] and pulsed [28, 30, 31]] can be used to achieve optical transfection. However, the transfection mechanisms are different for different laser systems. For CW lasers, the mechanism is probably due to the highly localized heating [39, 40] or photochemical reaction [29]. Phenol red is added to the buffer medium during transfection in order to increase the heat absorption and so subsequently to increase the transfection efficiency [29, 39-41]. For femtosecond lasers with high repetition rates (~80 MHz), the permeabilization event is most likely due to the creation of a low density plasma inducing chemical decomposition (bond breaking) in conjunction with multiphoton-induced chemistry on the cell membrane [42]. At much lower repetition rates (1 kHz) with increased pulse energy, small transient cavitation bubbles can be thermoelastically induced in the liquid and open small holes on the cell membrane [42]. Nanosecond lasers can generate electrons in the water, but also induce heating, cavitation bubble formation and thermoelastic stress, which lead to the formation of a shockwave [31, 42, 43]. Therefore, it is much easier to target an area covered with tens of cells than a single cell using a nanosecond laser for optical transfection. A comparison of the various laser sources and their efficiencies is shown in table 2.1 [38]. Femtosecond lasers are currently the most well understood powerful choice for single cell optical transfection. Theoretically, a femtosecond laser should also cause the lowest amount of damage to the cell due to the highly localized nonlinear absorption and therefore achieve the highest survival rate and transfection efficiency. Although by a similar mechanism, femtosecond lasers can manipulate biological cells in many different ways, such as optoinjection [44], microsurgery [45, 46] and nanopartical injection [47], but optical transfection will be the focus in this chapter.

Laser source: wavelength, pulse duration and repetition rate	*Reference*	*Likely mechanism of action*	*Transfection efficiency*
193 nm/308 nm, 6 ns, 200 Hz	[48]	Heating, thermoelastic stress	0.5%
355 nm, ns, Hz	[43, 49-51]	Heating, thermoelastic stress	0.3 – 38%
405/488 nm, CW	[29, 39-41, 52]	Hearting or photochemical; typically requires chemical absorbers in the medium such as phenol red	less than 30%
532 nm, ns, kHz	[53-55]	Heating, thermoelastic stress	30–80%
Approx. 800 nm, fs, greater than 1 MHz	[28, 30, 36, 56-73]	Multi-photon effect; generation of a low density free electron plasma cloud	often greater than 90%
1064 nm, ns, Hz	[74, 75]	Heating, thermoelastic stress	less than 2%
1554 nm, fs, MHz	[76]	Multi-photon effect; generation of a low density free electron plasma cloud	77%
2080 nm, a few Hz	[77]	Not known	41%

Table 2.1. *Laser sources used for optical injection, probable mechanisms of action and typical efficiencies. (Modified from Table 1 in [38] with newly added references)*

2.2. Mechanisms of Femtosecond Laser Mediated Cell Membrane Permeabilization

Throughout this thesis, cell transfection was instigated by a femtosecond Ti: Sapphire laser emitting at 800 nm, with an output pulse duration of ~100 fs and a pulse repetition frequency of 80 MHz (Coherent, MIRA). With this set of laser parameters, optical transfection was performed in the low-density plasma regime at pulse energies well below the optical breakdown threshold and only slightly higher than those used for nonlinear imaging. The induced moderate heating or thermoelastic stresses can be ignored. Increasing the laser power, cumulative heating will occur and long-lasting bubbles will be produced by tissue dissociation into volatile fragments, which cause dislocations far beyond the laser focus. Therefore long-lasting bubbles means that more damage to biological cells occurs and it should therefore be avoided.

2.2.1 The Principle of Plasma Formation

The process of plasma formation from laser induced breakdown in transparent biological media is schematically depicted in Fig. 2.1. The quasi-free electrons are generated by an interplay of photoionization and avalanche ionization. Quasi-free electrons, which are different from free electrons generated in gases, are used to describe the generated electrons by optical breakdown in condensed matter. These electrons have gained enough kinetic energy to be able to move freely without being captured by local potential barriers. For simplicity, the term “free electrons” will be used in this chapter.

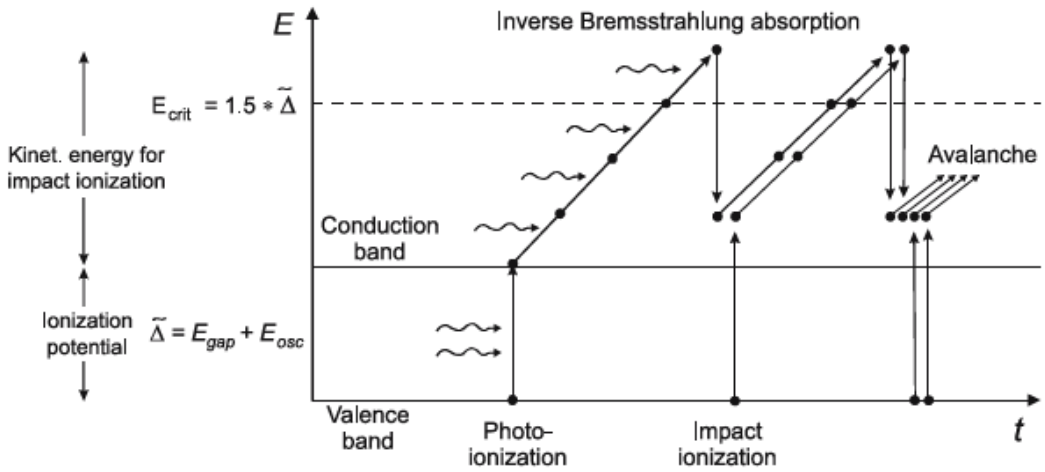

Fig. 2.1. *Interplay of photoionization, inverse Bremsstrahlung absorption, and impact ionization in the process of plasma formation. Recurring sequences of inverse Bremsstrahlung absorption events and impact ionization lead to an avalanche growth in the number of free electrons [42].*

Pure water can be used as a model instead of biological tissue to study the laser induced plasma formation in bulk material, since the optical breakdown threshold in water is very similar to that in biological tissue [78] and optical transfection is performed in a liquid environment. According to Sacchi, water can be treated as an amorphous semiconductor with a band gap Δ = 6.5 eV between valence and conduction bands [79]. However, under the irradiation of high peak power femtosecond pulses, the oscillation energy of the electron due to the electrical laser field has to be taken into account for the calculation of the band gap potential and the effective ionization potential of individual atoms can be written as [80]

$$\tilde{\Delta} = \Delta + \frac{e^2F^2}{4m\omega^2} \tag{2.1}$$

where ω and F denote the circular frequency and amplitude of the electrical laser field, e is the electron charge, and $1/m = 1/m_c + 1/m_v$ is the exciton reduced mass that is given by the effective masses m_c of the free electron in the conduction band and m_v of the hole in the valence band.

Under the scope of this thesis, multiphoton ionization and tunneling are two mechanisms thought to be governing the photoionization [42] (Fig.

2.1). Unlike single photon ionization where an atom or molecule absorbs one photon with the energy that is equal to or higher than the ionization energy, several photons are simultaneously absorbed during the multiphoton ionization process [81]. Tunneling is an ionization process that allows electrons escaping from an atom or molecule easily due to the intense electric field distorted potential barrier of the atom or molecule [80]. The relative contribution to the photoionization from these two mechanisms depends on the different field strengths and frequencies of the electromagnetic field. With relatively low frequencies and large field strengths, tunneling is more responsible for ionization, while with typical larger optical frequencies and moderate field strengths, multiphoton ionization occurs more easily [80]. At a wavelength of 800 nm, the transition between two mechanisms occurs at field strengths of about 100 – 200 MW/cm, corresponding to irradiances of 1.3 – 2.6 x 10^{13} W/cm^2 [82-84]. One example shows that the optical breakdown irradiance for 100 fs pulses in distilled water is 1.1 x 10^{13} W/cm^2, which is close to this transition and very close to the irradiance used in femtosecond optical transfection experiments. Therefore both multiphoton and tunneling ionization can be responsible for the photoionization in femtosecond optical transfection [85].

After the generation of the first free electron through photoionization, impact ionization will continue to produce more free electrons (Fig. 2.1). The first generated free electron can continue to absorb photons in a process called ‘inverse Bremsstrahlung’, which involves colliding with a third heavy charged particle (ions or atomic nuclei) to allow for energy and momentum conservation [86]. After several inverse Bremsstrahlung absorptions, the free electron is accelerated to a speed (kinetic energy) that is fast enough to ‘impact’ the other electron on the valence band and so two slow-moving free electrons, are thus created through the impact ionization (Fig. 2.1) [84, 87, 88]. These two electrons keep repeating the ‘inverse Bremsstrahlung’ process and ‘impacting’ more low energy electrons, and finally lead to an avalanche growth in the number of free electrons, if the irradiance is high enough, to overcome the losses of free

electrons through diffusion out of the focal volume and through recombination, and also if the energy gain through inverse Bremsstrahlung is faster than the energy loss by collisions with heavy particles. The whole process can be called ‘avalanche ionization’ or ‘cascade ionization’ (Fig. 2.1) [42].

For impact ionization to happen, the kinetic energy of the impacting electron must be large enough to assist the other electrons to overcome the effective ionization potential $\tilde{\Delta}$ and provide some extra energy for the collision with a third particle for the conservation of energy and momentum. This critical energy (kinetic energy), $E_{crit,}$ is decided by the band structure of the water molecule and can be assumed to be equal $E_{crit} = 1.5\ \tilde{\Delta}$ [42, 84, 89]. After overcoming the ionization potential $\tilde{\Delta}$, the rest $0.5\ \tilde{\Delta}$ is distributed among two free electrons and the other colliding particle. Therefore, after impact ionization, two free electrons have energies above the conduction band and need to gain less than $1.5\ \tilde{\Delta}$ to reach the critical energy [84, 90]. However, the average energy leading impact ionization is larger than E_{crit} because the impact ionization rate increases with kinetic energy and in order to achieve avalanche ionization, a very high ionization rate is needed [84, 89, 91]. Considering both factors, it is assumed that the average energy gain required for a free electron (above the conduction band) to cause impact ionization is $1.5\ \tilde{\Delta}$, as depicted in Fig. 2.1 [42].

To study optical transfection, the important range of plasma formation is from a point below the optical breakdown threshold to a point slightly over it. In aqueous media with femtosecond pulses, the indication of optical breakdown is the formation of cavitation bubbles. By contrast, from a theoretical point of view, the optical breakdown threshold is defined by the critical free electron density at the laser focus, above which the plasma becomes both strongly reflective and absorbing [83, 84, 90, 92, 93]. At 800 nm, the approximate value of the free electron density is 10^{21} cm^{-3} [42]. This is a constant because from experimental measurements, it has been shown that the bubble formation is always related to a plasma energy density with a fixed value [42].

2.2.2 Evolution of Free Electron Density and Breakdown Thresholds

Based on the qualitative description of the plasma formation process as discussed above, a numerical simulation has been developed to study the evolution over time of the free electron density ϱ_c under the influence of the laser field [42]. Considering the photoionization (including multiphoton and tunneling ionization), cascade ionization, and losses through diffusion of electrons out of the focal volume and recombination, the free electron rate equation can be written as [94]

$$\frac{d\varrho}{dt} = \eta_{photo} + \eta_{case}\varrho_c - \eta_{diff}\varrho_c - \eta_{rec}\varrho_c^2 \qquad (2.2)$$

The first term on the right hand side, η_{photo}, represents the free electrons produced by photoionization. The second term represents the electron production by cascade ionization; and the last two terms describe the electron losses. ϱ_c indicates the free electron density, η_{case}, η_{diff} and η_{rec} are the cascade ionization rate, diffusion loss rate and recombination rate respectively. The laser pulse is assumed to have a Gaussian time variation and focused into pure water through a microscope objective with a numerical aperture of NA = 1.3. More detailed numerical simulation can be found in [42].

From the numerical simulation, the evolution of the free electron density ϱ_c under the irradiation of a single 100 fs, 800 nm laser pulse at the optical breakdown threshold, is presented in Fig. 2.2(a) [42]. The time *t* is normalized with the 100 fs pulse duration (τ_L) and the 0 on the time axis in Fig. 2.2(a) indicates the center (peak) of a laser pulse. The contribution of photoionization to the total free electron density is plotted as a dotted line. Fig. 2.2(b) shows the maximum free electron density that can be achieved using different laser pulse irradiance ***I***, which is normalized with respect to the threshold irradiance $\boldsymbol{I}_R$.

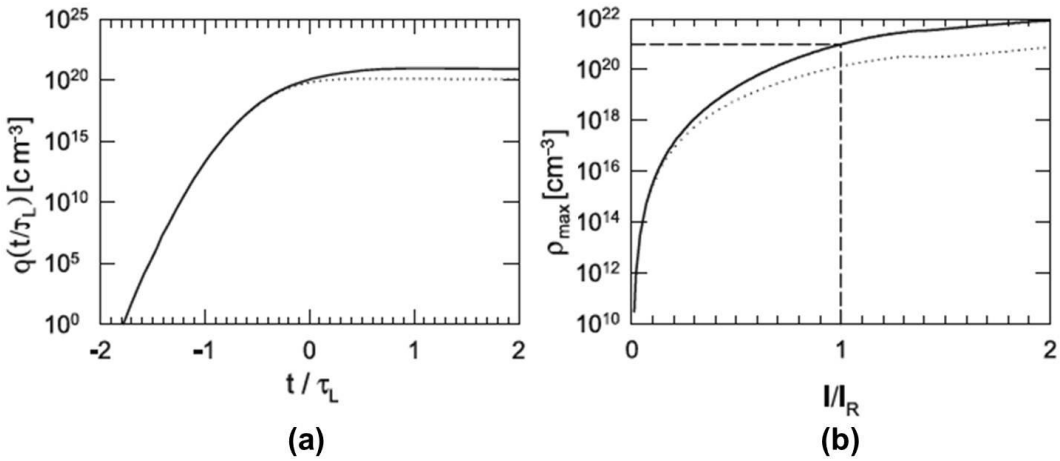

Fig. 2.2. (a): *evolution of the free electron density during the laser pulse at the optical breakdown threshold for 100 fs and 800 nm pulses. The time t is normalized with respect to the laser pulse duration τ_L. The contribution of multiphoton ionization to the total free electron density is plotted as a dotted line. (b): maximum free electron density ϱ_{max} achieved during the laser pulse as a function of irradiance, for the same laser parameters. The irradiance **I** is normalized with respect to the threshold irradiance **I**$_R$. The threshold **I**$_R$ and the corresponding value of ϱ_{max} are marked by dashed lines [42].*

Due to the ultrashort pulse duration of the femtosecond laser, a very high irradiance can be achieved and so produce free electrons through photoionization. With a single 100 fs pulse at 800 nm, the total number of free electrons generated through avalanche ionization is only 12 times larger than the number generated through photoionization [Fig. 2.2(a)]. Thus the contribution of photoionization cannot be ignored. It can be seen that the avalanche ionization can be initiated at irradiance values noticeably lower than the optical breakdown threshold, because there is never a lack of seed electrons for avalanche ionization [Fig. 2.2(b)]. The maximum free electron density can be reached at the relative irradiance value is shown in Fig. 2.2(b), from which and with the support of experiment results [92], it can be seen that plasmas with a wide density range below an optical breakdown threshold can be created using one

ultrashort pulse in bulk transparent media. The free electron density can be controlled through the tuning of relative irradiance values. Thus low density plasma mediated chemical, heating and thermomechanical effects can be precisely controlled by varying the irradiance. These effects are also very well localized due to the nonlinearity of the plasma formation process.

The irradiance and radiant exposure (irradiance multiplied by pulse duration) that is needed to reach the breakdown threshold with a critical free electron density of 10^{21} cm^{-3} is shown in Fig. 2.3 [42], from which it can be seen that pulse durations at the ranges below and above 10 ps show very different behaviours. For the pulse durations shorter than 10 ps, the threshold radiant exposure shows only a weak dependence on pulse duration. This reflects the fact that, when the laser pulses are shorter than 10 ps, free electrons can be produced in a very short time before the combination process starts and this set of produced free electrons (with a constant density at the threshold) results in a roughly constant energy density within the focal volume. This is proved by the bubble formation experiments that always require a specific plasma energy density, which varies little with different ultrashort pulse durations and wavelengths [42]. For the pulses longer than 10 ps, the recombination happens within one pulse duration time and therefore the longer the pulse, the larger the radiant exposure is needed. For the analysis of pulses longer than 10 ps, more information can be found in [42].

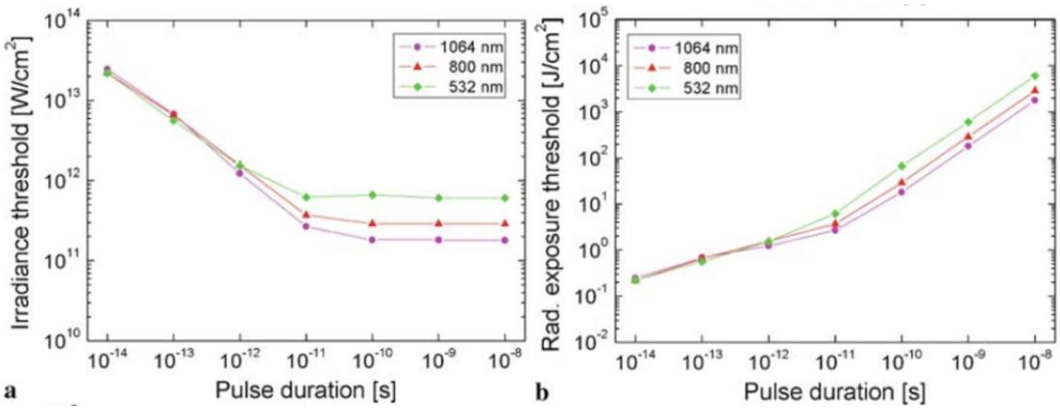

Fig. 2.3. *Calculated optical breakdown thresholds (10^{21} cm^{-3}) as a function of laser pulse duration for various laser wavelengths [42]. (a) Irradiance thresholds, (b) radiant exposure thresholds.*

2.2.3 Chemical Effects of Low Density Plasmas

Biological tissue is modified by low density plasma through chemical reactions. There are mainly two types of chemical effects. The first one, reactive oxygen species (ROS), such as OH* and H_2O_2, are generated through various pathways following ionization and dissociation of water molecules [95-97]. ROS have negative effects (causing cell damage [56]) on biological tissues. The second type of chemical effects can directly change the organic molecules in resonant electron-molecule scattering. Electrons captured into a molecule can cause the fragmentation of biomolecules [96, 98-100]. ROS and free electrons mediate cell membrane dysfunction and DNA strand breaks [56] and this is also believed to be the main mechanisms of the permeabilization of the membrane during femtosecond optical transfection. More discussion about the implications of laser induced low density plasma on biological cells and tissues will be presented in section 2.2.5 and more details about these chemical effects can be found in [42].

2.2.4 Temperature Evolution during Pulse Series

Thermal effects play a big role in some forms of laser surgery [101]. Therefore, to obtain a better understanding of femtosecond optical transfection, the temperature change near the laser focus needs to be investigated. In the previous sections, it was shown that the laser energy transferred to the medium forms plasma in the laser focus. After that, the fast moving electrons transfer the energy to heavy particles through collisions and non-radiative recombination processes, resulting in the heating of the atomic, molecular, and ionic plasma constituents [42]. For femtosecond lasers, the pulse duration is much shorter than the electron collision and the recombination process. Therefore, the plasma formation and heating (transferring of electron energy to heavy particles) can be treated as two consecutive and independent processes for the study of temperature evolution. The total energy delivered by one laser pulse can be calculated by simply multiply the total number of produced free electrons by the mean energy gain of them. Then taking into account the repetition rate of the laser (80 MHz), wavelength (800 nm), pulse duration (100 fs), free electron density, and properties of pure water, the evolution of the temperature distribution within the interaction volume can be calculated (Fig. 2.4).

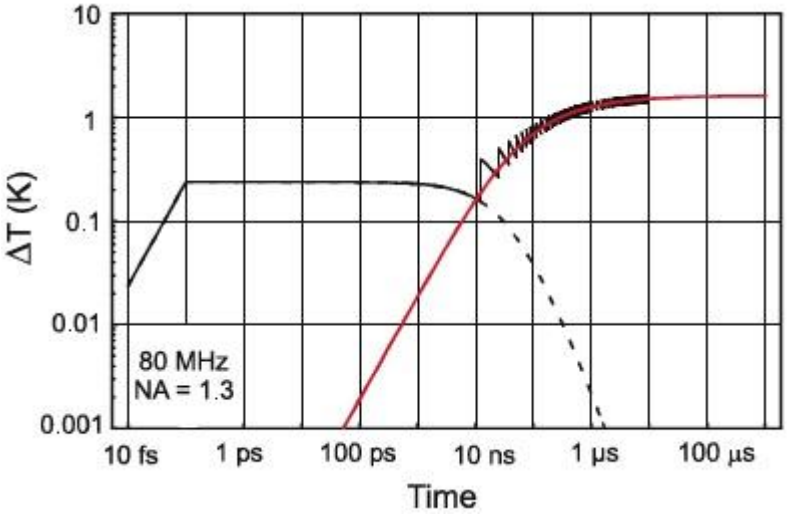

Fig. 2.4. *Temperature evolution (black line) at the center of the laser focus produced by a series 800 nm, 100 fs pulses focused into water at a NA = 1.3 with a repetition rate of 80 MHz. The volumetric energy density deposited per pulse is always 1 Jcm^{-3} at the focus center. The dashed lines represent the temperature decay after a single pulse. For comparison, the temperature evolution during CW irradiation with the same average power as for the pulsed irradiation is also shown (red line) [42].*

Fig. 2.4 shows the calculated temperature evolution at the center of the laser focus at a NA of 1.3 and with each pulse an energy density of 1 J cm^{-3} (corresponding to an irradiance value below the optical breakdown threshold) at the center of the initial temperature distribution is deposited [42]. For other values of the energy deposition, the shape of the curve in Fig. 2.4 will be the same but with a temperature increase (ΔT) proportional to the deposited peak energy density. For comparison, the temperature evolution during CW irradiation with the same average power as for the femtosecond laser, is also shown in the same graph (red curve).

An 80 MHz repetition rate corresponds to a delay of 12.5 ns between two consecutive femtosecond pulses. It can be seen that in Fig. 2.4 the temperature is first raised by 0.2 K by a single laser pulse and after 12.5 ns before the temperature drops back to the original state, the temperature increased again by the second pulse to a higher level. After

tens of microseconds the temperature is elevated to a balanced level, which is 6.8 times larger than the temperature raised by a single pulse. Moderate heat accumulation effects can be seen. With higher irradiance (still under the breakdown threshold), larger temperature rises can be achieved. However, thermal denaturation of biomolecules may only be a minor effect since more free electrons will be produced and induce chemical effects simultaneously [42].

2.2.5 Bubble Formation during Optical Transfection

The time interval for temperature rise under the irradiation of a single femtosecond pulse is much shorter than the acoustic transit time from the center of the laser focus to the surrounding medium. Therefore, the thermoelastic stresses caused by the temperature rise are confined in the focal volume and lead to the rise in local pressure [102-104]. Cavitation bubbles will be formed when the tensile strength of the liquid is exceeded (optical breakdown). However, for cell surgery with a laser of high repetition rate ~80 MHz, long-lasting (few seconds) bubbles will be created before the pulse energy reaches the level of cavitation bubble (sub-microsecond) formation. The long-lasting bubbles probably arise from the dissociation of biomolecules into volatile, non-condensable fragments [105-107]. The mechanisms of this dissociation can be attributed to free electron chemical and photochemical bond breaking as well as to the accumulative thermal effects [42]. During optical transfection, the appearance of long-lasting bubbles means more damage to the treated cell and it is therefore better if it can be avoided. The bubble formation does not belong to the mechanisms contributing to optical transfection and thus will not be introduced in this chapter. More specific information about this mechanism can be found in [42].

2.2.6 Conclusion

Normally for femtosecond optical transfection, a laser with a repetition rate of 80 MHz and pulse energies at the sub-nanojoule level, well below the optical breakdown threshold and less than one order of magnitude higher than those used for nonlinear imaging, is used [28, 57, 105, 108-112]. 40,000 to several million pulses are applied on the cell membrane to change its permeability so as to allow the delivery of foreign genetic material into the cytoplasm [28]. The different low density plasma effects and physical breakdown phenomena are summarized in Fig. 2.5, together with the experimental damage, transfection, and dissection thresholds on cells scaled by the corresponding values of free electron density and irradiance [42]. From Fig. 2.5 the relative position of femtosecond optical transfection compared with other modalities of cell laser surgery in terms of irradiance and free electron density can be seen. In comparison with intracellular dissection, optical transfection (membrane permeabilization) not only needs a larger laser dose, but also more applied pulses. The corresponding laser parameters are still within the regime of low density free electron mediated cumulative chemical effects but are already very close to the range where cumulative heating becomes effective. In this regime, no transient cavitation bubbles and long-lasting bubbles are produced. In the scope of this thesis, optical transfections are performed at irradiances (~4.4×10^9 W/cm^2) well below optical breakdown thresholds using 800 nm laser pulses at durations around 1 ps. The optical breakdown threshold at this point is ~10^{12} W/cm^2 [Fig. 2.3(a)]. Experiment evidence using transmission electron microscopy shows that during femtosecond laser pulse irradiation, pores of 0.5 – 1 µm in diameter are formed on fixed cells [113]. With properly selected laser parameters, cell survival rates higher than 90% after treatment can be achieved [28, 58, 62, 64, 65, 67]. Various cell membrane impermeable substances, such as fluorophore, monosaccharides, dyes [36, 56, 58-60, 62, 64, 65, 67], plasmid DNA [28, 30, 57, 59, 63, 64, 66, 67, 71, 114], mRNA [60, 115] and

even gold nanoparticles [47], have been delivered into cells.

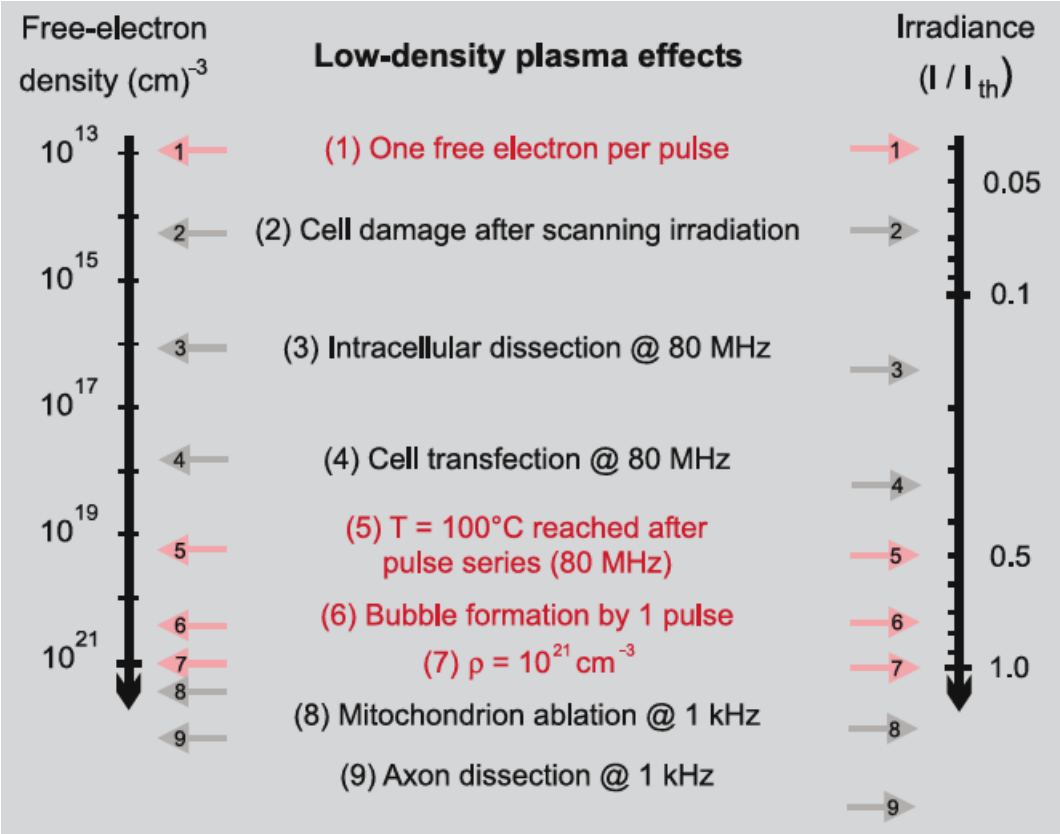

Fig. 2.5. *Overall view of physical breakdown phenomena induced by femtosecond laser pulses, together with experimental damage, transfection, and dissection thresholds for cells. The different effects are depicted together with the corresponding values of free electron density and irradiance. The irradiance values are normalized to the optical breakdown threshold defined by a critical electron density of 10^{21} cm^{-3}. All data refer to plasma formation in water with femtosecond pulses of about 100 fs duration and 800 nm wavelength [42].*

Generally speaking, in the regime of optical transfection, femtosecond lasers enable the creation of spatially and extremely confined chemical effects via the generation of free electrons through nonlinear absorption. A wide range of free electron densities below the breakdown threshold can be easily generated by tuning the relative irradiance value. Also due to the nonlinear nature of the plasma formation,

an effective volume below the diffraction limit can be achieved. This high precision technique can not only be applied to single cells or the surfaces of biological tissues, but also can penetrate at depth due to the high transmission of biological tissue at near infrared wavelengths.

One note of caution is that the mechanisms of femtosecond optical transfection discussed above are based on pure water, lacking the consideration of the absorption properties of biomaterials in the actual situation. More intermediate energy levels are also located within the band gap for water and this might lead to free electron generation at a lower irradiance and so lower the threshold for consequent chemical effects.

2.3. Development of Femtosecond Optical Transfection

Femtosecond optical transfection was first demonstrated by Tirlapur et al. in 2002 [28]. In their experiment, an 800 nm femtosecond pulsed laser beam from an 80 MHz Ti: Sapphire laser, with a mean power of 50 – 100 mW was tightly focused using a high NA objective at a sub-femtolitre focal volume at the cell membrane. Chinese hamster ovary and rat-kangaroo kidney epithelial (PtK2) cells were successfully transfected with plasmid DNA vector pEGFP-N1 encoding enhanced green fluorescent protein (EGFP) using this approach. The transfection efficiency was claimed to be ”100%” “irrespective of cell type”, although the definition of the transfection efficiency was not given [28]. A later work presented the first detailed study into transfection efficiency of this technique [30]. A similar setup was used and 4000 Chinese hamster ovary (CHO-K1) cells at a wide range of laser fluences were optically transfected. The results from this study are shown in Fig. 2.6. In the calculation of transfection efficiency, the fate of all of the cells treated with the laser including those that died directly as a result of laser manipulation was taken into account. The average transfection efficiency at a specific fluence of 1.2 μm/cm^2 was found to be 50 ± 10%, which was considered to be a true representation of the usefulness of this technique. Another recent study

also investigated the interaction between femtosecond laser pulses and biological cells in detail from several aspects [64]. This study not only successfully transfected a canine cell line (MTH53a) with a GFP expressing vector, but also calculated and experimentally verified that the relative volume exchange is 0.4 times the total cell volume during laser irradiation by measuring the membrane potential changes using patch clamping. The relationship between pore formation, its opening time and the membrane potential were studied as well. This system allowed optical transfection to be performed in a more controllable fashion.

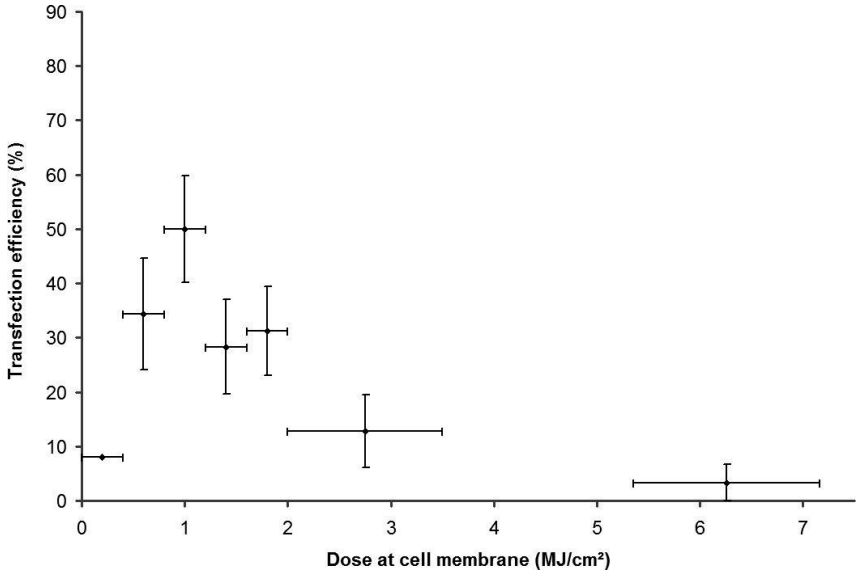

Fig. 2.6. *Transfection efficiency data for the optical transfection of 4000 cells. Exposure times varied from 10 ms to 250 ms, and average laser powers at focus varied from 168 mW to 225 mW. Total transfection efficiency as a function of cumulative energy per area of cell membrane irradiated is shown. Data points represent the average transfection efficiency; vertical bars represent the standard error of the mean (calculated for those points at which over 300 cells were optically transfected) and horizontal bars mark the bin range from which points were averaged [36].*

One of the engineering challenges that has prevented the optical transfection technique developing into a high throughput automated

transfection system, is the tightly focused laser beam has to be precisely targeted on the cell membrane. Based on mechanisms of femtosecond laser mediated cell membrane permeabilization presented in section 2.2, a beam focus needs to be as small as possible to generate enough free electrons through nonlinear absorption and keep the damage to the cell to the minimum (Fig. 2.7). A standard Gaussian beam focused through an objective has a very narrow axial effective range for transfection, owing to the small depth of focus; a mistargeting of as little as 3 μm results in a greater than 50% reduction in transfection efficiency (Gaussian beam in Fig. 2.8) [66]. Therefore, an experienced expert is always needed to manually target the laser focus on the cell membrane for each cell to perform optical transfection making it a relatively difficult and low efficiency process when compared with many other transfection methods.

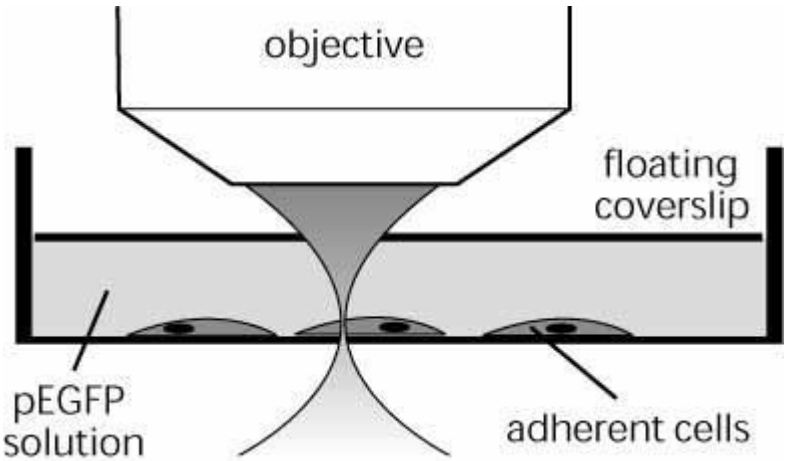

Fig. 2.7. *A typical configuration illustrated the relative position between focused laser beam and cells to be transfected. Due to the geometry of the focusing beam, the laser has to be accurately focused on the cell membrane (non-adhered side) to change its permeability to allow the surrounding pEGFP DNA solution entering the cell. Any mistargeting will decrease the power density and increase the interacting area on the cell of interest dramatically, which will lead to decreased transfection efficiency and cell viability [30].*

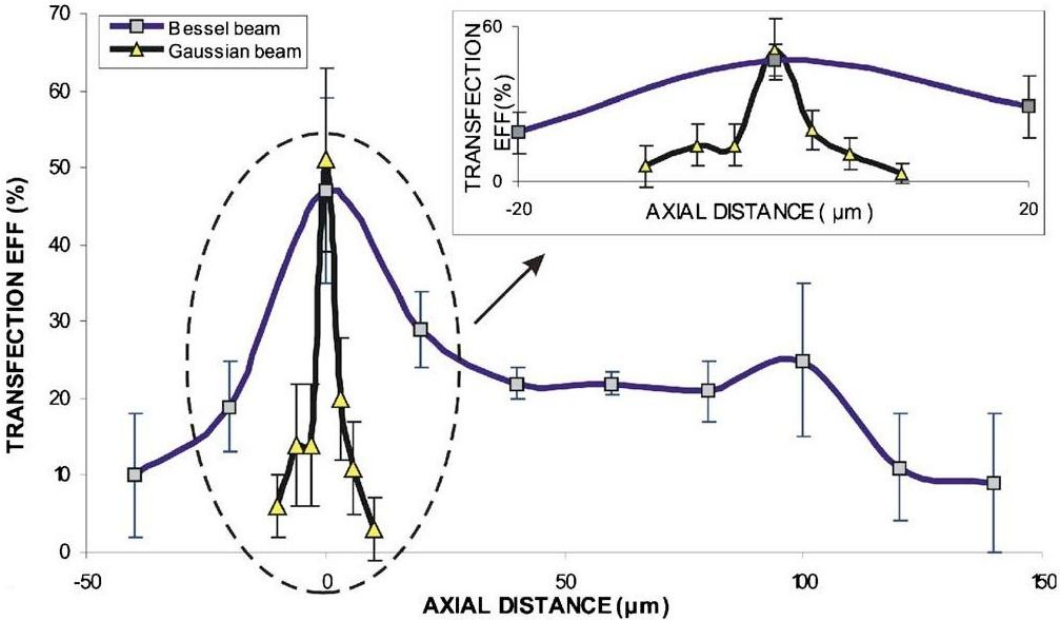

Fig. 2.8. *Bessel beam transfection vs Gaussian beam transfection. Bessel beam transfection of CHO-K1 cells was achieved for up to 180 µm along the propagation axis of the beam. Each data point corresponds to the average transfection efficiencies obtained at a specific axial position and incudes the number of spontaneously transfected cells, which varies between 0 and 5 for each sample dish. The inset shows the magnified image of the area around the focus. As can be seen that the successful transfection of CHO-K1 cells can occur over 20 times the axial distance when using a Bessel beam, as compared to the Gaussian beam (when considering the threshold of efficiency to be 20%) [66].*

In order to overcome this challenge, a non-diffracting light mode, a Bessel beam, was used for optical transfection [66]. The zeroth-order Bessel beam, with the central maximum theoretically approaching the wavelength of the illuminating light, is propagation invariant. That is the transverse profile of the beam remains unaltered during free-space propagation [116]. A finite approximation to a Bessel beam can be realized by illuminating a conical glass element known as an axicon with a Gaussian beam along the optical axis [116]. The emerging Bessel beam from the conical surface has a propagation distance given by

$$Z_{max} \approx \frac{\omega_0}{(n-1)\gamma} \tag{2.3}$$

where ω_0 denote the beam waist of the illuminating Gaussian beam, n and γ are the refractive index and opening angle of the axicon. The central maximum propagates several Rayleigh ranges without significant spreading and thus offers a focal rod of light. Targeting this type of beam on the cell membrane obviates the need for precise focusing and allows the permeabilization to happen over large axial distances. A comparison of transfection efficiencies using Bessel and Gaussian light modes at a range of axial distances is shown in Fig. 2.8, from which it can be seen that the transfection of CHO-K1 cells is achieved for up to 180 µm along the propagation axis of the beam using a Bessel beam and the successful transfection of CHO-K1 cells can occur over 20 times the axial distance when using a Bessel beam, as compared to the Gaussian beam (when considering the threshold of efficiency to be 20%) (inset, Fig. 2.8). Application of a Bessel beam thus alleviates the requirement of precise targeting and opens the possibility of automation of optical transfection technique.

Another approach using a dynamic diffractive optical element, namely a spatial light modulator (SLM), for the automation of optical transfection was demonstrated by Antkowiak et al. [69]. The SLM can modulate light spatially in amplitude and phase, thus providing full control over the lateral and axial position of the beam with submicron precision. The problem of accurate laser focusing on the cell membrane can be alleviated by sequentially irradiating the cell membrane at three axial positions separated by 1 µm with a delay of 700 ms between doses. Computer control of the SLM and the shutter allows the precise delivery of a timed sequence of doses. Their system also enabled unassisted and untargeted raster scan irradiation which provided a higher throughput transfection of adherent cells at the rate of 1 cell per second (Fig. 2.9). The laser beam was moved from spot to spot, rather than scanned in a continuous manner in a predefined procedure. Depending on the cell

plating density and the required number of cells to be treated, the computer controlled motorized stage moves from one region to another to cover a predefined area.

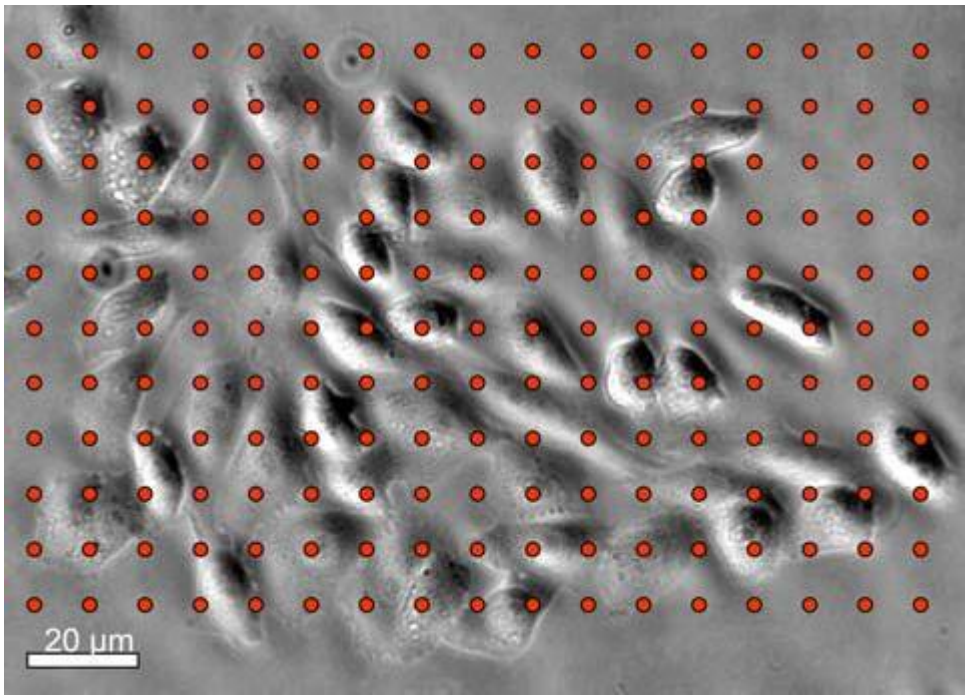

Fig. 2.9. *Illustration of the raster scan irradiation. The grid (10 x 10 µm) covers the whole area of the dish in a untargeted manner [69].*

Apart from the previously mentioned advancing of optical transfection technique from engineering aspects, significant transfection efficiency enhancement can also be achieved biochemically [70, 72]. Praveen et al. modified the conventional optical transfection procedure by incorporating a suitable synthetic peptide in the buffer medium during optical transfection, assisting DNA import into the cell nucleus [72]. This synthetic peptide consists of a nuclear localization signal at one end and a cationic peptide at the other end. The nuclear localization signal binds to the nucleus while the cationic end binds to the negatively charged DNA, helping the DNA plasmid enter the nucleus. A 3-fold enhancement in the transfection efficiency for adherent CHO-K1 cells was achieved. Additionally, the amount of required plasmid DNA can also be reduced by

70% without compromising the transfection efficiency. Cells in the suspension were also optically transfected for the first time with the help of this synthetic peptide.

As it was previously discussed in this thesis, optical transfection can transiently change the permeability of the cell membrane so that plasmid DNA can enter the cytoplasm. However, in order for the DNA to be transcribed it has to be delivered into the nucleus of the cell and this process mainly relies on the mitotic division of the cells, when the nuclear membrane is disassembled. The plasmid DNA in the cytoplasm may suffer from degradation as it stays in the cytoplasm, thus decrease the transfection efficiency. Therefore if the plasmid DNA is delivered into cytoplasm during cell division, the transfection efficiency can be promoted. Mthunzi et al. synchronized the CHO-K1 and Human Embryonic Kidney (HEK-293) cells at M (cell division or mitosis) and S (DNA synthesis) phases before doing the optical transfection [70]. The results show that both cell lines at the S phase give highest optical transfection enhancements compared to unsynchronized cells at random phases and cells at the M phase (Fig. 2.10).

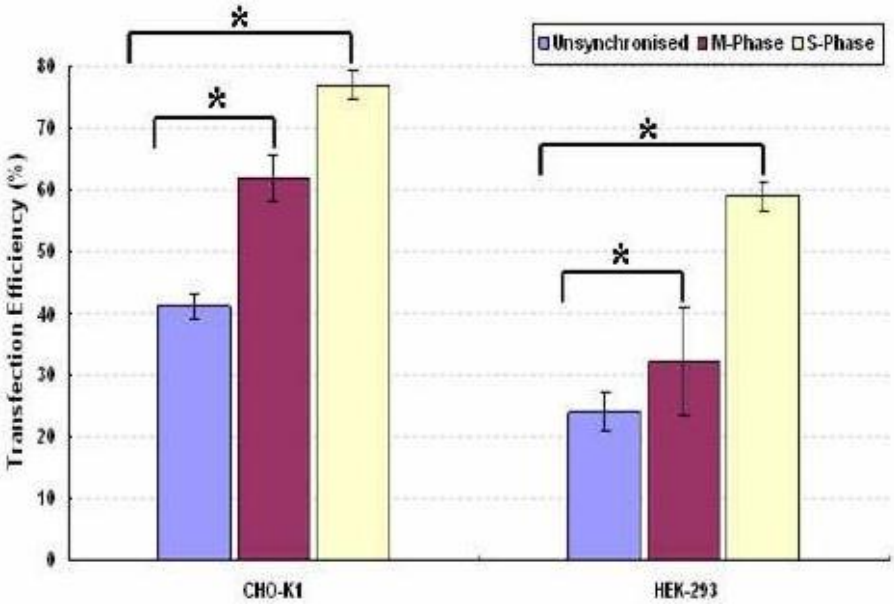

Fig. 2.10. *Synchronized CHO-K1 and HEK-293 cells at the M phase give the highest optical transfection efficiency compared to unsynchronized cells at random phases. Optical transfection of cells at S phase also shows enhanced transfection efficiency. Error bars represent the standard error of the mean (n = 3 experiments of 50 irradiated cells). * indicates data sets are significantly different from each other within relative cell lines [70].*

As early as 2003, Zeira et al. applied femtosecond optical transfection technique *in vivo* on tibial muscle cells of mice [57]. Enhanced *in vivo* gene expression was achieved with negligible risks of tissue damage. 10 µg naked DNA was first injected into the tibial muscle of mice followed by application of the femtosecond laser beam for 5 s, focused to 2 mm in depth upon an area 95 x 95 μm^2. This resulted in the highest intensity and duration of gene expression with no histological biochemical evidence of muscle damage. Although this work used raster scanning instead of single cell targeting, it demonstrates that optical transfection has the potential to become a simple, safe, effective, and reproducible method for therapeutic gene delivery. Another *in vivo* optical transfection experiment was performed on zebrafish [117]. Single zebrafish blastomere cells at the two, four, eight and sixteen cells stage were optically

transfected with a GFP expressing plasmid using an 800 nm femtosecond laser source. 24 hours post-fertilization, a wide distribution in the protein expression was observed in the resulting larva. These optically transfected embryos finally developed into fully functional animals.

Recently, optical transfection has started to be used to tackle difficult biological questions. mRNA of controllable quantities was optically transfected into neuronal dendrites rather than cell bodies to study the importance of subcellular localization on protein function [60]. Another published work showed that transfer of the transcriptome (the sum of all mRNA species within the cell) from differentiated rat astrocytes into a non-dividing differentiated rat neurons resulted in the conversion of the neuron into a functional astrocyte-like cell [115]. 16 pores on the cell membrane created by femtosecond laser pulses were used to facilitate this transfer. Mouse embryonic stem cells can also be transfected and differentiated using optical transfection [70].

In recent years, along with the above mentioned femtosecond laser mediated optical transfection techniques, fiber based miniaturized optical transfection, moving towards potential clinical applications, has also been developed which forms the main theme of my thesis and will be discussed thoroughly throughout this thesis.

2.4. Delivery of Pulsed Laser Through an Optical Fiber

2.4.1 Introduction

Optical transfection has been traditionally performed using free-space (bulky) optical setups, which have several drawbacks, such as expensive, difficult to manipulate and not suitable for *in vivo* and clinical environments. These problems can be overcome by using optical fibers to replace free-space setups. The detailed pros and cons will be discussed based on specific fiber based optical transfection systems throughout this thesis.

In the next few chapters, optical fibers [single mode fiber (SMF), coherent fiber bundle and large mode area photonic crystal fiber (LMA-PCF)] will be used to deliver femtosecond pulses. However, important issues arise during the delivery of the ultrashort optical pulses (normally of sub-picosecond duration at ~nanojoule energy per pulse) which are typically used for optical transfection through optical fibers. Ultrashort pulses of extremely high peak power can interact with the glass fiber core, which leads to a distortion of both the pulse shape and spectrum through a nonlinear process known as self-phase modulation (SPM). Under the high peak power, the local refractive index is raised transiently and this leads to a phase delay and a subsequent spectral distortion in the pulse in a nonlinear manner [118]. Another effect known as chromatic or group velocity dispersion (GVD) occurs when the light of different wavelengths travels through optical fiber at distinct speeds [118]. There are two sources of GVD in optical fiber: material and waveguide dispersion. Material dispersion results from the dispersive nature of the silica glass: light of different wavelengths travels at different speed [118]. Waveguide dispersion results from the fact that different proportions of the pulse energy at different wavelengths, transmit through the fiber cladding [118, 119]. These two dispersion mechanisms cancel each other at the so-called zero-GVD wavelength. Under the effects of both SPM and GVD, pulses propagating through an optical fiber, undergo temporal stretching and a consequent pulse peak power decrease [120-122]. In order to achieve optimized fiber based optical transfection, it is necessary to understand the effects of femtosecond laser pulses propagating through an optical fiber.

2.4.2 Dispersion

2.4.2.1. Group velocity dispersion

A glass fiber core is a dispersive material, and its refractive index varies with the wavelength of light. Since the pulse comprises of a range of different wavelengths, each of them propagate at a different group velocity, and so the pulse duration is stretched in the optical fiber. This type of dispersion is called material dispersion and it is characterized using a parameter called the dispersion coefficient, D_λ, in the unit of ps/km-nm. D_λ characterizes how long the pulse duration (with an original spectral width) would be after it travels through an optical fiber of a certain length. The wavelength dependence of D_λ for a silica-glass fiber is shown in Fig. 2.11. At wavelengths smaller than 1.312 µm, the D_λ is negative, which means the proportion of long wavelength light propagates faster than those of short wavelength. At the wavelength that is normally used for optical transfection, λ_0 = 800 nm, the D_λ is around -110 ps/km-nm.

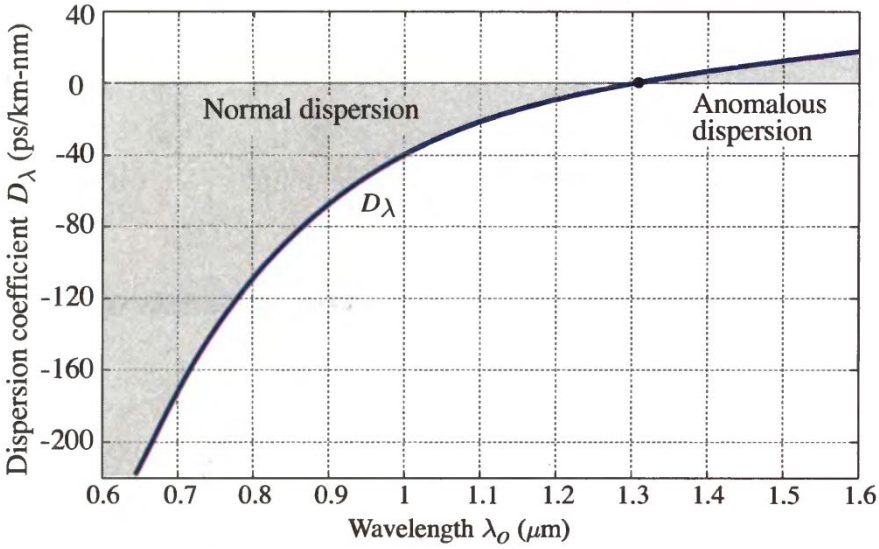

Fig. 2.11. *Dispersion coefficient D_λ for a silica-glass fiber as a function of wavelength λ_0 (Figure 9.3-5 in [118]).*

When pulses propagate through a waveguide, such as a SMF, the

field distribution in the fiber depends on the ratio of the core radius to the wavelength. Thus the relative distribution of optical power in the fiber core and cladding depends on the wavelength. Since the refractive indices and the resulted phase velocities in the core and cladding are different, the propagating velocities of each wavelength component are altered. For a SMF of the wavelength around 1.312 μm, where the material dispersion is trivial, waveguide dispersion dominates. Waveguide dispersion is characterized using a parameter called a waveguide dispersion coefficient, D_ω, in the units of ps/km-nm. D_ω characterizes how long the pulse duration (with an original spectral width) would be after it travels through an optical fiber of a certain length.

Combined material and waveguide dispersion is called chromatic dispersion, or GVD. Generally waveguide dispersion plays a minor role when compared with material dispersion. However, the former does shift the wavelength dependence curve (Fig. 2.11) to a new position.

2.4.2.2. Self-phase modulation

SPM happens when the ultrashort pulses with extremely high peak power propagate through an optical fiber. The local refractive index is raised transiently due to high peak power and so induces a phase delay and a subsequent spectral distortion in the pulse, in a nonlinear manner [118]

An ultrashort pulse with a Gaussian temporal shape and a constant phase at time t can be expressed as:

$$\mathrm{I(t)} = I_0 \exp(-\frac{t^2}{\tau^2}) \tag{2.4}$$

where I_0 is the peak intensity, and τ is half the pulse duration.

The optical Kerr effect is a case that causes a variation in the refractive index proportional to the local irradiance I of the light, which can be expressed as:

$$n(I) = n_0 + n_2 \cdot I \tag{2.5}$$

where n_0 is the linear refractive index and n_2 is the second order refractive index of the fiber core.

For an ultrashort pulse passing through a point in the fiber core, the transiently raised refractive index variation can be obtained by substituting (2.4) into (2.5) and take the derivative of $n(I)$ with respect to time t:

$$\frac{dn(I)}{dt} = n_2 \frac{dI}{dt} = n_2 \cdot I_0 \cdot \frac{-2t}{\tau^2} \cdot \exp(\frac{-t^2}{\tau^2}) \quad (2.6)$$

The instantaneous subsequent phase variation of the pulse induced by refractive index variation is:

$$\phi(\mathrm{t}) = \omega_0 t - kx = \omega_0 t - \frac{2\pi}{\lambda_0} \cdot n(I)L \quad (2.7)$$

where ω_0, λ_0 and L are the center frequency, vacuum wavelength and propagation distance of the pulse. The phase shift leads to a frequency shift of the pulse, which is obtained by:

$$\omega(\mathrm{t}) = \frac{d\phi(t)}{dt} = \omega_0 - \frac{2\pi L}{\lambda_0} \frac{dn(I)}{dt} \quad (2.8)$$

and then substitute (2.6) into (2.8):

$$\omega(\mathrm{t}) = \omega_0 + \alpha \cdot t \cdot \exp\left(\frac{-t^2}{\tau^2}\right) \quad (2.9)$$

where

$$\alpha = \left.\frac{d\omega}{dt}\right|_0 = \frac{4\pi L n_2 I_0}{\lambda_0 \tau^2} \quad (2.10)$$

Plotting the equation 2.9 out, shows that the leading and trailing edges of the pulse shift to lower [“redder” (higher) wavelengths] and higher [“bluer” (lower) wavelengths] frequencies, while the peak of the pulse is not shifted (Fig. 2.12). The spectral width of the pulse is thus broadened. For the portion of the pulse in the center near the peak, the frequency shift is approximately linear and can be expressed as:

$$\omega(\mathrm{t}) = \omega_0 + \alpha \cdot t \quad (2.11)$$

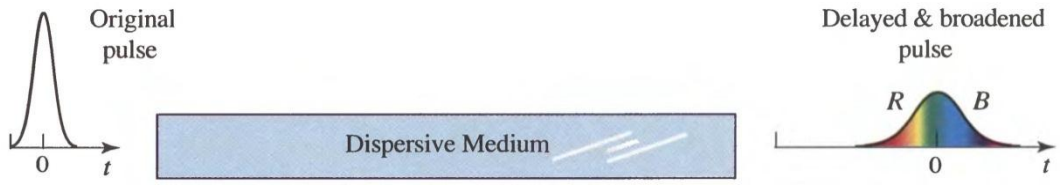

Fig. 2.12. *A pulse propagating through a dispersive medium undergoes a frequency shift due to SPM. Leading and trailing edges of the pulse shift to lower (higher wavelengths) and higher (lower wavelengths) frequencies, while the color of the pulse peak is not shifted. Along with GVD and other dispersion sources in the medium, the ultrashort pulse is normally broadened (Figure 5.5-3 in [118]).*

From the above discussion it appears that the optical Kerr effect induces a rise in the localized transient refractive index (2.6), which leads to the phase delay (2.7) and a subsequent optical frequency shift (2.9) of the ultrashort pulse. The pulse envelope in the time domain is not affected at the beginning, however, GVD and other dispersion sources in the fiber core will immediately act on the pulse (Fig. 2.12). In the region of normal dispersion (Fig. 2.11, zero dispersion may shift from 1.312 µm due to waveguide dispersion), the dispersion coefficient is negative, therefore the “redder” portions on the leading edge propagate faster than the “bluer” portions on the trailing edge of the pulse and the pulse is broadened temporally. On the other hand, in the regions of anomalous dispersion (Fig. 2.11), the pulse is compressed. For the application in this thesis, 800 nm femtosecond laser pulses are always broadened when passing through an optical fiber. Although the propagation of ultrashort pulses through an optical fiber has been theoretically studied, the best method to find a pulse’s properties is still by measuring it directly [120-122].

2.5. Summary

This chapter focused on the introduction of mechanisms of femtosecond laser mediated cell membrane permeabilization and briefly described other laser transfection techniques. Instead of biological tissue,

pure water was used as a model to illustrate the plasma formation in bulk material since the optical breakdown threshold in water is similar to that of biological tissue and in addition optical transfection is performed in liquid environment. Plasma formation through a highly focused femtosecond laser beam in pure water was discussed thoroughly. Briefly summarising, the first free electron is generated through photoionization, and the following recurring sequences of inverse Bremsstrahlung absorption events and impact ionization lead to an avalanche growth in the number of free electrons.

After a plasma is formed under the irradiation of a single 100 fs, 800 nm laser pulse at the optical breakdown threshold, a simulation was then developed to study the time evolution of the free electron. Ionization and electron losses were considered in the simulation. The simulation shows that the electron density can be very well controlled through the tuning of the relative laser irradiance value, and a wide density range below optical breakdown threshold can be created. Calculated optical breakdown thresholds as a function of laser pulse duration for various laser wavelengths were also presented. Pulse duration at the ranges below and above 10 ps show very different behaviours due to the time it takes for the combination process to happen after free electrons were generated.

Low density plasma induced chemical effects (ROS and free electron mediated fragmentation of biomolecules) were also discussed and are believed to be the main mechanism behind membrane permeabilization during femtosecond optical transfection. Temperature evolution within the laser focus is also explored through numerical simulation and it excludes a highly localized moderate heat accumulation effect being a major mechanism for cell membrane permeabilization. The simulation shows that long-lasting bubbles created under the parameters used for optical transfection are lethal to the biological tissue and should be avoided.

After the introduction of mechanisms of femtosecond optical

transfection, a review of the development of this technique was presented. Fiber based optical transfection is the main topic of this thesis, therefore it is necessary to understand the effects of femtosecond laser pulses propagating through an optical fiber. Two ultrashort pulse dispersion mechanisms, GVD and SPM, were introduced.

Chapter 3:

3. Microlensed Optical Fibers: Emerging Applications and Techniques of Fabrication

3.1. Introduction

The last few decades have seen technological advancements in areas such as communication and healthcare with the use of photonics technologies. A key factor which has enabled this revolution was optical fiber technology. Today optical fibers are widely used as optical waveguides in telecommunications and they have become more important as interconnectors in microelectronics. However, the applications of optical fibers are not just limited to being used as a waveguide to send digital signals for communication. Specialized optical fibers can be used as mechanical and chemical sensors for remote sensing applications. Also optical fibers are used for delivering a high power laser beam for applications such as laser cutting [119, 123]. Another emerging area where optical fibers play an important role is bio-medical optics. Optical fiber based devices have helped the miniaturization of optical diagnostic probes such as optical fiber based endoscopes which enable *in vivo* sensing and imaging within the human body where direct human actuation is not possible.

Although optical fibers are small in size and are flexible, the output beam profile is naturally divergent. This decreases the light intensity and increases the beam diameter significantly after the light leaves the fiber. There are several applications where such a divergent output beam profile is not desirable, and so it is required to focus or collimate the output beam from the fiber. One of the solutions to this issue is to use micro-optic components fixed near the tip of the fiber. However fabrication of such micro-optic components are technically challenging due to the requirement of precise polishing, which makes it relatively expensive. Also it needs a

proper housing to hold both the fiber and the micro-optic components. This would make the overall size of the device at least one order of magnitude bigger when compared to the diameter of the actual optical fiber [119]. An alternative approach would be to fabricate microlens structures at the tip of the optical fiber itself. This will help by not increasing the total size of the device.

Microlensed optical fibers were first used in the area of optical communications where they were used for collimating or focusing the output beam from a single mode fiber to increase the coupling efficiency between fibers or between a laser diode and a fiber [124-126]. There have been several techniques developed to achieve fabrication of such microlensed fibers. The majority of these techniques were developed and inspired by the requirement of a specific application. There were also some generic techniques which were developed for the general modification of the output beam profile of an optical fiber.

There are several bio-medical imaging and spectroscopic techniques which require fiber probes. The trend towards fiber optic probes based on *in vivo* bio-imaging was initiated by early studies on chemical sensing and spectroscopy using fiber optic fluorescence probes [119, 127]. Such systems were used for real-time *in vivo* monitoring of the chemical dynamics of tissues [128] and for disease diagnostics [129, 130]. Although fiber probes were used for bio-medical purposes since the early 1980s, the last decade has seen an unprecedented growth in this field. Fiber based endoscope has become a commonly used tool for disease diagnosis and for visualization during laparoscopic surgeries [131, 132]. Micro-endoscopy is another burgeoning field where fiber based systems have proven to be useful [133]. Fiber probes have been implemented in the miniaturization of advanced bio-imaging techniques such as confocal two photon microscopy [46] and optical coherence tomography [134, 135]. Another field where fiber based miniature microscopes can find applications is in the field of nano- or micro-surgery [45, 71, 133].

While the majority of bio-medical applications mentioned before used a probe head with micro-optic components to modify the output beam profile, there have been several studies reported in the last 10 years, where micro-structured fibers were used in probes. The field of bio-imaging started using micro-structured fibers for scanning near-field optical microscopy (SNOM), where the fiber tip with a sharp nanometric protrusion is required for near-field imaging [136-141]. In recent years, lensed fibers are now being used for other imaging techniques. One of the imaging modality which has used several micro-structured fiber based probes was optical coherence tomography (OCT) [142-144]. Combination of the technique of micro-structuring at the tip of the fiber with a specially fabricated photonic crystal fiber, helped to achieve desired functionalities suitable for bio-imaging [145, 146]. Micro-structured optical fibers were also used for fiber based optical manipulation systems [147-150] and fiber based optical transfection systems [63, 71, 151].

It is evident that micro-structured fibers have found applications beyond the field of optical communication in recent years. The field of bio-medical optics is embracing this technology to realize miniaturized optical probes for a variety of applications which range from fundamental biology research to medical diagnostics. In order for the transition towards hand-held or endoscopic systems several other advanced imaging techniques or spectroscopic techniques may adopt micro-structure fiber technology in the near future.

In order for the fabrication of micro-structured fibers, there have been several methods reported to date. Each fabrication methods has its own advantages and disadvantages based on various factors such as the type of lens it can fabricate, fabrication cost, through-put, reproducibility and ease of implementation. Hence there does not exist a single fabrication technique, which is versatile enough to achieve all the different types of structures required for the various applications. It is essential to choose the right fabrication method to create structures that are required for a particular application. In this chapter, I provide a list of the fabrication

techniques reported over the last three decades for producing micro-structured lens. While most of these techniques were developed to cater to the needs of a specific application, there are some techniques which are not limited to a specific application. Since these techniques were developed for a wide variety of applications, a one to one comparison of this technique would not be sensible. So this chapter will focus on the fabrication technique with special discussions on the flexibility and ease of its implementation. Hence this chapter can be used as a guide to choose the right fabrication method for a specific application, such as the works presented in Chapter 4, 5 and 6.

3.2. Arc Discharge Technique

Arc discharge is a technique which is widely used for fiber splicing. Microlensed fibers can be fabricated using this technique using a commercial fiber fusion splicer. The process relies on thermal effects during fusion arc discharge, which meld the tip of the optical fiber. As the tip is melted, surface tension causes the melted portion to become a rounded hemisphere, with the diameter of the hemisphere being determined by the heat distribution and by the amount of material raised above the glass melting temperature [Fig. 3.1(A)]. In order to focus the output beam from an optical fiber, the beam waist (determined by the fiber core diameter) and the radius of curvature of the lens to be fabricated, need to be comparable. Due to the relatively large diameter (compared with the fiber core) of the fiber tip, the lenses formed using arc discharge always have a large radius of curvature which limits the extent to which the output beam profile can be modified with such microlenses. A solution to this limitation is to splice a piece of coreless silica fiber to the single mode fiber using arc discharges, to expand the output beam. The length of the coreless silica fiber controls the extent to which the beam can be expanded. An arc discharge was applied to the tip of the coreless silica piece to form a microlens [Fig. 3.1(B)]. A relatively long working distance

of ~1 mm and a beam spot of ~10 µm was obtained using this fabrication protocol [142, 143, 145, 146, 152-156]. If a smaller beam focus was needed, a thinner piece of silica rod can be used with a compromised working distance [Fig. 3.1(C)] [124, 157]. In the case that the rod diameter was too small to be cleaved, an arc discharge can be used to cut the silica rod and form the lens simultaneously. By changing the length of silica rod, beam expanding and the subsequent working distance and focus diameter of the lensed fiber, can be adjusted. The coreless fiber can be replaced with a multimode fiber (MMF) of different diameter to expand the output beam and create lens of different diameter [143, 153, 154].

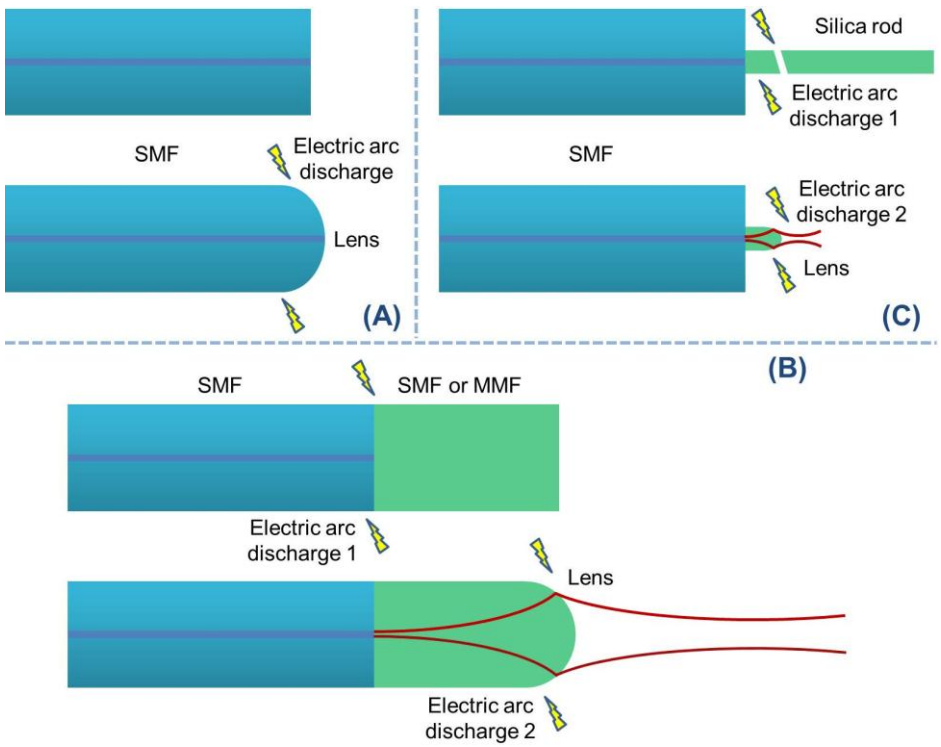

Fig. 3.1. *The lensed fiber fabrication using arc discharge technique. (A) Electric discharge was applied at the cleaved tip of an optical fiber, which melted the material, resulting in a convex microlensed tipped fiber. (B) In order to achieve tighter focusing a coreless silica fiber was spliced at the fiber end to expand the beam waist comparable to the radius of curvature of the microlens. (C) Coreless silica fiber with a diameter comparable to that of the size of the core of the fiber was spliced at the tip of the fiber to obtain microlensed fiber with tighter focusing.*

For applications that require coupling multiple wavelengths to the fiber, a microlens can be fabricated at the apex of a photonic crystal fiber with endlessly single mode characteristics, instead of a SMF [143]. A microlensed fiber fabricated using a hollow core fiber can be used for the delivery of a high peak power pulsed laser beam. Ryu, *et al* reported a microlensed fiber probe, based on a double-cladding fiber and related parts, suitable for simultaneous measurements of optical coherence tomography and fluorescence spectroscopy [142]. The arc discharges can also be used as a heating source to create a tapered fiber tip through a heating-pulling process before the lens fabrication process [125, 158]. This is generally a flexible technique whose fabrication parameters can be tuned to fabricate a tailored probe with specifically required properties.

Arc discharge has been used for fabricating microlensed fibers for a variety of applications such as: to increase the coupling efficiency between laser diodes and single mode fibers [124, 125, 153, 155, 157, 158], to create an optical free-space interconnector [152] and for OCT [142, 143, 145, 146]. However, there are difficulties associated with it, such as low fabrication efficiency, low reproducibility and the inability for batch fabrication, have all prevented this technique to be used for wider applications.

3.3. Laser Micro-machining Technique

There are two types of laser micromachining technique using a CO_2 laser. The first one normally utilizes the laser as a heating source and adopts a heating-pulling scheme. The fiber can be either pulled to split or be cleaved at a required point before melting the tip to form a lens. Using this method, very sharp tips can be obtained and they have been widely used as scanning probes in the field of scanning near-field microscopy [126, 159-162].

In the second type, a pulsed CO_2 laser is normally focused on the tip of a spinning fiber (Fig. 3.2). The beam ablates the fiber tip by cutting

and heating simultaneously. The shape of the lens can be controlled by the relative position and movement between the fiber and laser focus. This is controlled by a computer and so the microlens profile can be modified by appropriate changes in the movement commands [126, 163-166]. In order to increase the coupling efficiency, a hyperbolic shaped microlens is preferred over hemispherical shaped microlens. The ability of laser micro-machining to modify the fiber tip with submicron precision, allows the fabrication of such aspheric shapes which is difficult to achieve otherwise. A near 100% coupling efficiency has been claimed using such an aspheric microlensed fiber [166]. CO_2 laser heating fabrication results in more consistent lens curvature than the arc discharge technique, resulting in better reproducibility. However, this technique also shares some drawbacks with the arch discharge technique such as low fabrication efficiency and its unsuitability to be used for batch fabrication.

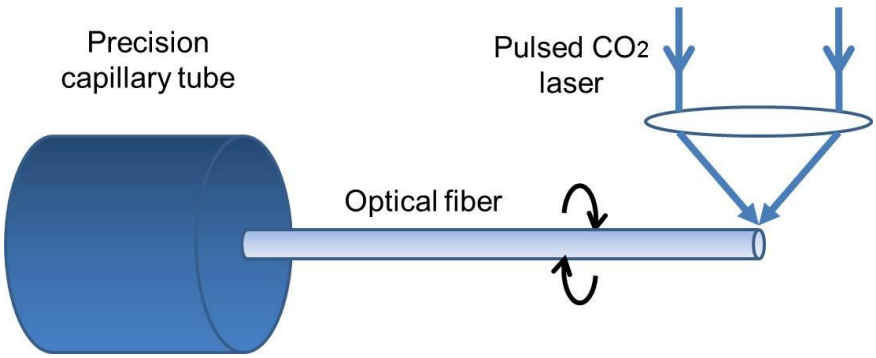

Fig. 3.2. *Schematic diagram of the fabrication of hyperbolic shape microlens on the tip of an optical fiber using a pulsed CO_2 laser.*

3.4. Polishing Technique

Another approach to fabricate a microlensed fiber is using a polishing technique, which is often combined with other techniques such as chemical etching and fusing for obtaining the desired structures [167-176]. For some micro-structured fiber tips with simple shapes, a wedge for example, it is possible to perform manual polishing. However, in most of

the cases, a fiber polisher or beveller (Fig. 3.3) is used to achieve fiber tips with complex micro-structures. Automated polishing also offers high reproducibility, smooth surface and higher throughput. The basic polishing procedure is shown in Fig. 3.3: an optical fiber, which can be rotated around its axes with a controllable speed and angle, is slightly pushed against a spinning abrasive disk at an angle. A microscope is used to inspect the whole process and a computer is needed to control all the fabrication parameters for the automation.

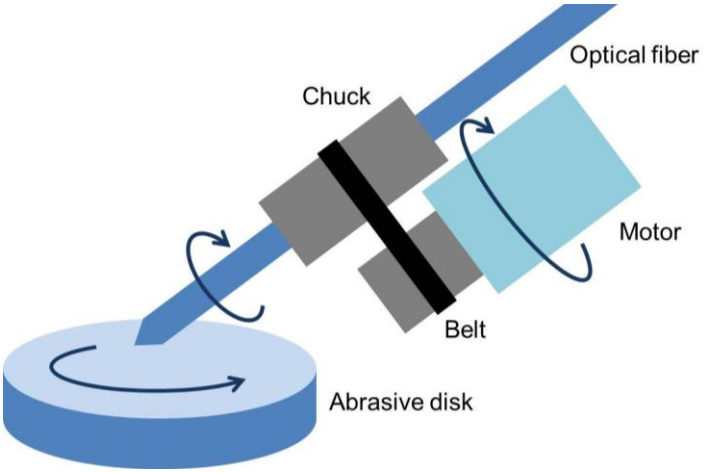

Fig. 3.3. *Schematic diagram of the automated fiber tip polishing procedure. The tip of an optical fiber, loaded onto a motorized beveller was pressed against an abrasive disk to create a microlensed at the tip of the fiber. The contact angle, speed of rotation and the force with which the fiber tip was pressed against the abrasive disk were controlled to obtain desired lens structure.*

Fibers with a wedge shaped tip [168, 169] and an elliptical microlensed tip [167, 171, 173, 174, 177], which are fabricated using this method have been used to increase the coupling efficiency between SMF and laser diodes, whose beam profile is highly elliptical. The wedge shaped fiber tip resembled a cylindrical lens which corrected for the phase front mismatch between laser beam and optical fiber [Fig. 3.4(A)]. The lengths and curvatures of the two axes of the elliptical microlens can be tailored using this method [Fig. 3.4(B-F)]. This resulted in a higher

coupling efficiency through better corrections for the mismatching between elliptical Gaussian output beam profile of the laser diode and optical fiber.

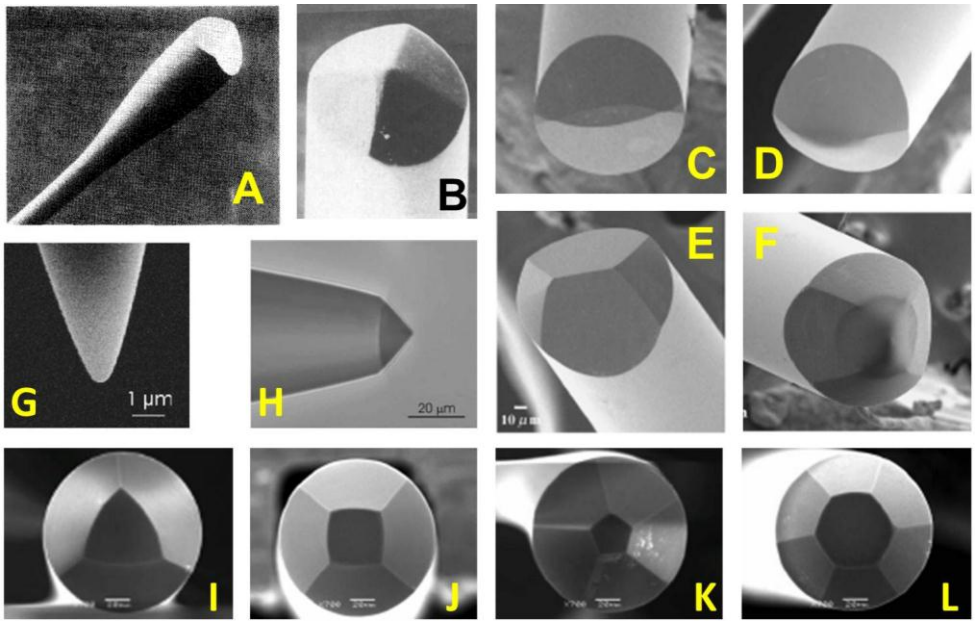

Fig. 3.4. *Different types of fiber tip fabricated using polishing based technique. (A) Wedge shaped microlens [168]; (B) Elliptical microlens [167]; (C, D) Elliptical microlens [177]; (E, F) Elliptical microlens [174]; (G) Fiber tip for scanning near field microscopy [170]; (H) Axicon tipped fiber [172]; (I-L) polygon pyramid tipped fiber [176].*

Held *et al*. fabricated a probe for high resolution SNOM using a polishing method combined with chemical etching (section 3.5) [170]. In this study, a fiber with a suitable tapered tip was obtained using chemical etching with subsequent polishing of the fiber tip to achieve a curvature radius of the tip in the nanometer range, as well as a smooth surface to allow a good aluminum metallization [Fig. 3.4(G)]. An optical resolution of < 80 nm for SNOM was demonstrated using this probe. An axicon tipped optical fiber was also fabricated using polishing for the generation of Bessel-like beams [Fig. 3.5(H)] [172]. Any desired micro-axicon cone angle can be produced by this technique. In order to fabricate an axicon tipped fiber, a heat-pulling technique was first applied to the optical fiber to

generate a tapered tip with a radius of curvature of a few micrometers which was followed by polishing. The heat-pulling stage helped to reduce the fabrication duration to < 5 minutes. Recently, a periodical variable torque technique has been developed to facilitate the polishing technique to fabricate optical fibers with different types of end faces [176]. Periodical pressure was applied to the fiber against the spinning abrasive disk while the fiber rotating around its axes, so as to fabricate not only an elliptical microlens but also a polygon pyramid tipped fiber [Fig. 3.4(I-L)].

Polishing when combined with other methods allows fabricating a variety of microstructures at the tip of an optical fiber and also offers a smooth surface. Most of these structures can be achieved in an automated single step polishing procedure. Hence a relatively high fabrication yield can be achieved using polishing techniques. The lens fabricated is independent of the nature of the fiber (core diameter, doping, and refractive index) and a high reproducibility is guaranteed with this technique. However requirement of high stability and high precision in positioning is required for the successful implementation of this fabrication technique, which makes it technically challenging.

3.5. Chemical Etching

Chemical etching using a buffered hydrofluoric (HF) acid has been widely used in processing dielectric materials. Optical fibers consisting of silica material can be chemically etched by a buffered HF solution. This method can also be used to create a lensed optical fiber when using a suitable buffered HF and etching setup. The fabrication method can be mainly divided into three categories: selective chemical etching, protection layer method and tube etching. Also there have been several procedures where combinations of these methods along with other techniques, were used for micro-structuring the tip of an optical fiber.

3.5.1 Selective Chemical Etching

For selective chemical etching [63, 71, 114, 144, 150, 178-189], a HF aqueous solution of ammonium fluoride (NH_4F) has been used as an etchant to modify the shape of a fiber tip. Due to the variation in doping of the core of an optical fiber, the etching speed of the core and cladding are different. By varying the ratio of HF to NH_4F, the relative etching speed between the core and cladding of the fiber can be adjusted. When the ratio is right, the etching speed of the cladding is faster than the etching speed of the core, resulting in a conical lens at the end face of an optical fiber [Fig. 3.5(A)]. When dipped into the etchant, due to the difference in etching rate, initially a volcano shaped structure forms at the cleaved fiber tip. As the etching process progresses, this structure becomes sharper and eventually evolves into a conical shaped axicon. Meanwhile the cladding diameter decreases at a constant speed (Fig. 3.6). After the conical lens was formed, the axicon apex angle remains almost constant for the remaining etching process [182].

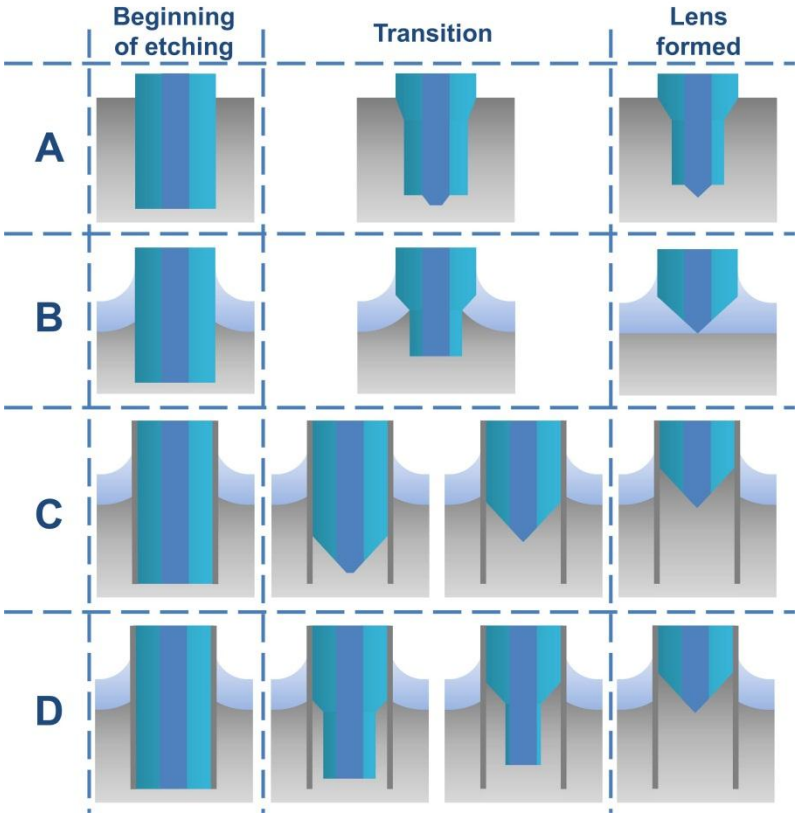

Fig. 3.5. *Schematic diagram describing the progress of etching process in three chemical etching schemes. (A) The selective chemical etching. (B) Protection layer method. (C) Tube etching with etchant impermeable fiber jacket. (D) Tube etching with etchant permeable fiber jacket.*

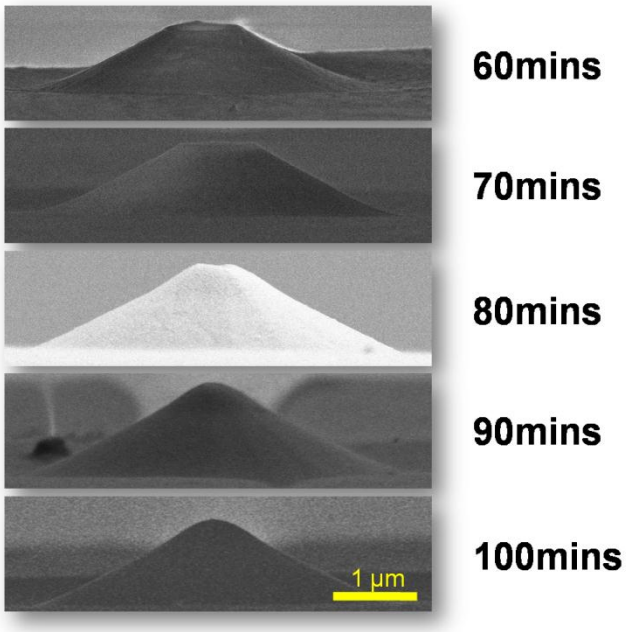

Fig. 3.6. Scanning electron microscopy (*SEM) images of the various stages of axicon lens formation during selective chemical etching.*

In order to establish the relationship between the apex angle of the chemically etched axicon on the end face of an optical fiber, and the ratio of NH_4F to HF, we have previously fabricated a series of axicon tipped fibers using freshly made etchant comprising of HF (48 – 51 % in water) and NH_4F (40% in water), and commercially available optical fibers (SM800-5.6-125, Thorlabs, UK) with a cladding diameter of 125 µm, mode field diameter of 5.6 µm at ~22 °C (Fig. 3.7). The etching times varied from tens of minutes to ~2 hours. Fig. 3.6 shows the various stages in the formation of the axicon tipped fiber for a ratio of NH_4F to HF equals to 2.

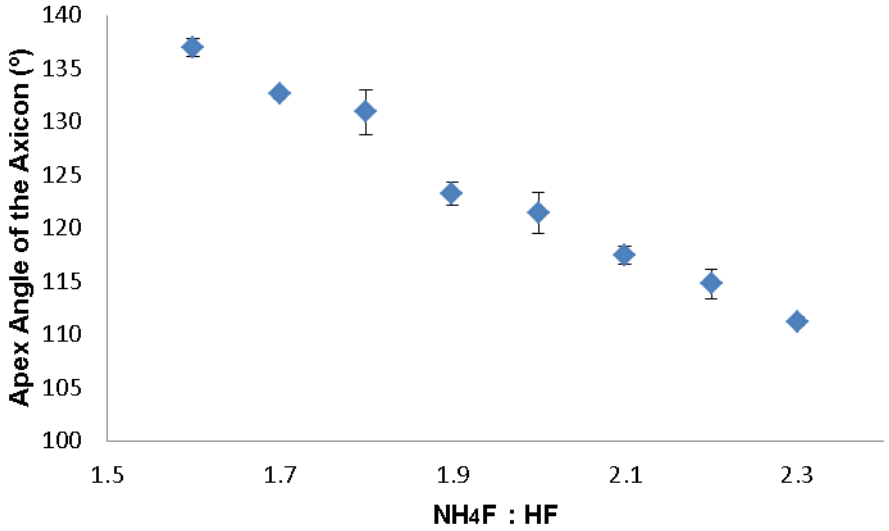

Fig. 3.7. *The relationship between apex angle of the axicon lens and the etchant mixing ratio of NH_4F to HF. The apex angle can be controlled through etchant combination. 3 to 7 axicon tipped fibers were fabricated and measured for each data point. The error bars are the standard deviation.*

Selective chemical etching is a flexible, inexpensive method for axicon tipped fiber fabrication with high reproducibility. The lens made from the core is always created exactly on the centre of the end face of an optical fiber. Batch fabrication can be easily realized and also multicore fibers or coherent fiber bundles with thousands of cores, can be treated by this method to create an array of identical axicons [114, 186, 187, 190]. This method has been used to increase the coupling efficiency between single mode fibers and a laser diode [179, 180]. A nearly diffraction-limited focused spot was generated by the fiber fabricated using this method [181]. By attaching a gold nanoparticle to the chemically etched fiber tip, in order to increase the optical signal collection efficiency, the fiber has been used as a chemical and biological sensor on a nanometer scale [183]. Optoelectrochemical sub-micrometer - or even nanometer - sized sensors have been achieved using this structure [184, 186, 187]. The axicon tipped fibers fabricated by this method have also been applied in optical manipulation [150], optical transfection [63, 71, 114] and OCT [144].

3.5.2 Protection Layer Method

The etching process of protection layer method is illustrated in Fig. 3.5(B) [162, 188, 191-198]. The optical fiber is inserted into the etchant solution underneath a protection layer, which should not be chemically reactive and miscible with the etchant. Various types of oil can be used as a protection layer which has the added advantage of low density allowing it to cover the top surface of the etchant. During the etching process, due to surface tension, by the time the conical tip was formed, the tip is covered by the protection layer, resulting in self-termination of the etching process as shown in Fig. 3.5(B).

The cone angle depends not only on the original fiber diameter, but also on the interfacial tensions (of etchant solution, protection layer and fiber surface). This makes it difficult to tailor the desired cone angle [162]. A solution is to build up statistical data by trying fiber etching with different protection layers [162]. It has been reported that changing the temperature and acid concentration can also adjust the cone angle [192]. Various scanning probes have been fabricated based on this protection chemical etching method [192-195].

The protection layer etching method is again an inexpensive self-terminating process with high reproducibility. The oil layer helps to slow down HF evaporation. While the availability of several parameters such as temperature, acid concentration and the protection layer material to tune the fabrication process offers flexibility, this makes calibration of this technique difficult. Also the fiber tip fabricated with protection layer method leaves a rough surface.

3.5.3 Tube Etching

A method called tube etching has been suggested to improve the smoothness of the microstructure fabricated at the tip of the fiber [199-201]. This method is similar to the protection layer method except the fiber

is etched with its jacket on. Depending on the permeability of the fiber jacket to the etchant, the tip formation is slightly different as is shown in Fig. 3.5(C, D). A smoother tip can be obtained using this technique which would help in improved metallization of the fiber tip, resulting in higher light transmission and higher reproducibility. This method is less sensitive to vibration and temperature fluctuation during etching. Fibers fabricated using this tube etching method, have also been used for optical manipulation of microscopic objects [149, 202].

3.5.4 Multistep Etching

There are several design parameters for fabricating an ideal optical scanning probe. The tip curvature radius (tip diameter) should be small with a small cone angle to increase the imaging resolution which depends on the tip diameter. The cladding diameter should be as small as possible to avoid contact with the samples (especially when uneven samples are scanned). The tip surface should be smooth for high quality metallization which decreases the light leakage. Also the fabrication procedure which can offer high reproducibility of the tip structure is preferred.

Obviously, the cladding diameter can be decreased by increasing the selective chemical etching time, but the sharpness of the tip will be compromised in such long time etching process, especially for small cone angled tip [203]. Therefore a multistep etching process was chosen to reduce the cladding diameter while retaining the sharpness of the probe tip. The first step involved reducing the cladding diameter, and the second step was for sharpening the tip (made from fiber core) [Fig. 3.8(B)] [190, 203-205]. The smallest cone angle of 14º, a tip diameter of 3 nm, and a cladding diameter of 8 µm was obtained using this protocol [190]. Detailed study about apex shape and transmission of the fiber tip with additional etching can be found in [204] and [205] respectively. To further increase the transmission efficiency a triple-tapered aperture probe was built with the help of focused ion beam (FIB) technique [Fig. 3.8(C)] [139]. Another

approach using multistep etching fabricated a pencil-shaped (without the edge of cladding) fiber probe [Fig. 3.8(D, E)] [206, 207]. The pencil shape gives the probe more flexibility when scanning a sample with rough surface.

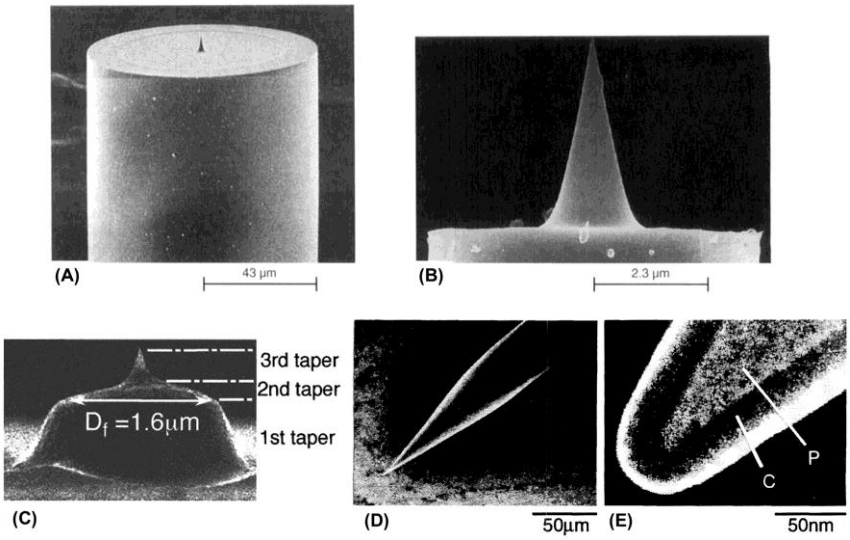

Fig. 3.8. *(A) A probe fabricated by one step selective chemical etching method [190]; (B) a probe fabricated by two step etching with a reduced cladding diameter [190]; (C) a triple-tapered probe [139]; (D)(E) an example of pencil shaped probe [206].*

Although the multistep etching procedures are more complicated than the basic etching methods mentioned earlier, probes with tailored properties can be fabricated with this approach. The probes fabricated with this technique have been successfully used in SNOM [136-138, 207].

In short, chemical etching is a simple, inexpensive and flexible method. Although the etching process is time consuming, this method is suitable for batch fabrication and is highly reproducible. It is worth noting that the etching method does not change the core diameter as happens in the pulling method; therefore, the optical beam profile in the core is well preserved, avoiding any loss due to the distortion of the fiber core. However the HF based etchant solution is highly dangerous and therefore extra care is required while handling this chemical.

3.6. Microlens Fabrication Using Photosensitive Polymers

All the microlens fabrication techniques mentioned so far, modify the shape of the material at the fiber tip to fabricate a microlens. Another approach to fabricate a microlens at the tip of the fiber, is to use photosensitive polymers (photopolymers). There have been several methods reported for fabricating polymer microlenses at the tip of an optical fiber [208-211]. Usually photosensitive polymers such as photoresists or epoxy, which can be cured using UV exposure, are used for fabricating these polymer microlenses. Although this technique offers the flexibility to fabricate a wide variety of structures with some of the reported protocols being easy and cheap to implement, polymer lenses are not usually suitable for applications that requires the delivery of high power or ultra-short pulsed laser beams. However there have been reports where femtosecond lasers have been delivered through polymer microlensed fibers [71]. The fabrication procedures can be divided into two categories depending on the curing process adopted – single-photon polymerization and two-photon polymerization.

3.6.1 Single-photon Polymerization Technique

In single-photon polymerization, a UV beam is normally used for the curing of the photopolymer, which is a linear process and the threshold of the polymerization corresponds to the energy that the curing beam delivers. The general approach in this fabrication method is to create a structure of uncured photopolymer at the tip of the fiber by dipping the fiber into the relatively high viscous photopolymer or dropping a drop of photopolymer at the cleaved tip of the fiber. Due to surface tension, usually a hemispherical structure of the uncured photopolymer is formed at the tip of the fiber, which is cured by exposing it to a UV beam.

Several methods of polymer microlensed fiber fabrication using single-photon polymerization have been proposed [71, 208, 209, 212-214].

One of the easiest methods is to dip vertically and raise the cleaved optical fiber from the photopolymer such that a photopolymer hemisphere on the fiber tip is formed due to the polymer surface tension. Then this hemisphere is cured using UV light as shown in Fig. 3.9(A) [215]. A normal commercial UV lamp can be used for curing through flood exposure and does not require any specialized optical alignment. The curvature of the lens can be varied by slightly pushing the polymer hemisphere to touch a glass surface, from which part of the polymer is removed due to its viscous nature [215]. Another approach uses a nano-syringe to control the amount of polymer deposited on the fiber end face so as to change the curvature of the microlens [212, 214]. A piece of coreless silica fiber (CSF) or MMF can be added between the optical fiber and polymer lens for the expansion of the output beam [208, 209, 212, 214], which is similar to the configuration used in Fig. 3.1(B).

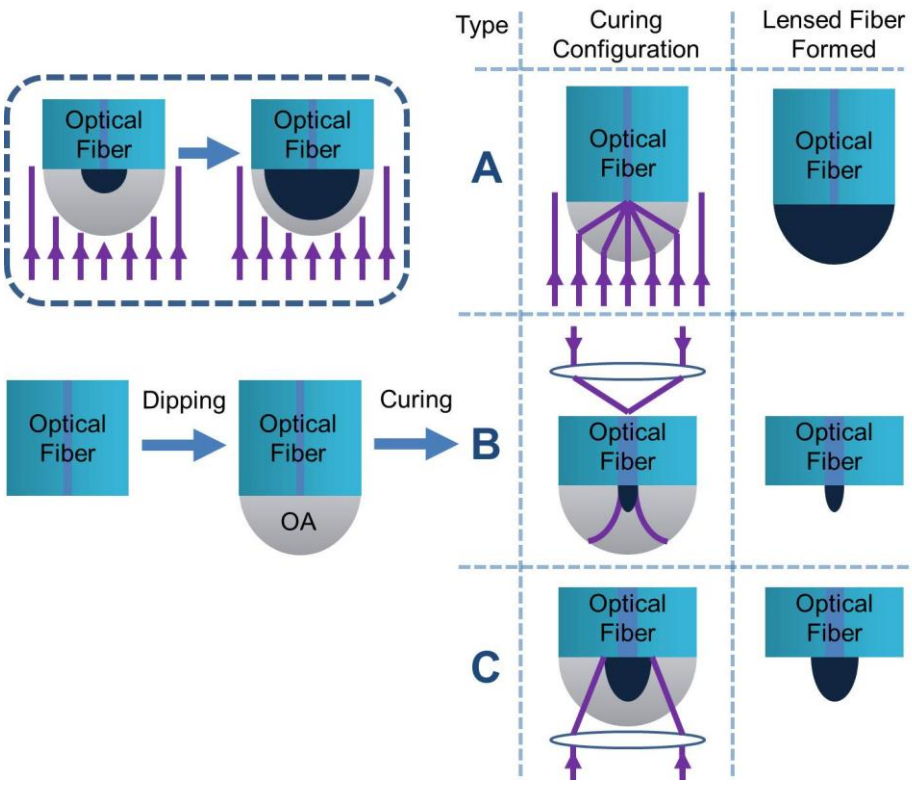

Fig. 3.9. *lensed fiber fabrication using single-photon polymerization technique.*

Another approach is as shown Fig. 3.9(B) [211, 216-222]. In this procedure, the photopolymer hemisphere, which was formed at the tip of an optical fiber, was cured with the curing beam which was then coupled into the optical fiber from the other side. By carefully controlling the curing power and time, a variety of lenses can be fabricated. Lens formation is based on the gradual growth of an optical waveguide (cured part) in the liquid environment and the lens shape is decided by the output beam intensity distribution (Fig. 3.10).

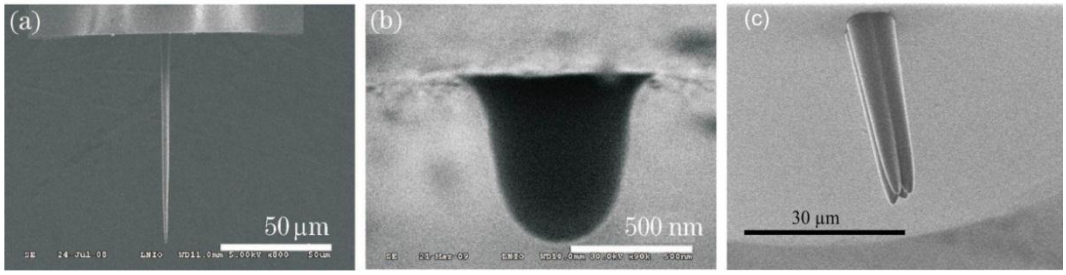

Fig. 3.10. *Examples of the polymer lens created at the end face of an optical fiber using the configuration in Figure 9(B). (a)&(b) [218], (c) [222].*

A modification of this technique was demonstrated using the reflow property of the photopolymer [210]. The various stages of this fabrication process are shown in Fig. 3.11. Instead of forming a polymer hemisphere at the fiber end face, a layer of photoresist is coated on the fiber tip. The curing is done using a UV beam coupled through the same fiber. After developing, a photoresist cylinder is formed exactly on top of the core area. The cylinder was then melted by a post-baking process which allowed reflow of the cylindrical structure resulting in a lens shape. If the fiber is to be used for ultrahigh power applications, the curvature of photoresist lens can also be transferred into the glass core by etching down the tip with the polymer microlens structure through dry etching [210]. The thickness of the polymer cylinder can be more precisely controlled using a spray coating technique so as to increase the reproducibility of this fabrication method [223].

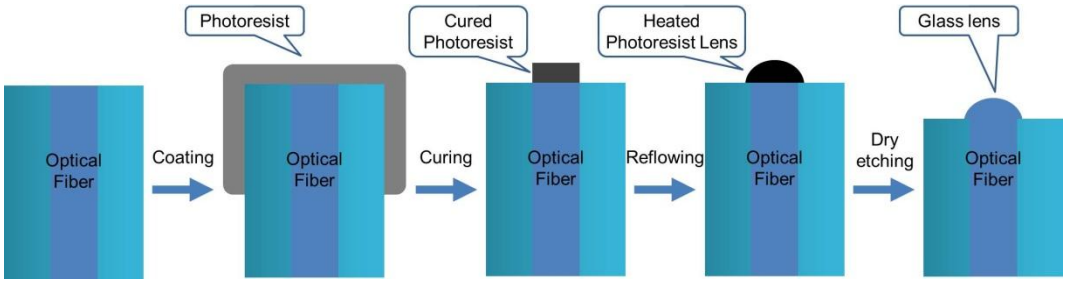

Fig. 3.11. *The fabrication of lensed fiber utilizing the reflow property of the photopolymer.*

In all the single-photon polymerization techniques mentioned above, the beam profile of the curing beam was not a factor in order to achieve the desired microstructures at the tip of the fiber. In those methods, the main parameters that decide the final structure were the shape of the uncured material at the tip of the fiber and the exposure time and power of the curing beam. This however limits the flexibility of this method. Chapter 5 will report a new fabrication method for fabricating polymer microlens using single-photon polymerization in detail. In this technique, instead of flood exposure using a UV lamp or curing using the UV beam coupled through the fiber itself, a UV diode laser (wavelength = 405 nm) is used to facilitate the curing process as shown in Fig. 3.9(C). When a laser beam is used for the curing process, it is possible to modify the beam profile of the curing beam to control the curing process. Thus it is possible to sculpt the desired microstructure at the tip of the fiber by modifying the beam profile of the curing beam. This allows higher flexibility in order to fabricate desired structures with better control and reproducibility. Since a diode laser is used as curing source, it is relatively cost-effective and easy to setup this system. An example of the lensed fiber fabricated using this method is shown in Fig. 5.1.

The same approach can also be used for fabricating collimating microlenses with a hemispherical shape. This can be achieved by curing the hemispherical polymer using a collimated laser beam instead of a focused laser beam. The self-focusing property of the photopolymer hemisphere allows gradual growth of a hemisphere at the tip of the fiber

as the exposure time progress [Fig. 3.9(inset)]. The size of the final polymer lens formed can be precisely controlled and lenses with a range of radii of curvatures can be achieved with this approach as seen in Fig. 3.12 [215]. The microlens starts to grow from the center outwards. The curing continues until the lens reached the required size, and the un-polymerized polymer can be removed by rinsing the tip of the fiber in ethanol or acetone. Using a photopolymer with different physical properties (eg its viscosity) and changing the convergence of the curing beam, it is also possible to adjust the shape of the lens.

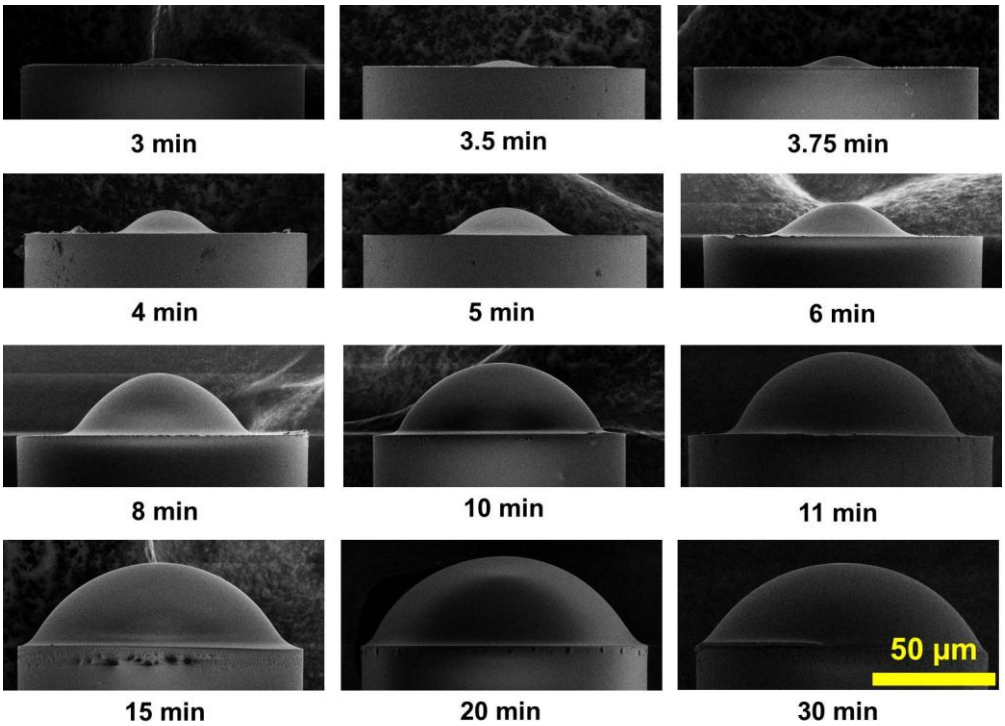

Fig. 3.12. *SEM images of the various hemispherical lenses fabricated with collimated laser beam by varying the exposure time.*

Using this single-photon polymerization technique, microlensed fibers can be fabricated in a single-step procedure except when using the thermal reflow method. For polymer lenses fabricated with this technique, the surface roughness of the lens is not a concern and a high quality surface can be easily obtained. This is a relatively inexpensive fabrication

technique with a relatively high throughput. With a little creativity, a variety of tailor made lenses can be produced. However, while the multi-parameter space (material properties, curing beam properties etc.) offers the flexibility to fabricate a wide variety of structures with this fabrication protocol, this makes it difficult to optimize this fabrication technique for fabricating a lens with specific parameters.

3.6.2 Two-photon Polymerization Technique

This is a relatively new and promising technique to fabricate microstructures on the cleaved tip of an optical fiber. It is one of the applications of the three-dimensional microfabrication technique with photopolymers, which traditionally involves loading a three-dimensional computer aided design (CAD) drawing on a computer, which controls the scanning of an optical beam to obtain the desired structure. In traditional photolithography, a UV beam exposed to a two dimensional photoresist layer through a photolithography mask, solidifies the photopolymer. The uncured photopolymer is washed away after the exposure. The solidified area is then covered with another layer of photopolymer, and the process is repeated in order to obtain a three-dimensional structure [224]. This is a very complicated and time consuming process. In addition, it is impossible to fabricate some specific structures using this fabrication protocol. The layer-by-layer structure also limits the longitudinal resolution. Curing using a tightly focused UV beam to improve the longitudinal resolution, is also impractical due to the significant absorption at the non-focused area.

Using a near infrared femtosecond laser and UV sensitive polymers, it is possible to overcome these limitations. Two-photon absorption is a third order non-linear process. At high intensities, which is often achieved using a focused femtosecond laser beam whose peak pulse power is high, the energies of two photons combine together to promote the molecule to an excited state, which then proceeds along the normal photochemical reaction pathway [32]. The rate of two-photon absorption is proportional to

the square of the light intensity (photon density) [225]. When a tightly focused near infrared femtosecond beam is shone on a UV sensitive polymer, at the focal spot and where there is sufficient photon density available, the material absorbs the NIR photons through a two-photon process. Thus the material at the focal volume is cured leaving the rest of the material unaffected. This allows sculpturing of the desired structure with a high resolution with point by point scanning. Once the scanning process is over, the uncured material can be washed away using solvents like ethanol or acetone. It is even possible to achieve a resolution below the diffraction limit of light with this technique, which allows the fabrication of complicated 3-dimensional microstructures [Fig. 3.13(A)].

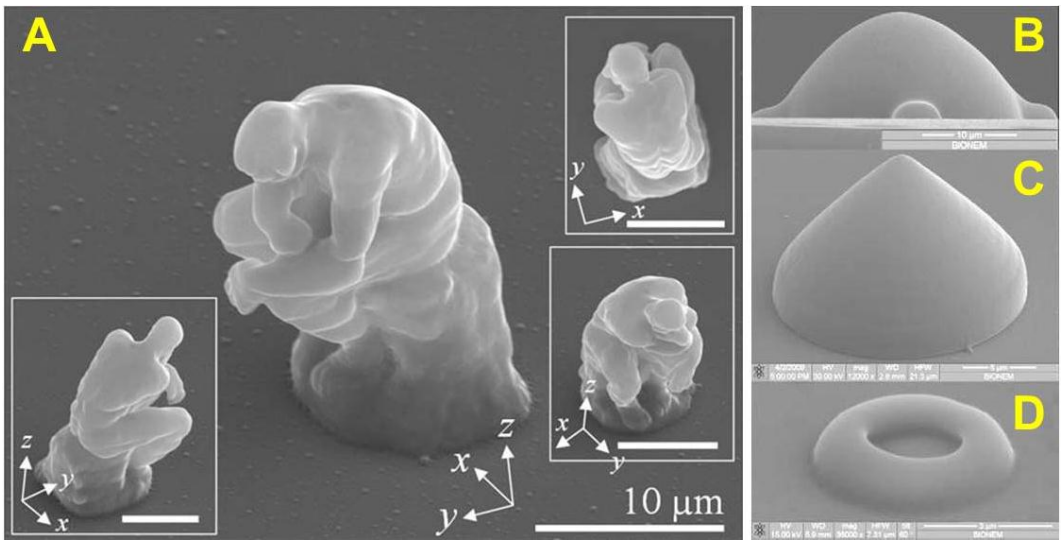

Fig. 3.13. *(A) Micro-"The Thinker" that is about 20 µm tall fabricated using two-photon polymerization technique. Reprinted from [226]. (B-D) Different micro-optic elements, fabricated at the end face of an optical fiber by two-photon polymerization technique: (B) convergent lens, (C) axicon lens, and (D) ring shaped phase mask. (B-D) are reprinted from [227].*

Since its first demonstration in 1997, the two-photon polymerization technique has matured so that it is used in a variety of applications [228]. The resolution of this technique depends on the numerical aperture of the objective lens, wavelength and intensity of the laser, exposure time,

scanning pattern, and the properties of the photopolymer. Many kinds of material, from traditional photopolymers such as urethane acrylates and epoxies to newly developed materials including inorganic-organic hybrid polymers, biopolymers, photoresists and hybrid polymers containing metal ions, have all been used for fabricating microstructures using this technique. This fabrication technique has found applications in areas such as photonics, microfluidics, microfabricated microelectromechanical systems (MEMS) devices, bioengineering and micro-magnetics. A detailed discussion on this technique is outside the scope of this thesis and can be found elsewhere [225, 229-232].

Using this technique, a polymer microlens or any other microstructure can be easily created at the end face of an optical fiber [Fig. 3.13(B-D)] [227, 233-235]. A high quality surface profile and smoothness with spherical symmetry are generally required for creating a high quality output beam. Therefore, unlike the parallel linear scanning pattern employed for traditional two-photon polymerization [236-241], Guo *et al*. used the annular scanning mode cooperated with continuous variable longitudinal scanning spaces, to achieve a high quality microlens with a surface roughness of ~20 nm [233]. Under the same scanning pattern, Liberale *et al*. fabricated spherical microlenses and a conical microlens of arbitrary angles at the end face of an optical fiber, from which a Bessel-like beam was generated [227, 235]. Malinauskas *et al*. fabricated spherical and aspheric microlenses on the optical fiber end face using a novel method that can reduce by 100 fold the fabrication time, but this is dependent on the shape and volume of the structure to be fabricated [234]. To achieve this, only the outer shell of the microlens was solidified using a laser, with their interior being polymerized using a post-fabrication UV treatment. An average surface roughness of ~30 ± 3 nm was obtained, which is less than a tenth of an optical wavelength in the visible spectral range and hence is acceptable for optical devices.

Using the two-photon polymerization technique arbitrary shapes can be fabricated. With the help of optical modeling software, it is possible

to design complex optical surfaces to suppress aberrations and tailor output beam profile. However, the higher ensuing cost limits the wider application of this relatively new technique.

3.7. Focused Ion Beam Milling

FIB milling is a pure physical process. The ions collide with the specimen and precisely remove the material at the sub-micrometer level. Therefore, by scanning a FIB of specific energy over a substrate with a pre-designed route and specific dwell time at each point, a micro-structure can be sculptured. This technique mills directly on the substrate, therefore no others preparation is needed. Normally a FIB machine is equipped with a scanning electron microscope (SEM), which when used in the same experimental chamber, simultaneously allowing the checking and automated drift correction of the sample during the fabrication process.

A lens-like structure can be fabricated using an exposure pattern composed of a series of concentric rings with different diameters, thickness and ion dosage. However, the re-deposition effect, which depends on several factors such as the milling sequence, the angle between the FIB and the sample, milling depth and dwelling time, all causes material accumulation at certain areas. Hence it is hard to achieve a linear relationship between the ion dosage and the milling depth, especially at deeper depths. For example, the previous milled area is always filled with redeposit material sputtered from the newly milled location, which causes the depth of the previous milled area to being reduced. Another effect is the modification of the physical properties of the substrate under ion bombardment. The high dosage induced heating effect can change the milling rate. Compensation methods are needed to achieve the designed lens profile. Ion beam induced charging can be neutralized using negative electron beams or applying a conductive metal layer on the sample.

Schiappelli *et al*. fabricated a spherical lens on the tip of SMFs [242]. The profile of the fabricated lens was very well reproduced in ten layers each 100 nm thick [Fig. 3.14(A, B)]. This lens was used to couple the output light into a waveguide with increased coupling efficiency. A nonlinear equation was applied to rectify the nonlinear relationship between ion dosage and milling depth. Cabrini *et al*. fabricated an axicon lens on the cleaved top of a SMF [243]. They divided a series of concentric milling rings into various sub-rings of very small milling dosage and used a scanning pattern that leaves as much time as possible between two superposition of the same ring to provide a slower heating and formation of re-deposition [Fig. 3.14(C)]. A Bessel-like beam was generated and this fabricated axicon tipped fiber was used for optical manipulation [150, 243]. Callegari at el. first fabricated a parabolic lens with a similar method [243] on silicon substrate to optimize the fabrication parameters [Fig. 3.14(D)] [244]. With a maximum milling dwell time in the linear range, the re-deposition happened at a large milling angle (deeper depth) – the edge of parabolic lens – was minimized. A Fresnel phase lens was then produced on the center of the tip of an optical fiber using these parameters [Fig. 3.14(E, F)]. The surface roughness was characterized by an atomic force microscope (AFM) to be 3.6 nm for the central part of the Fresnel phase lens. At a wavelength of 840 nm, a spot size of 740 nm FWHM was achieved with the Fresnel phase lensed fiber [244].

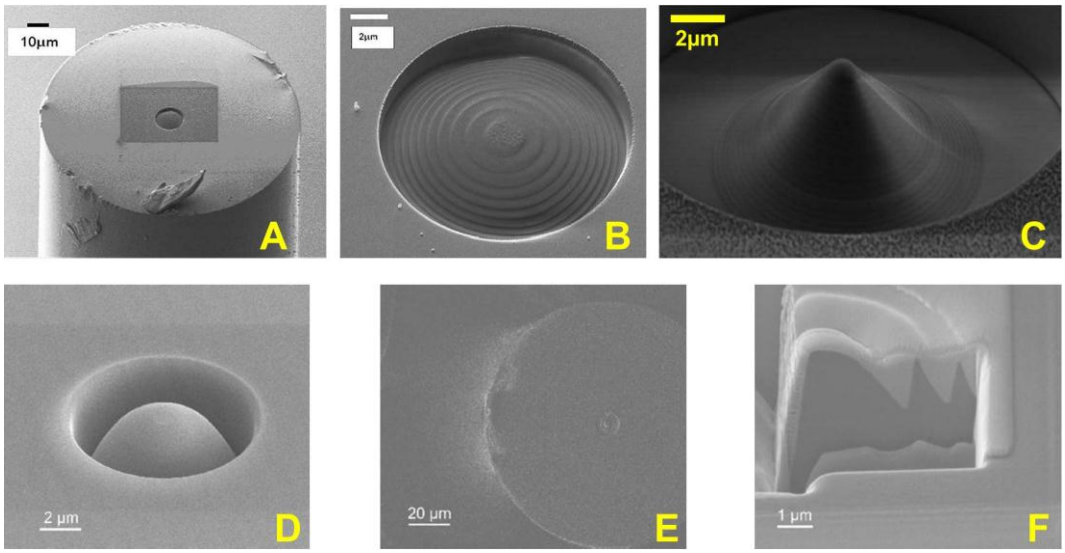

Fig. 3.14. *Lens tipped fibers fabricated using FIB. (A) [242]; (B) [242]; (C) [243]; (D) [244]; (E) [244]; (F) [244].*

It is worth mentioning that during the milling process, especially when using a high energy beam, the implantation of ion may occur. The implantation depth may reach up to tens of nanometres for the energy used for microlens milling. This will result in a decrease in the optical transmission; however, normally it is acceptable for conventional optical usage. The re-deposition can also be compensated by tilting the sample stage to decrease the angle between the sample and the FIB. Chemical gas assisted etching with gases like Cl_2 or XeF_2 can also be used to degrade the re-deposition effect. More information about this FIB technique is available at [245].

The FIB milling technique is a high resolution, flexible technique. It directly sculptures structures on the substrate without the need of other assistance. High profile microlenses can be created in a single step on the end face of optical fiber although complex compensation calculations are normally required. The whole milling process may take minutes to hours and the manufacturing cost is relative high when compare with other lensed fiber fabrication methods. Mould microfabrication on metal material for mass production replication might be realized in the future to decrease the cost.

3.8. Summary

As can be seen from the discussions in previous sections, the approaches in fabricating microstructures at the tip of the fiber varies a lot from melting the tip of the fiber to sculpting structures on the tip using mechanical or optical methods. Table 3.1 summarizes the pros and cons of each of these techniques which would help one to choose the right fabrication method for a specific application.

Fabrication method	**Advantages**	**Limitations**
Arc discharge technique	Ease of use. Low cost. Commercial fiber fusion splicer can be used. Can fabricate long working distance microlenses. Suitable for high peak power pulsed laser applications.	Low reproducibility. Low fabrication efficiency. Manipulation becomes more difficult when smaller silica rod was used. Not suitable for batch fabrication.
Laser micro-machining technique	Hyperbolic shape microlens can be fabricated for increasing coupling efficiency.	Low reproducibility and flexibility. Not suitable for batch fabrication.
Polishing technique	Axicon, wedge and polygon pyramid tipped fiber can be made. Single step fabrication. The lens fabricated is independent of the nature of the fiber (a pure physical process). Smooth surface. Fast fabrication speed. High reproducibility.	A fiber beveller is required. Complex shaped lenses require computer aided control. Very challenging to fabricate traditional spherical surface.
Chemical etching	Flexible, inexpensive and high reproducibility. Cone angle of the tip can be easily adjusted. Microlens is self-aligned. Multicore fiber can be etched to make multiple microlenses. Suitable for batch fabrication. A self-terminating process with	Highly dangerous etchant involved. Sensitive to temperature. Rough surface for protection layer etching. . Unable to fabricate traditional spherical surface. Complex etching procedures for multistep etching.

	protection layer. Using multistep etching sharp probes (with nanometre radius curvature) with tailored properties can be fabricated.	
Single-photon polymerization technique	With ingenious design various types microlens tipped fiber can be made. Single step procedure. High quality surface. Inexpensive. Fast fabrication. Most of the fabrication methods are suitable for batch fabrication.	Difficult to optimize the parameters. Not suitable for high power applications.
Two-photon polymerization technique	Highly flexible. High precision. Arbitrary structures can be made. Possible to design complex optical surfaces to suppress aberrations and tailor output beam profile.	Relatively expensive method. Not suitable for high power applications. Not suitable for batch fabrication.
Focused ion beam milling	Highly precise fabrication. Pure physical process.	Expensive method. Implantation of ion may occur which would decreases the transmission efficiency of the material. Require complicated non-linear modeling Low throughput. Not suitable for batch fabrication.

Table 3.1. *Comparison of various microlens tipped fiber fabrication techniques.*

3.9. Conclusion

In this chapter, I have discussed the details of various microlensed fiber fabrication methods. While choosing a suitable microlensed fabrication method for a specific application there are several factors to be considered such as operating wavelength, output beam profile, optical break down threshold, fabrication cost, instrumentation and throughput. The design requirements for microlensed fibers are so diverse due to the

diversity of the fields in which they are used; there is no single fabrication technique which can be chosen as the best. Each fabrication method has its own merits and each of them caters some specific requirements depending on the field of application. Even though the field of microlensed fabrication has seen lot of technological advancements over the past decade, there is still room for optimizing these techniques in terms of reproducibility, flexibility and throughput so that they would be commercially viable for various applications. Such commercially viable techniques would greatly aid fields like bio-medical optics in realizing miniaturized fiber based probes for endoscopic or handheld imaging and microscopy.

Chapter 4:

4. Axicon Tipped Fiber for Cellular Transfection

4.1. Introduction

The delivery of therapeutic and other biologically relevant agents into cells which are otherwise membrane impermeable remains an essential requirement in the study of biological cells. At present, there are various transfection methods used to solve this problem including chemical, physical, viral, electrical, and optical techniques [246]. Among these, optical transfection is a technique which offers single cell selectivity, specificity, sub-cellular resolution, high transfection efficiency and good post-transfection cell viability. By tightly focusing a laser beam on the cell membrane, optical transfection can transiently and locally increase the permeability of the cell's plasma membrane to permit for example nucleic acids to be internalized. Femtosecond laser assisted transfection has proven to be a very effective method to date, amongst the use of alternative laser systems with an excellent potential for targeting single cells *in vitro* [28, 30, 38, 64, 67]. However, most of the optical transfection techniques that have been used employ free-space (bulky) optical setups for targeting light to the transfection site. The transfection efficiency achieved by these setups is highly dependent on the alignment of these optical setups, the quality of the optical transfection beam and accurate targeting of the beam focus on the cell membrane, so an expertise in optics is necessary to achieve efficient transfection. This approach also limits the potential application of the technology for *in vivo* experiments.

A fiber based system would offer not only compactness but also the advantage that, once the laser has been fiber coupled, no specialised optical alignment is required to perform optical transfection. Optical fibers could also be integrated with endoscopic techniques, which might lead optical transfection into the clinical arena. In this chapter the efficiency of

femtosecond transfection of CHO-K1 cells with a novel axicon tipped optical fiber is studied.

4.2. The Fabrication of an Axicon Tipped Optical Fiber

The output beam from a cleaved optical fiber is naturally divergent, which makes it inappropriate to use for optical transfection. As discussed in Chapter 2, a tightly focused femtosecond laser is vital for the success of optical transfection. Therefore, a mechanism to focus the output beam from an optical fiber had to be developed. One option is to use a microlens tipped fiber, which can be fabricated using various methods. Melting the fiber tip by a heating source to form a lens is the most widely used methods to fabricate microlensed fibers to increase the coupling efficiency into optical fibers in the communication field [145, 161]. However, the reproducibility of this method did not meet the requirements of my application and only lenses with a comparatively large radius of curvature can be fabricated. Polishing techniques [170, 176] can make axicon lenses of different angles; however, this technique is complex, time consuming and expensive. To obtain a high quality lensed fiber using a polishing technique, a computer controlled complex polishing pattern is needed. There are also other methods using photoresist reflow [210], two-photon lithography [233], FIB milling [243] or a combination of a few techniques [161]. However, these methods have drawbacks such as low-precision, limited flexibility, high cost, or they can only fabricate polymer lenses that are not suitable for high peak power pulsed laser. For a detailed discussion about these fabrication methods please see Chapter 3.

In the presented work, a selective chemical etching method was used to fabricate an axicon lens in the centre of a carefully cleaved fiber end face [178-182]. This method was chosen over potential others due to several considerations: this method is a simple single-step, flexible, inexpensive method for axicon tipped fiber fabrication with high reproducibility. Batch fabrication can also be easily realized. The lens is made from the core therefore it is automatically aligned with the fiber core

and thus suitable for a higher power application compared with a lens made from polymer. Furthermore, this method can be applied to most single mode silica optical fibers.

HF solution and an aqueous solution of NH_4F are normally used as an etchant to modify a fiber tip. The tip of a piece of carefully cleaved optical fiber is first dipped into the etchant (Fig. 4.1). The etching rates of the core and cladding of the fiber are different and, by varying the ratio of HF to NH_4F, the relative etching speed between core and cladding of the fiber can be adjusted. The etching speed of the cladding can be controlled faster than that of the core, by choosing a suitable ratio. A protruding axicon lens is then created at the end face of an optical fiber. It can be seen from Fig. 4.1 that a volcano shape is created before it evolves into an axicon shape. This is due to the fact that the slower etched core is exposed to the etchant gradually. The etching rates for both core and cladding are constant at a set temperature. Therefore once the axicon has formed its apex angle remains constant and the diameter of the cladding decreases at a constant speed.

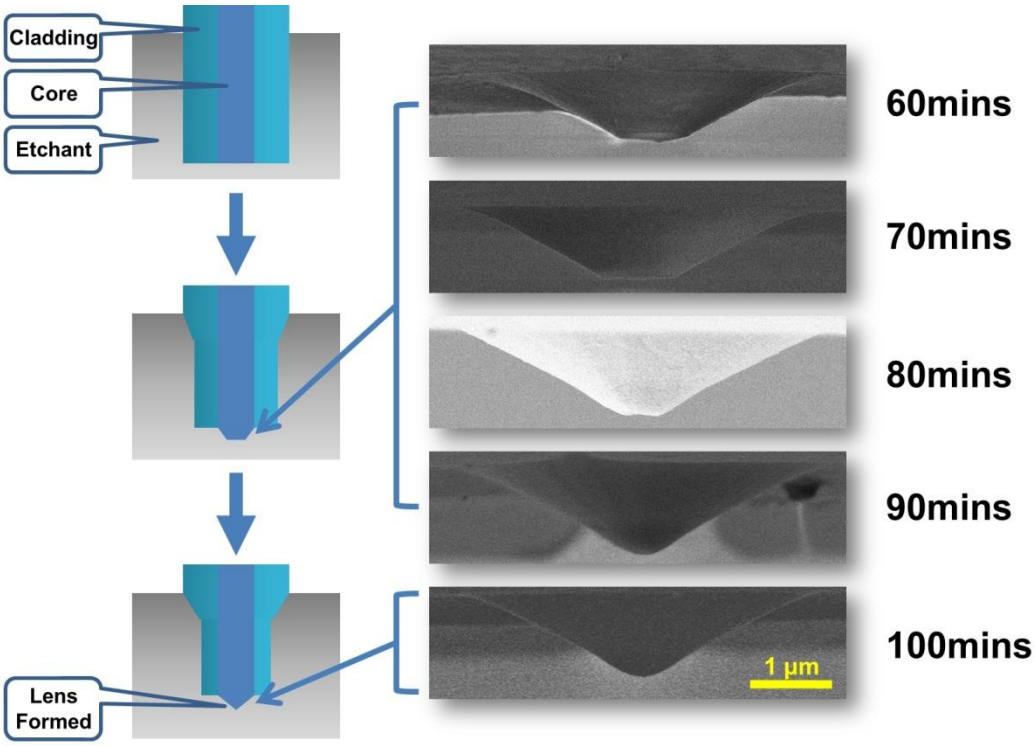

Fig. 4.1. *The fabrication of an axicon tipped optical fiber using a selective*

chemical etching method. An optical fiber tip is first dipped into the etchant. Due to the different etching rate between the fiber core and cladding, an axicon lens is produced in the form of a volcano shape on the end face of an optical fiber. Shown are the SEM images of the lens formation (using an etchant comprising of NH_4F:HF = 2) at different stages.

In order to discover the relationship between the apex angle of an axicon and the mixing ratio of etchant, a series of axicon tipped fibers were made using freshly made etchant comprising HF (48% - 51% in water) and NH_4F (40% in water) at different mixing ratios, and using commercially available SMF (SM800-5.6-125, Thorlabs, UK) with a cladding diameter of 125 µm, and mode field diameter of 5.6 µm at ~22 ºC (Fig. 4.2). The etching durations were from tens of minutes up to ~2 hours dependent on the formation of the axicon lens. The result of each fiber (axicon apex angle) was checked using a SEM. Two examples of axicon tipped fibers with different axicon apex angles etched using differing etchant combination ratios, can be seen in Fig. 4.3. With a ratio of NH_4F:HF = 2.3 and an etching time of 120 minutes, an axicon apex angle of 111.2 ± 0.4 º (mean ± standard deviation, N = 3) was fabricated [Fig. 4.2, Fig. 4.3 (b, d)] and was subsequently used in the following optical transfection experiment. A detailed discussion of axicon tipped fiber characterization and theoretical modelling will be presented in the next section (Chapter 4.3).

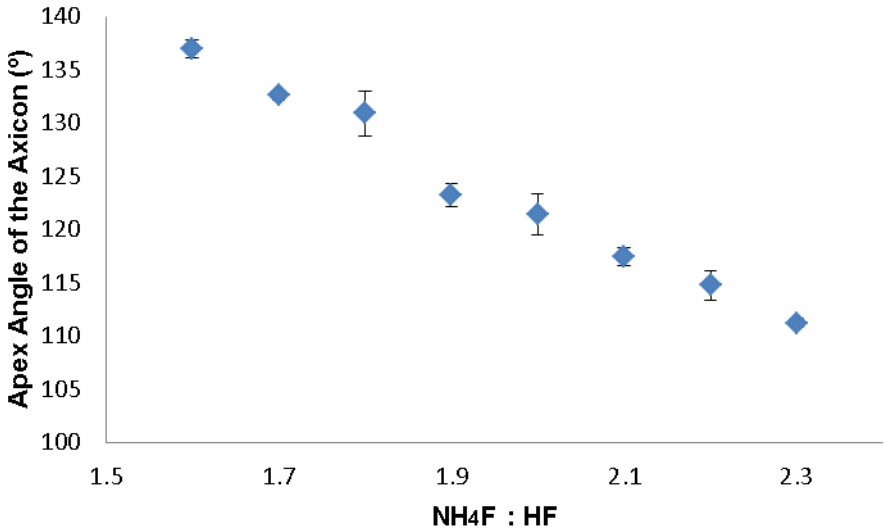

Fig. 4.2. *The relationship between apex angle of the axicon lens fabricated using selective chemical etching method and the etchant mixing ratio of NH_4F to HF. 3 to 7 fibers were fabricated at each mixing ratio. The error bars indicate the standard deviation.*

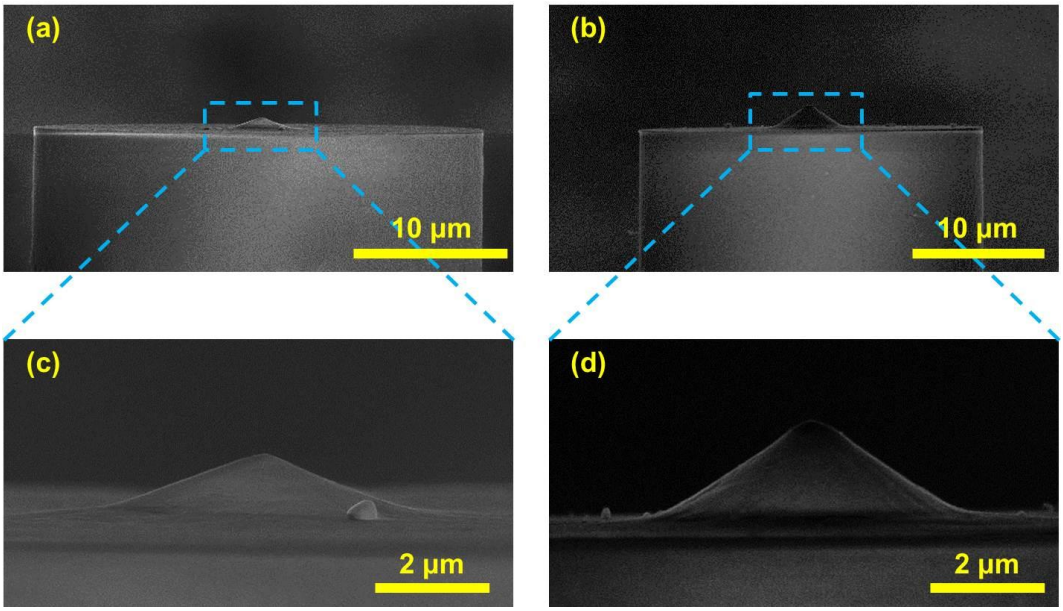

Fig. 4.3. *SEM images of axicon tipped fibers fabricated using etchant comprising NH_4F : HF = 1.6 [(a), (c)] and 2.3 [(b), (d)]. Axicon lenses with different apex angles can be readily seen.*

4.3. The Characterization and Theoretical Modeling of the Output Beam from an Axicon Tipped Fiber

4.3.1 The Characterization of the Output Beam from an Axicon Tipped Fiber

For characterization of the output beam from an axicon tipped fiber, an 800 nm pulsed femtosecond laser was first coupled into an axicon tipped fiber through a fiber collimator (Thorlabs, F810FC-780). The fiber output light was then analyzed from a series of lateral cross sections obtained in a water medium (since the optical transfection will be performed in a liquid environment) using a 60X water immersion objective (X60 Olympus UPlanSApo) in conjunction with a CCD (Charge coupled device) camera (WAT-250D) (Fig. 4.4). The fibers were mounted and positioned by being taped onto a vertical post whose movement was controlled by a xyz translation stage with 1 μm resolution.

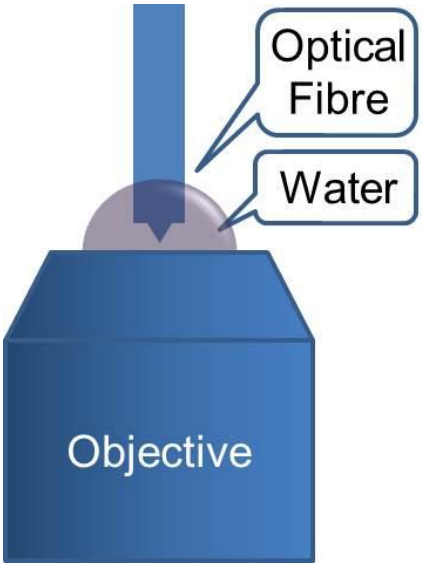

Fig. 4.4. *The setup for measurement of the output light from an axicon tipped optical fiber.*

Due to optical aberration it was difficult to determine the relative position between the output beam and the fiber itself. For example, by

shining a torch (white light) on the fiber end face from the side, I could locate the end face of the fiber tip through an objective using the setup shown in Fig. 4.4. However, after switching off the torch light and starting to image the cross-section of the output beam (800 nm), keeping the fiber and objective still, the position of the cross-section observed was not coincident with the fiber end face. The cross-section at that time is actually a few micrometers behind the axicon lens, inside the fiber, due to the chromatic optical aberration. Therefore an alternative method was adopted: if we define the apex of the axicon as the origin of a Z axis pointing in the direction of beam propagation, then images of the fiber (with an axicon of ~110 ºC made in etchant comprising of NH_4F:HF = 2.3) output beam cross section from around -8 µm to 25 µm at 1 µm interval along Z axis can be obtained (Fig. 4.5). From Fig. 4.5, it can be seen, for example, that the cross-sections at -3 and -2 µm show dark holes in the center. This is because the image is taken through the axicon lens. It is a virtual image rather than a real one. Therefore the first cross-section that shows a Gaussian distribution after the images with dark holes at their center was defined as 0 µm.

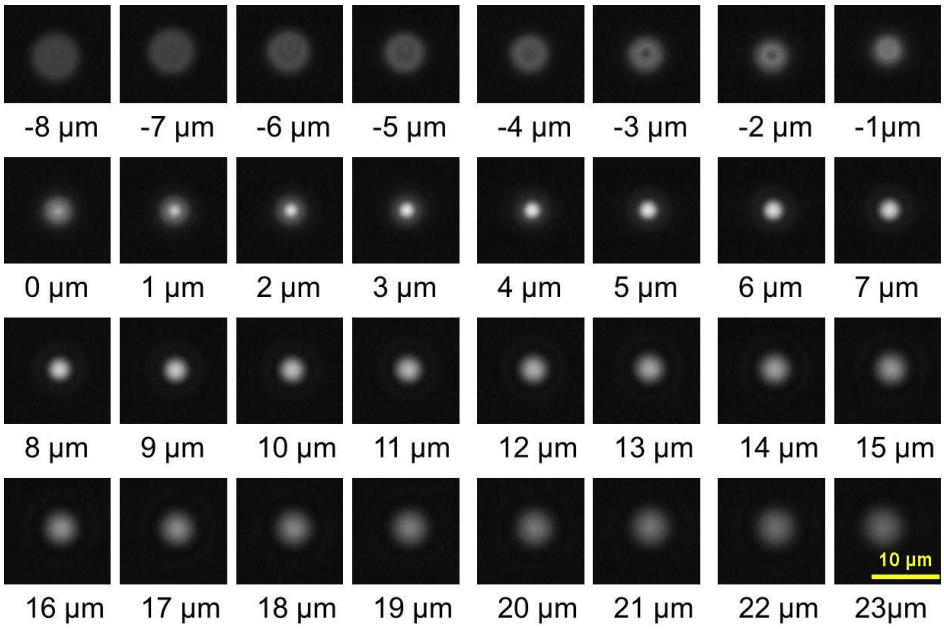

Fig. 4.5. *Images of the cross sections of the output beam from an axicon tipped fiber taken at different position from -8 µm to 23 µm along Z axis.*

Measurements like those shown in Fig. 4.5 were performed for each fiber in order to characterize the relationship between the axicon apex angle and the output beam profile. During the measurement, the laser intensity was adjusted to ensure the image with the highest intensity is under saturated and the whole series of images was taken with a constant laser power. From Fig. 4.5 the diameter for each cross section and therefore the working distance [defined as the distance from the apex of axicon to the cross-section with smallest diameter (focus) along Z axis] of the axicon tipped fiber could be obtained (Fig. 4.6). Each cross-section of the output beam, it was assumed to have a perfect Gaussian distribution and the beam diameter was defined as the width where the intensity falls to $1/e^2$ times the maximum value. The focus diameter can also be deduced (Fig. 4.7). The interpretation of Fig. 4.6 and Fig. 4.7 will be presented in section 4.3.2 along with the information obtained from theoretical modeling.

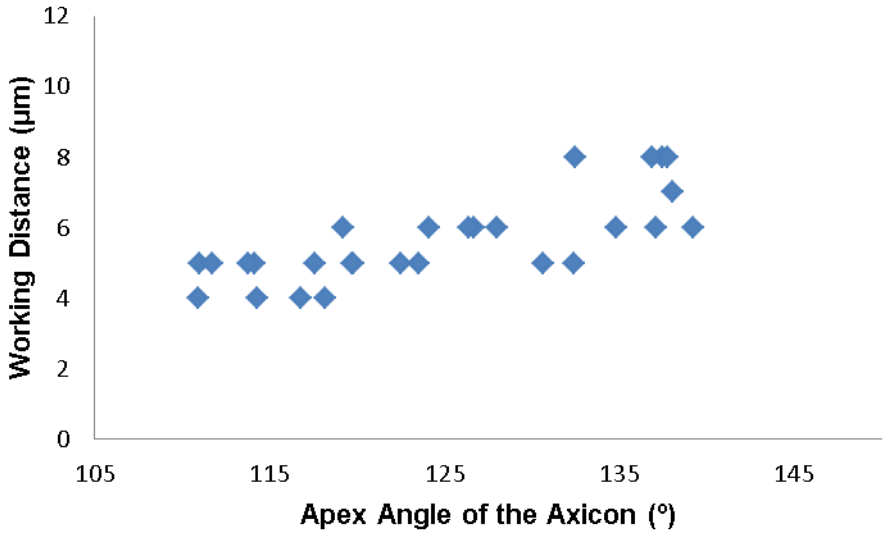

Fig. 4.6. *The relationship between apex angle of the axicon and working distance obtained from measured data.*

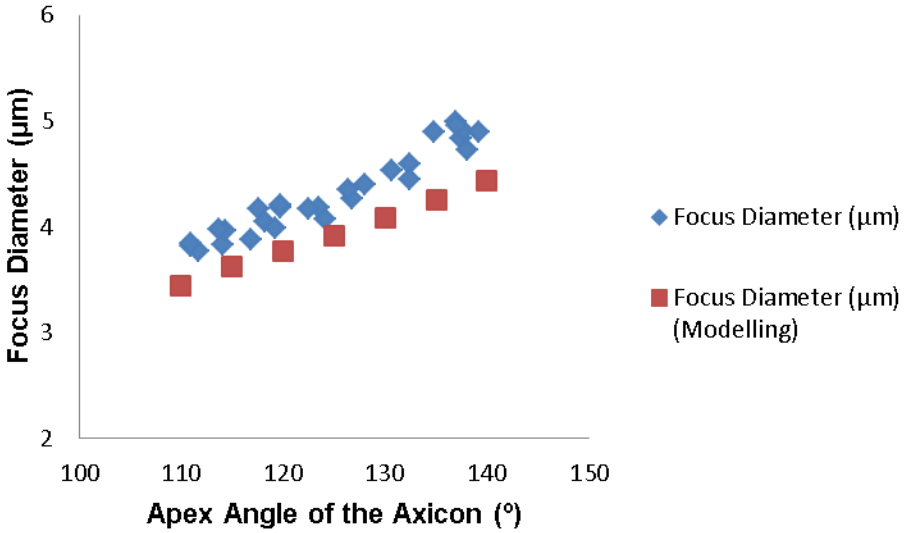

Fig. 4.7. *The relationship between apex angle of the axicon and focus diameter of the output beam. Blue and red points indicates the measured data and the data predicted by modelling.*

4.3.2 Theoretical Modeling of the Output Beam of an Axicon Tipped Fiber

To understand and optimize the fiber properties, the output beam from an axicon tipped fiber was analyzed using a computer model modified from the literature [247]. In this model an axicon tipped fiber core was divided into two parts: a bare tipped fiber and an axicon. The plane wave, with Gaussian intensity distribution, traveling through the fiber core to the end face (Fig. 4.8, Plane 1) of the bare tipped fiber, was modified by the axicon and the surrounding medium (water) as it traveled to Plane 2 (Fig. 4.8), which was defined at the apex of the axicon perpendicular to the beam axis. The field at Plane 2 was obtained by assigning a phase shift, calculated using geometric optics, taking into account the refractive index of the axicon and the surrounding medium to each component of the plane wave at Plane 1. The light field at Plane 2 was then decomposed into a spectrum of plane waves (spatial spectrum) by a Fourier transformation. The spatial spectrum for any plane behind Plane 2 was obtained by assigning the corresponding phase shift to each of the plane wave

components, and the light field was retrieved by an inverse Fourier transform. Using this approach, the light intensity distribution corresponding to the square of amplitude of light field distribution can therefore be therefore obtained. A Hankel transformation was used to reduce the calculation from 2D to 1D (1 dimensional) [248].

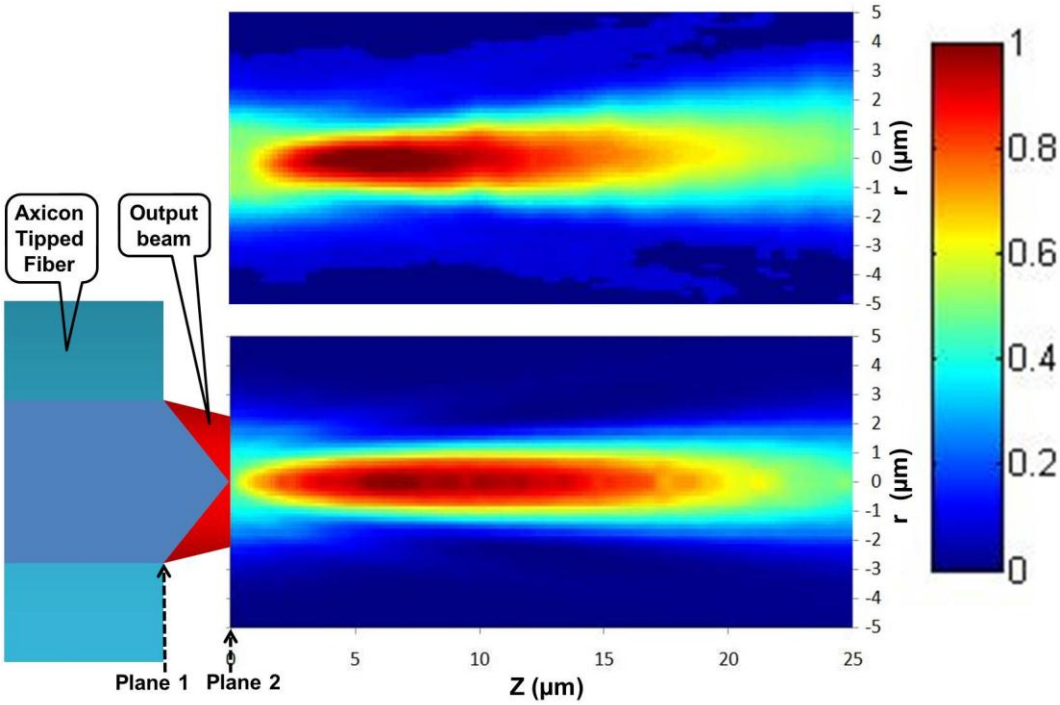

Fig. 4.8. *The measured (top) and simulated (bottom) output beam intensity profiles of the axicon tipped fiber in water where r and Z are cylindrical coordinates with the Z axis pointing in the direction of the beam propagation. Experimental data used are from Fig. 4.5. On the right of the simulated graph light traveling through the fiber core reaches the fiber end face (Plane 1) and enters water after it is modified by an axicon lens. The simulation starts from Plane 2 towards the direction of the beam propagation.*

The lower image in Fig. 4.8 shows the theoretical results of the azimuthally averaged intensity profile of the beam as a function of the distance from the apex of the etched axicon in water. A 5.6 µm mode field diameter of the fiber, a 110º axicon apex angle and a wavelength of

800 nm were used in this model. The refractive index of the core and surrounding medium were assumed to be 1.5 and 1.33 respectively. The upper image in Fig. 4.8 is the experimental result, stacked using Image J, using the data in Fig. 4.5. The experimental findings are in good agreement with the theoretical predictions. The MATLAB source code for this theoretical simulation can be found in Appendix A.

Using this model the axial intensity profiles of the output beam from axicon tipped fibers with different axicon apex angles can be generated. The input powers are identical for all the fibers. The working distances of each axicon tipped fibers are the same, 6 µm, except for 110º axicon, which slightly shifted to ~5.4 µm. The result is consistent with experiment measurements (Fig. 4.6), which show that changing axicon apex angle from 110º to 140º does not greatly affect the working distance. However, from the relative intensity around the focus (6 µm on Z axis), we can see that the peak intensity decreases as the axicon apex angle increases (Fig. 4.9). The 110º axicon therefore showed the best enhancement of the intensity since the input power in each case was the same.

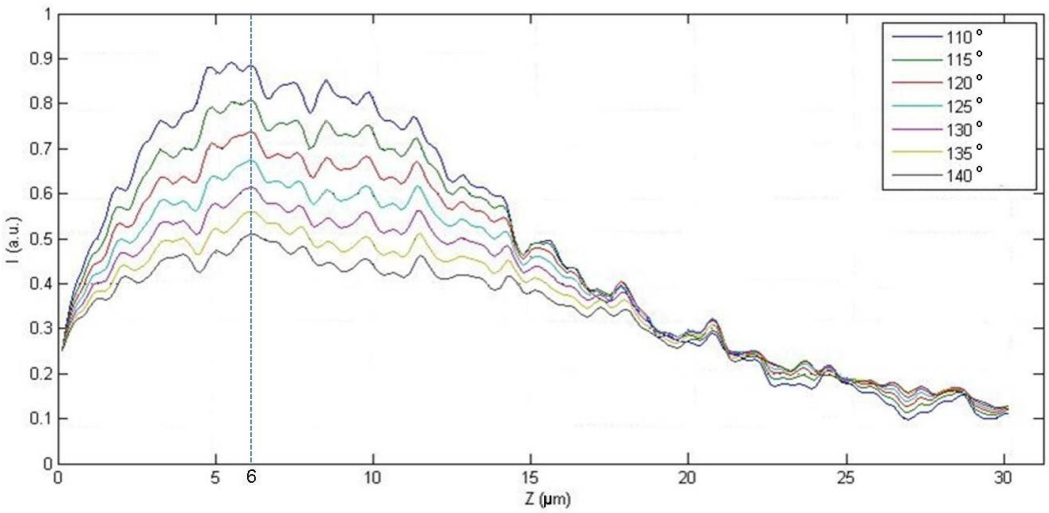

Fig. 4.9. *The axial intensity profiles of the output beam from axicon tipped fiber with axicon apex angles from 110º – 140º.*

Also from this model the lateral intensity profiles cross the centre of

the output beam focus could be generated (Fig. 4.10). From this normalized graph, it is clearly seen that the focus diameter is increasing as the axicon apex angle increases. If we treat these intensity distributions as Gaussian distributions the focus diameters (the width at $1/e^2$ of maximum intensity) can be obtained (Fig. 4.7, Fig. 4.10). The theoretical values are slightly smaller than the experimental measurements. This may be due to the imperfection of the axicon and the geometric optics approximation between Plane1 and Plane 2 in Fig. 4.8. However, both theoretical modelling and experiment measurements indicate that the fiber with an axicon of 110º gives the smallest beam focus, which is around 3.7 to 3.8 µm.

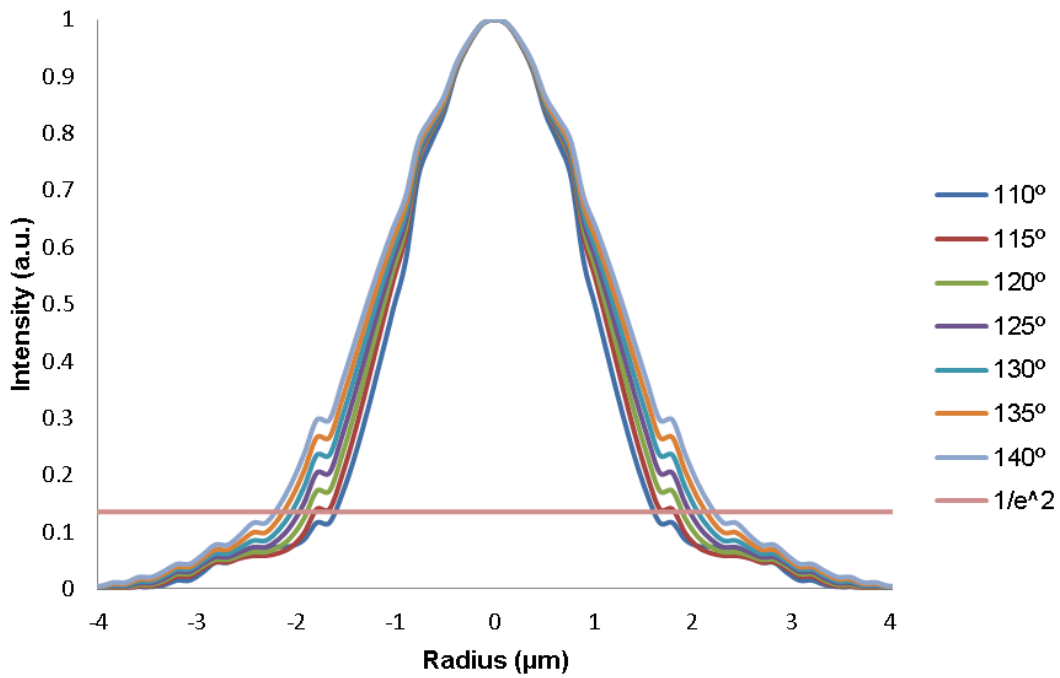

Fig. 4.10. *Normalized lateral intensity profiles of the focus of the output beam from axicon tipped fiber with axicon apex angles from 110º to 140º.*

4.3.3 Summary and Conclusion

Axicon tipped optical fibers with axicon apex angles between 110º and 140º were analysed through both experimental measurement and theoretical simulations. Due to the nature of my axicon tipped fiber

fabrication method, selective chemical etching, as the axicon apex angle decreased, the cladding of the fiber tip decreased as well. For the fiber with an axicon of 110º, the cladding diameter is around 30 µm. With any fiber tip smaller than this, the fiber proved to be too fragile and thus unstable during the optical transfection experiment. Also, as the axicon becomes sharper the transmission efficiency of the fiber will decrease due to total internal reflection in the axicon area. For the optical transfection experiment, a tight focus at a relative remote distance is preferred. Fig. 4.7 and Fig. 4.10 show that a 110º axicon generates the smallest focus and from Fig. 4.6 and Fig. 4.9 we can see that by varying axicon apex angle from 110º to 140º the working distance is only affected slightly. Also, if we take into account the height of the axicon itself, the actual working distance (from Plane 1 to the focus along Z axis in Fig. 4.8) for a 110º axicon is actually longer. From the relative focus intensity in Fig. 4.9, it is clearly seen that the fiber with the 110º axicon gives the best intensity enhancement. Therefore, based on the above considerations, the fiber with an axicon of 110º was chosen for the following optical transfection experiment [Fig. 4.3 (b), (d)].

4.4. Experimental Procedure

4.4.1 Experimental Setup

Cell transfection was instigated by a femtosecond Ti: Sapphire laser emitting at 800 nm, with an output pulse duration of ~100 fs and a pulse repetition frequency of 80 MHz (2 W average power, Coherent, MIRA). At the exit of the axicon tipped fiber, the pulses undergo stretching due to non-linear phenomena occurring inside the fiber such as SPM and GVD. The pulse duration of the output beam against the length of axicon tipped fiber at 30 mW output power was measured using a home built autocorrelator (Fig. 4.11) [249]. The pulse duration of bare tipped fiber was also measured in the same conditions and no significant difference was

found. Therefore it is safe to assume that the amount of pulse stretching caused by the axicon lens can be ignored. In order to keep the pulse duration as short as possible, and considering the physical limitation of the experiment setup, the length of the axicon tipped fiber was set to be 35 cm which stretched the pulse to ~800 fs.

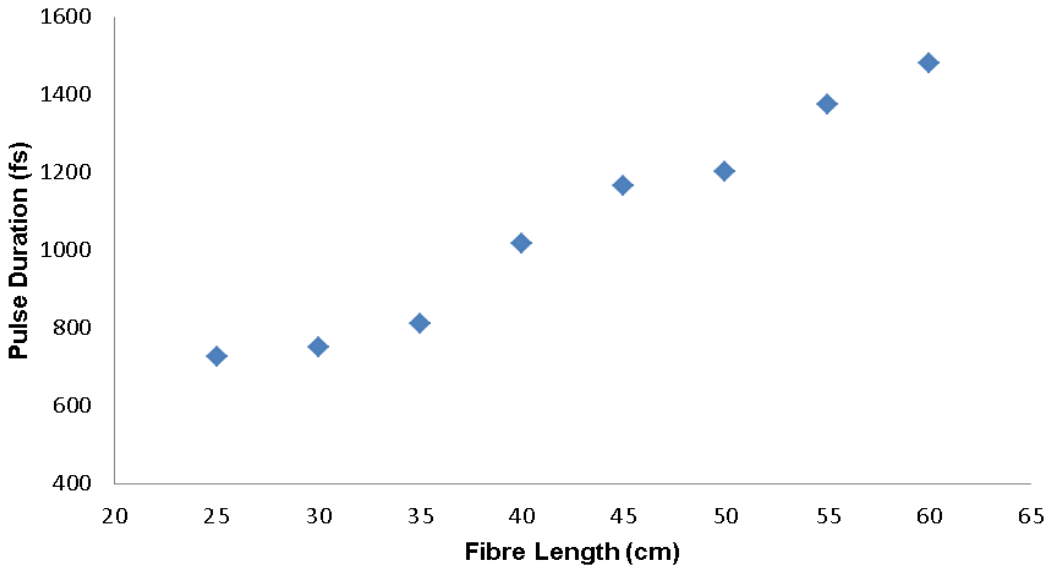

Fig. 4.11. *The pulse duration of the output beam against the length of axicon tipped fiber at 30 mW. Femtosecond laser pulse is stretched in the optical fiber.*

A home built experiment setup based on a Nikon inverted microscope (TE-2000U) was used for the optical transfection experiment as shown in Fig. 4.12. A half-wave plate was used to adjust the laser polarization direction before it was directed into a combination of a half-wave plate and an optical isolator (Laser2000, UK, I-80-2), which were used to eliminate back reflection from the beam path. A magnifying telescope (L1 + L2) of magnification 1.6X was used to expand the incoming laser beam which was subsequently coupled to the 35 cm long optical fiber, through a fiber collimator (Thorlabs, F810FC-780). The overall coupling efficiency for fiber collimator and axicon tipped fiber was ~35%. The fiber output power was adjusted using a variable neutral density (ND) filter wheel (not shown in Fig. 4.12) appropriately placed in

the beam path. The sample dish was held on the microscope stage and imaged from below.

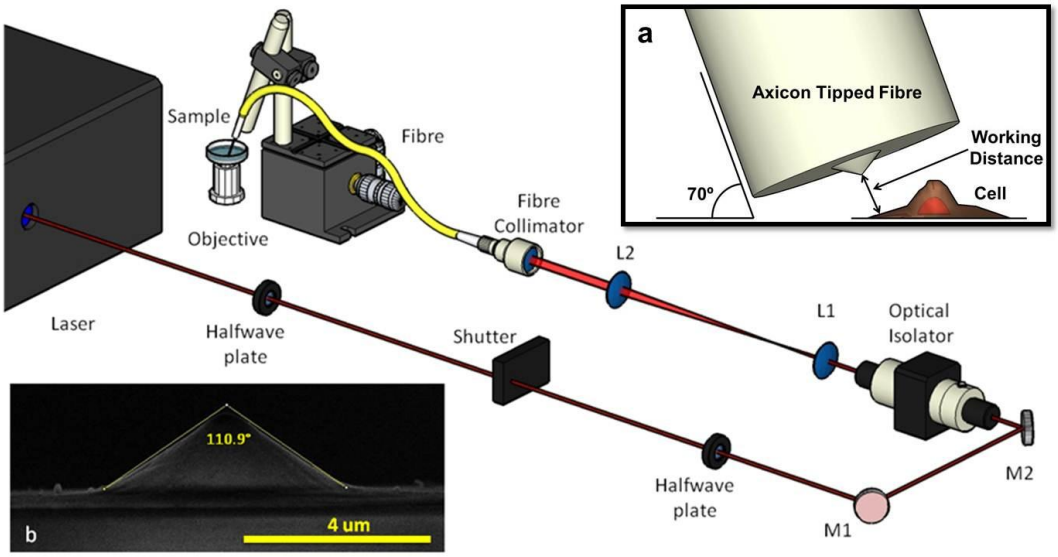

Fig. 4.12. *Schematic of the experimental setup for fiber based optical transfection. The femtosecond laser beam passes through two half-wave plates, a shutter and an optical isolator. The beam is then directed by two mirrors (M1, M2) and expanded 1.6X by a lens pair (L1, L2) before entering the fiber collimator. The optical fiber is inserted into the sample dish, which is held on the microscope stage, and is controlled by a xyz translation stage. The microscope is omitted from this diagram for simplicity. Inset (a), which is drawn to scale, shows the position of the fiber with respect to a cell during the experiment. Inset (b) is an SEM image of an axicon of 110.9º fabricated at the tip of an optical fiber.*

During optical transfection the average power of the beam was kept at 30 mW, with a peak power per pulse of 0.47 kW. A mechanical shutter (Newport, UK, model 845HP-02) controlled the time duration of the laser dosage on the cell membrane. Each cell was irradiated with 3 – 5 laser doses. The duration of each dose was experimentally optimized to be 100 ms. The number of laser doses was experimentally determined to be the most successful number in conjunction with a dose duration of 100 ms. The peak intensity of the pulse was estimated to be ~4.4 x 10^9 W/cm^2 and

the total energy per dose was estimated to be 3 mJ.

The fiber was mounted on a xyz translation stage and carefully inserted into the medium (Fig. 4.12). Due to restrictions imposed by the geometry of the inverted microscope and the illumination from above, the fiber could not be accommodated vertically between the sample stage and microscope condenser without disrupting the imaging path. Also as it is clearly seen in Fig. 4.12(a), which is drawn to scale, if the fiber was positioned at an angle much smaller than 70º with respect to the substrate plane, the beam focus cannot reach the cell or can only focus on the center of the cell. During optical transfection, beam focusing is normally targeted to the cell membrane near the edge of a cell grown on the substrate. In this manner, focusing near the edge rather than on the center of a cell, significantly higher transfection efficiencies can be achieved. At an angle higher than 70º, the fiber would obstruct the illumination from above. The optimum angle for placing the fiber was experimentally defined to be 70º. The imaging effect of the cell using this configuration can be seen in Fig. 4.13, in which a cell, underneath the fiber, is under irradiation by the laser beam. From this configuration we can also see another advantage that the selective chemical etching method can provide: the decreased fiber cladding size (compared with bare tipped fiber whose cladding diameter is 125 µm) permitted the placement of the axicon at a short distance from cells. Normally during an experiment, the fiber was positioned at 70º with respect to the substrate plane, and was lowered until it reached the substrate. Then the fiber was lifted up by 1 to 3 µm depending on the shape of the cell so as to catch the cell membrane on the edge Fig. 4.12(a). During the experiment, the cell sample dish was held on the microscope sample stage, therefore to target a cell both fiber and cell sample dish can be moved.

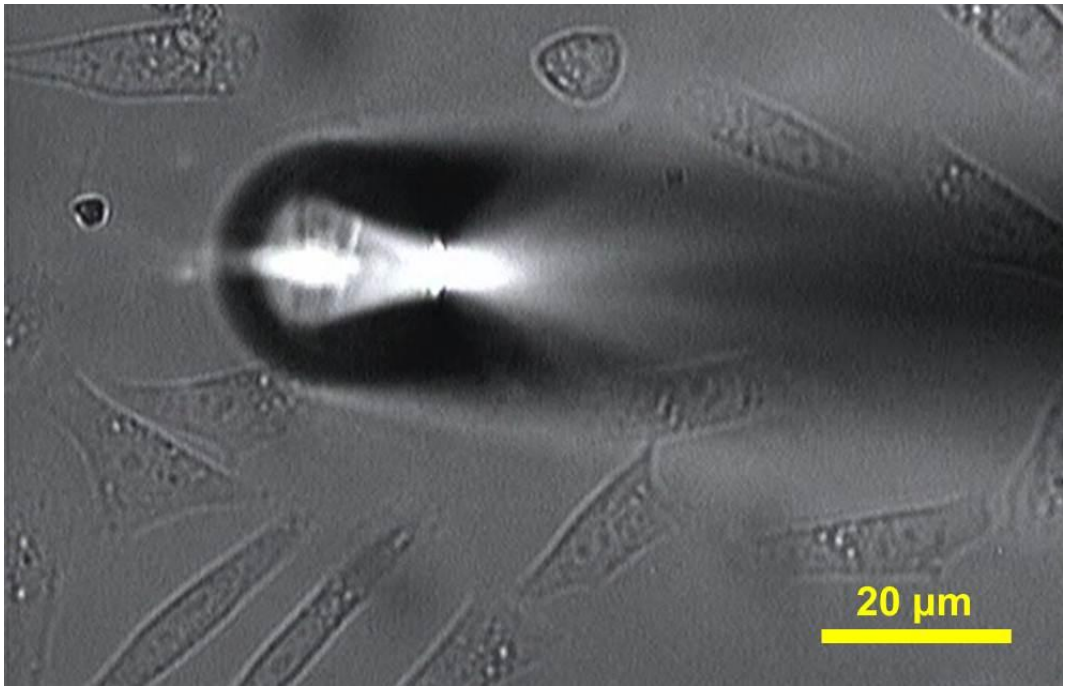

Fig. 4.13. *The imaging effect during optical transfection with an axicon tipped fiber. The image was taken from below with illumination from above. It can be seen that a cell is irradiated by the laser beam emitted by the axicon tipped fiber which is positioned at an angle. Due to the similar refractive indices of the fiber (~1.55) and surrounding medium (~1.33), the illumination can pass through the fiber and the cell underneath the fiber can be imaged.*

4.4.2 Sample Preparation

CHO-K1 cells were routinely cultured in modified eagles medium (MEM) (Sigma, UK) containing 10% fetal calf serum (FCS) (Sera Laboratories International, UK), penicillin (100 units/ml, Sigma, UK), streptomycin (100 µg/ml, Sigma, UK), and L-Glutamine (2 mM, Sigma, UK) in a humidified atmosphere of 5% CO_2 /95% air at 37 ºC. Cells were grown to sub-confluence in 30 mm diameter glass-bottomed petri dishes (World Precision Instruments, Stevenage, UK) in 2 ml of culturing medium. Prior to experimentation, the cell monolayer was washed twice with 2 ml OptiMEM (Invitrogen, UK) and for all experiments, the sample was bathed in 1 ml solution of OptiMEM containing 9 µg/ml mitoDsRED plasmid,

encoding a mitochondrially targeted *Discoideum sp*, red fluorescent protein (BD Biosciences, Oxford, UK).

Before the experiment, a circle with a diameter of a few millimeters was drawn on the underside of the sample dish and only selected cells from within this circle were laser treated. After laser treatment, the cell monolayer was washed twice with 2 ml of culturing medium before it was bathed in 2 ml of culturing medium and returned to the incubator. The sample was viewed under a fluorescent microscope 48 hours later, where successfully transfected cells within the circle expressed the red fluorescent protein. Fluorescent cells outside the circle were categorized as spontaneously transfected cells.

4.5. Results of Transfection

Fig. 4.14 shows an example of successfully transfected fluorescent cells. As in our previous studies, the transfection efficiency was defined as the number of cells correctly expressing the targeted red fluorescent protein 48 hours after laser treatment, divided by the total number of cells that were laser treated in a particular area of interest [30, 246]. To monitor for potentially spontaneously transfected cells, each photoporated sample dish was accompanied by a control sample dish in which cells were cultured, bathed in plasmid DNA solution and then experienced the fiber presence in the absence of laser radiation. During the whole course of this experiment, comprising 30 cells per dish for 15 dishes, 450 cells in total were laser treated. The transfection efficiency for each dish varied from 10% to 67% with an average transfection efficiency of 30.22% (with a standard error of the mean of 5.36%). The number of spontaneously transfected cells varied between 0 – 2 cells for each sample dish. Our result shows that the efficiency of the axicon tipped fiber based optical transfection technique is comparable to that of the free-space transfection [30].

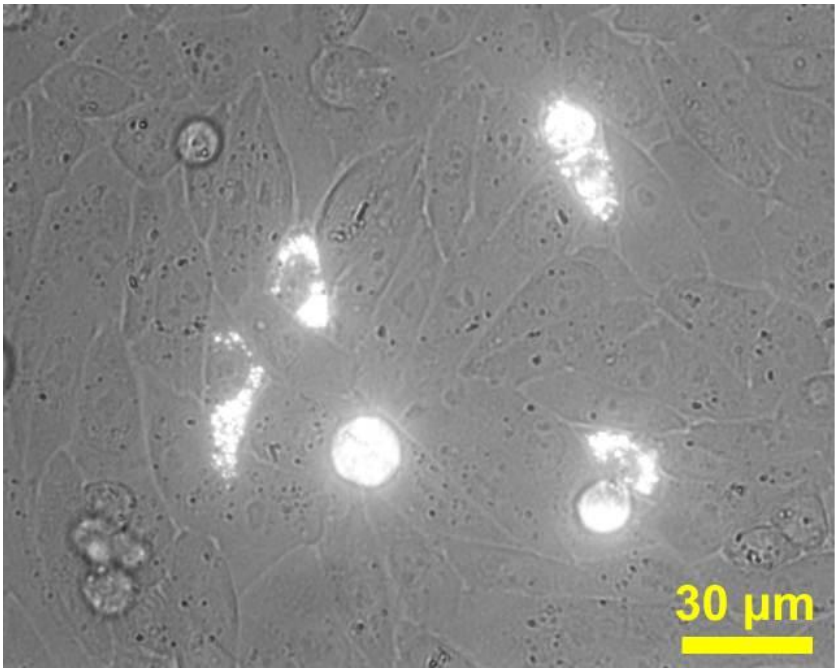

Fig. 4.14. *Successfully transfected CHO-K1 cells (bright cells) embedded in the cell monolayer. The picture was taken with both bright field illumination and fluorescence excitation. The bright fluorescent cells show the successful optical transfections while the other cells are left unaffected.*

During the experiment, the duration of laser treatment for each dish was controlled to be less than 25 minutes, so as to keep both potential airborne contamination and evaporation from the dish at a minimum. After laser treatment, the cells were kept for inspection for up to 5 days and no contamination (fungal, bacterial, etc.) was found and the cells showed a healthy appearance.

When targeting the beam focus on the cell membrane, sometimes there was accidental contact between the fiber tip and the cell. When this happened, the whole dish was disposed of and the fiber was cleaned using a sonicator. The output beam of the fiber was checked again to confirm that the fiber tip was not damaged. Damaged fibers were replaced for any subsequent experiments.

4.6. Summary and Conclusion

In this chapter I have shown successful axicon tipped fiber based optical transfection of CHO-K1 cells. A selective chemical etching method was adopted for fabrication of axicon tipped optical fibers. This method provides many advantages over the alternatives in this particular application of fiber based optical transfection. The fabrication and characterization of axicon tipped fibers and properties of the output beam in water have been discussed in detail. A theoretical model has been developed, which provide good simulation and prediction of the output beam from an axicon tipped fiber. Finally, based on experimental characterization, theoretical modeling and taking into consideration of some physical limitations, a fiber with an axicon of ~110º was chosen to perform optical transfection. A new experimental configuration, to include accommodation of the fiber into a microscope based optical transfection setup, positioning of the fiber relative to CHO-K1 cells, and imaging has been developed. The transfection efficiencies achieved compare favourably with the traditional free-space transfection technique.

Fiber based optical transfection provides greater flexibility over traditional methods and opens new directions towards tissue transfection, *in vivo* experiments in animal models and potential clinical applications. However, there are technical barriers that must be overcome before the fiber based optical transfection technique goes to a higher level of acceptance. The relatively short working distance of the axicon tipped fiber makes the manipulation during an experiment very difficult and slows down the photoporation process. Methods that can increase the working distance of a lensed fiber need to be developed. In the next chapter various newly developed lensed fiber fabrication methods will be presented. Fiber induced pulse stretching will reduce the two-photon effect and decrease the transfection efficiency. Although a 800 fs pulse duration proves to be adequate for optical transfection, a 35 cm long fiber lacks flexibility for application in a clinical environment. In the future, pulse

compensation techniques, LMA-PCF and hollow core PCF could be used to reduce the GVD and SPM effects, thus decreasing the pulse stretching and increasing the fiber length. Single cell selectivity is one of the unique advantages of optical transfection technique. With the use of optical fiber techniques combined with a localized drug delivery system, this advantage can greatly promote use of *in vivo* or clinical environment. In Chapter 5, the first attempt to build up such a system will be presented. A fiber based transfection technique could be potentially particularly useful for studying neurons *in vivo* or *ex vivo*, by selectively manipulating individual neurons within a large cell population.

This technique could be potentially commercialized. One of the possibilities for commercialization is the integration with endoscopy technique by passing the optical fiber over the working channel of a conventional endoscope, hence new functions, such as imaging, illumination and drug delivery could be readily realized. The optical fiber can also be used as a sensor *in vivo* by measuring the collected fluorescent signal from a pathological area [129]. In the following chapters, attempts to improve optical transfection technique towards potential use in clinical applications will be introduced.

Chapter 5:

5. Integrated Optical Transfection System Using a Microlens Fiber Combined with Microfluidic Gene Delivery

5.1. Introduction

Section 2.3 briefly reviewed the development of the traditional femtosecond optical transfection technique, which is performed using an expensive and bulky microscope-coupled optical system. In Chapter 4, a new approach was successfully demonstrated for cellular transfection, using an axicon tipped single mode optical fiber, fabricated using a selective chemical etching method. The inexpensive fiber based optical transfection method not only miniaturizes the whole system, but also potentially finds a new approach towards commercialization of the optical transfection technique. However in all these traditional and fiber based *in vitro* optical transfection experiments, the foreign genetic material to be transfected are homogenously mixed in the cell buffer medium. This arrangement is not compatible with the modern clinical endoscopy techniques and many *in vivo* experimental configurations. In the future, needle injection could be used in animal models for agent delivery, but it is not localized and increased physical damage may be induced. On occasion, particularly when using an injection agent that is precious or toxic, minimizing the amount of agent is paramount.

Development of an integrated system for localized gene delivery through a microfluidic system is necessary in order to move optical transfection technology towards *in vivo* applications. However, combining a micro-capillary based gene delivery system to the traditional bulk optics based system is not easily achieved, since the beam is delivered from outside of the sample dish through the microscope objective, while the drug has to be delivered within the sample medium. Hence the solution was to use fiber based light delivery system and combine it with a micro-

capillary based gene delivery system to achieve spatial localization of both optical transfection beam and gene delivery.

To the best of my knowledge, the only reported fiber based femtosecond optical transfection technique before this work used an axicon tipped optical fiber for light delivery (Chapter 4) [63]. However the HF based etching makes the fabrication procedure of axicon tips hazardous and also the transfection efficiency is very sensitive to the quality of the axicon tip. In addition, the short working distance produced by the axicon makes the targeting of the beam focus at the cell membrane very difficult: particular care has to be taken to make sure both fiber tip and cells are not damaged. The relatively large beam focus spot compared with traditional techniques may decrease the transfection efficiency. These limitations make axicon tipped fiber based optical transfection a non-viable technique for use in wider advanced invasive applications. Another solution is to fabricate a microlens at the tip of an optical fiber, whose properties can be tailored in order to obtain the optimum output beam characteristics for optical transfection and cell transfection.

Microlensed fibers are widely used in the field of communication for increasing coupling efficiency between terminals and interconnect [208]. These fibers are also used in the field of biomedical optics as endoscopic probe heads for OCT [143, 145], two-photon microscopy [250], scanning near-field optical microscopy [218] and spectroscopy [251]. As discussed in Chapter 3, there are various fabrication procedures reported for the fabrication of microlensed fibers. Considering the previously mentioned drawbacks of axicon tipped fiber based transfection, here I report a simple, inexpensive method for fabricating a polymer microlens at the tip of a standard optical fiber using commercially available UV curable adhesive. This method has been briefly described in Chapter 3 as one of the single-photon polymerization methods and the detailed fabrication process will be presented in this chapter. The SEM image of the fabricated microlens is shown in Fig. 5.1. This fabrication procedure affords the flexibility to tailor

the lens characteristics by changing the parameters of curing the adhesive. The microlenses yield a very small focal spot (2~3 μm) at a relatively large working distance (~20 μm). The efficiency of femtosecond transfection with this novel microlens was studied with CHO-K1 cells and HEK-293 cells.

Further, using the microlensed fiber mentioned above, an integrated system was engineered and this new system achieves highly localized delivery of DNA-containing fluid during transfection which is the first of its kind. In order to image cells during transfection, a MMF based illumination system was also embedded into the integrated system. This new integrated system was then used for the successful optical transfection of CHO-K1 cells and HEK-293 cells with MitoDsRed. Also the amount of DNA required for transfection could be reduced as the DNA is delivered locally, close to the cell to be transfected. I suggest that this miniaturized optical transfection system could readily be adapted for a myriad of *in vivo* applications, including the optical injection of membrane impermeable drugs.

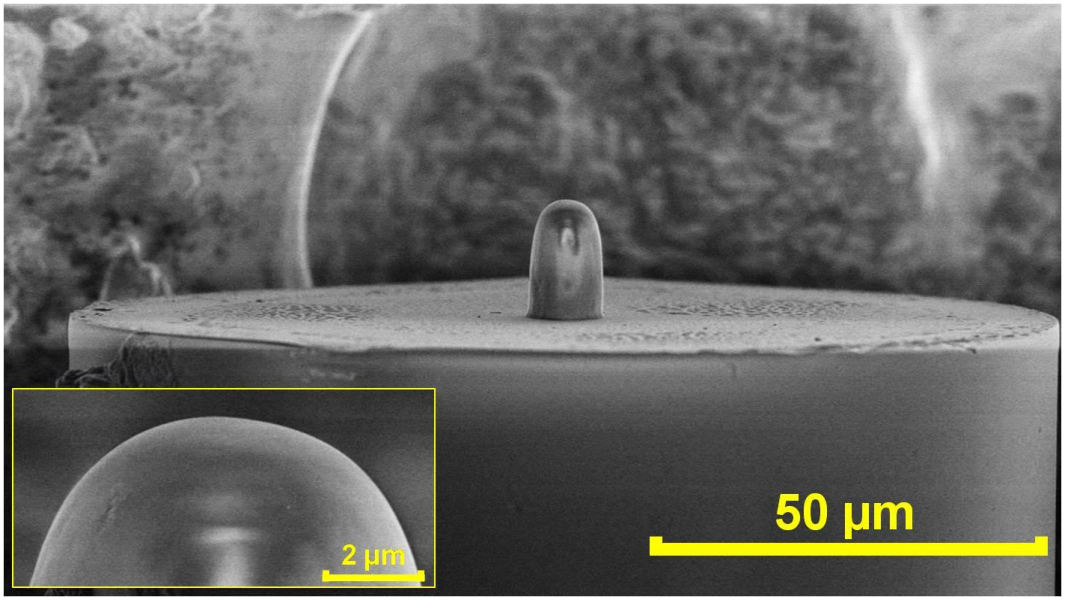

Fig. 5.1. *SEM image of the polymer microlens fabricated at the facet of an optical fiber. (inset): shows the apex of the microlens.*

5.2. Experiment

5.2.1 Fabrication and Characterization of Microlens Tipped Fiber

The polymer microlens was fabricated onto the tip of a standard SMF fiber by using a UV curable adhesive, cured with a focused UV beam. The commercially available SMF had a mode field diameter of 5.6 µm, cladding diameter 125 µm, and an operating wavelength of 830 ± 100 nm (Thorlabs, SM800-5.6-125). A UV curable adhesive (Norland, NOA 65) with optimum sensitivity for curing in the 350 – 380 nm range was used as the photopolymer for fabrication of the microlens due to its good adhesion to glass, fast curing time, easy processing, suitable refractive index (1.524 for polymerized resin) and high transmission efficiency (~98%) at 800 nm. These characteristics make the polymer lens ideal for the delivery of high peak power pulsed laser light without damaging the structure.

The basic approach in this fabrication method was to dip the cleaved tip of a fiber into the uncured adhesive and raise the tip out of the adhesive as slow as possible so that there would be a drop of adhesive stuck onto the tip through surface tension. Further, using an appropriate beam profile of a violet diode laser (Toptica Photonics CVLS-LH050-2V1, λ = 405 nm, maximum output power = 40 mW) the adhesive was cured using a controlled power and exposure time in order to achieve the desired parameters for the microlens.

The schematic diagram of the setup used to cure the optical adhesive so as to fabricate the ‘microstick’ is shown in Fig. 5.2. A violet diode laser beam was shaped to TEM_{00} mode by coupling it to a SMF (Thorlabs, S405-HP) through a fiber coupler (10X objective lens). The optical fiber was carefully cleaved and the end face was examined using a SEM to make sure a flat end face was obtained. The lateral beam profile of the output beam was measured using a long working distance objective (Mitutoyo x100 infinity-corrected, 6 mm working distance) to confirm a high quality TEM_{00} Gaussian beam profile. A high quality beam profile and

good alignment of the system were essential for this fabrication method. The beam, directed by a 5 cm tube lens and a beam splitter, was focused by an objective (x60 Nikon) at the end face of a fiber. The lens was placed at ~6 cm away from the fiber to make the beam converge. After dipping the tip into the adhesive, the fiber on which the microlens was to be fabricated was vertically mounted on a xyz translation stage with 1 µm resolution. The fiber tip was imaged onto a CCD camera (WAT-250D) to position the curing beam at the centre of the fiber end face. A small portion of the laser light split from the laser output (not shown in Fig. 5.2) could be used to help finding the centre of the fiber end face by coupling the laser into the Optical Fiber 2 from the other side and imaging the visible core from below. The curing beam from below was then accurately focused on the bright core on the Optical Fiber 2 end face. This process guarantees the accurate alignment between the curing beam and the optical fiber, which is a common problem in many lensed fiber fabrication techniques (Chapter 3). A symmetrical diffraction pattern of the focused curing beam on the end face of the Optical Fiber 2 also indicates a good alignment of the system. The exposure of the curing beam was controlled by a shutter (Newport, UK, model 845HP-02).

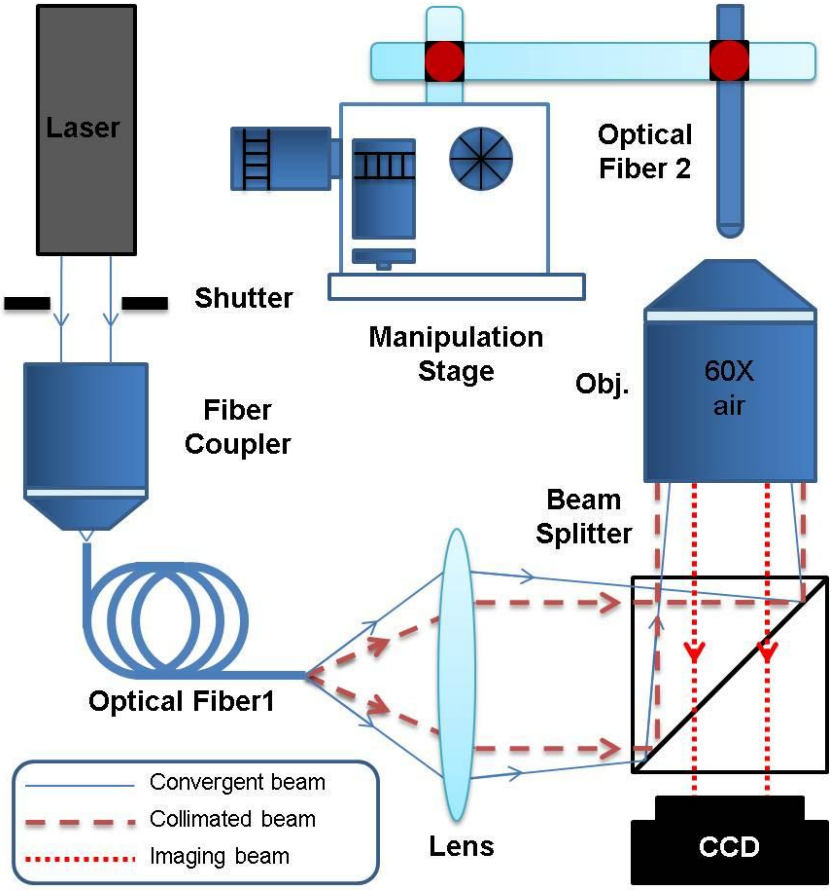

Fig. 5.2. *Microlens tipped fiber fabrication setup (method 1). A violet diode laser (405 nm) is coupled into a SMF (Optical Fiber 1) through a 10X objective lens to obtain an output beam with near-perfect Gaussian lateral distribution. The beam, directed by a 5 cm tube lens and a beam splitting cube is focused by a 60X objective at the cleaved facet of a fiber. The lens is placed at 6 cm away from the Optical Fiber 1 to make the beam converging. The fiber on which microlens is to be fabricated (Optical Fiber 2) is mounted in the setup using a xyz stage with 1 µm resolution, after dipping it into the uncured UV adhesive which forms a drop of the adhesive at fiber tip. The adhesive at the tip of the Optical Fiber 2 is cured for 5 s with the laser power of 0.5 mW.*

The steps involved in microlens fabrication are schematically shown in Fig. 5.3. A well cleaved optical fiber was vertically dipped and raised from a drop of UV curable adhesive as slowly as possible such that a hemisphere of adhesive on the fiber tip would be formed. The size of the

hemisphere is mainly decided by the properties of the adhesive (such as surface tension, elasticity) and the pulling speed of the optical fiber from the adhesive only affects the hemisphere size slightly. By doing the pulling as slowly as possible the size of the hemisphere can be kept as constant as possible. This fiber was then mounted to the curing setup as shown in Fig. 5.2. Keeping the power of the laser below the threshold (<0.1 mW), where the curing process would not be initiated, the laser beam was positioned at the centre of fiber tip facet and defocused by 20 µm from the tip of the fiber in order to get the correct beam shape which could produce the desired lens structure. The power of the laser was increased to 0.5 mW to start the curing process. At the beginning of the polymerization process, UV adhesive would partially cure around the centre of fiber facet followed by a growth towards the direction of the laser. After an exposure for 5 s, the unpolymerized adhesive was removed using acetone and a 'microstick' (an extended microlens as shown in Fig. 5.1) was created. At the apex of 'microstick' a curved facet was formed which acts as a focusing surface for the output beam from the fiber and the 'microstick' acts as an extension that allows the output beam to expand before it is being focused by the apex.

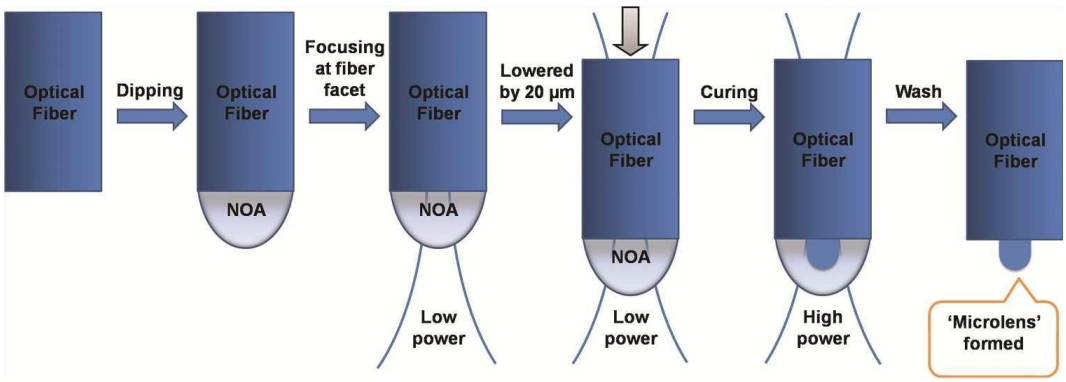

Fig. 5.3. *Steps involved in the fabrication of lens at the tip of the fiber. The relative position between the fiber and the curing beam was adjusted through these steps in order to find a suitable curing beam distribution, which can fabricate a lens-like structure.*

The fabrication procedure is highly flexible, and by changing the parameters such as the light distribution (which is controlled by convergency of the curing beam and the relative position between the end face of the fiber and the focus of the curing beam) near to the focus of the curing beam, intensity of the curing beam (for controlling the curing speed) or curing time (which decides the size of the fabricated structures), it was possible to fabricate different structures at the tip of the fiber as shown in Fig. 5.4 which shows that, the structures created are strongly related to the beam distribution. In order to obtain a lens-like structure, curing parameters were optimized through a series reiterative experiments and within each experiment, one of the parameters was adjusted slightly.

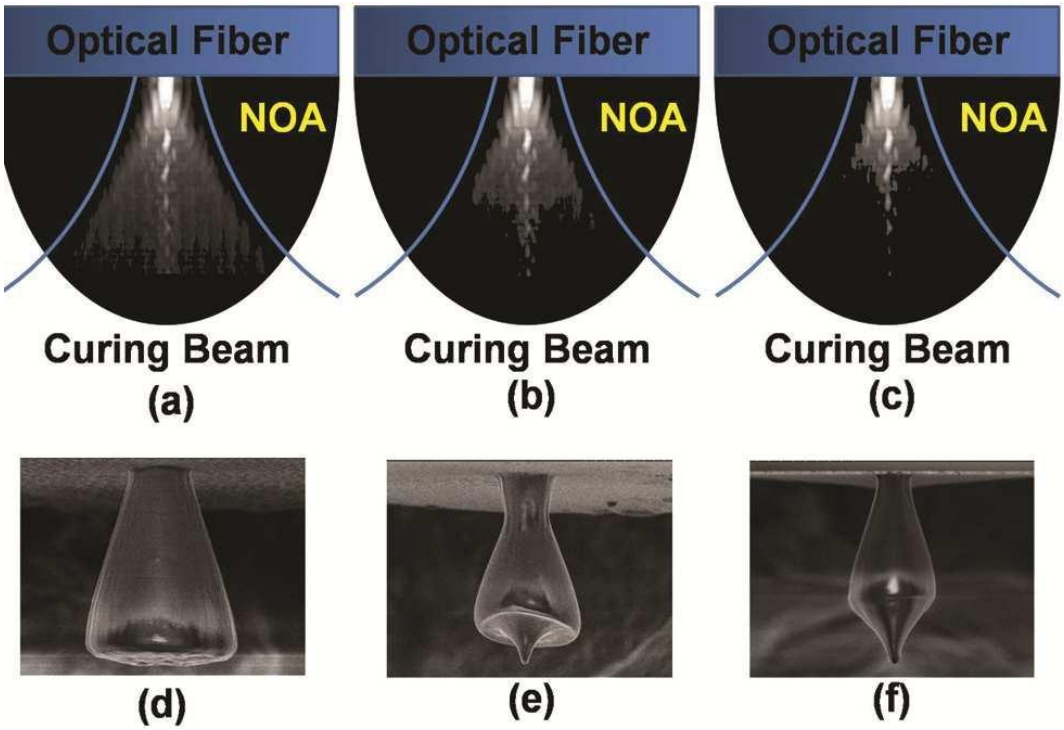

Fig. 5.4. *Different structures can be made by changing the curing beam distribution. Using curing beam (a), (b) and (c) with appropriate laser power and curing time structures like (d), (e) and (f) respectively were fabricated.*

The fabricated lens was characterized by using SEM and beam profiling. One of the SEM images of the microlens at the tip of the fiber is

shown in Fig. 5.1. The physical parameters of the lens were estimated from the SEM images. The height of the lens was estimated as 11 ± 1 µm, base diameter 7 ± 1 µm and top diameter 5 ± 1 µm.

The output beam profile was characterized in a similar way as described in Section 3.3.1. Briefly, an 800 nm laser from a Ti-Sapphire laser (Coherent, MIRA) was coupled to the microlens tipped fiber and the output beam from the microlens was profiled in water from a series of lateral cross-sections with a 5 µm step change using a water immersion objective (x60 Olympus UPlanSApo) (Fig. 5.5) in conjunction with a CCD camera (WAT-250D). The working distance of the lens (distance of the focal plane from the apex of the lens) and the diameter of the focal spot were estimated from the beam profile (Fig. 5.5). The estimated working distance of the beam was 20 ± 2 µm, the focal spot diameter was 3 ± 0.05 µm and the beam divergence was 15º.

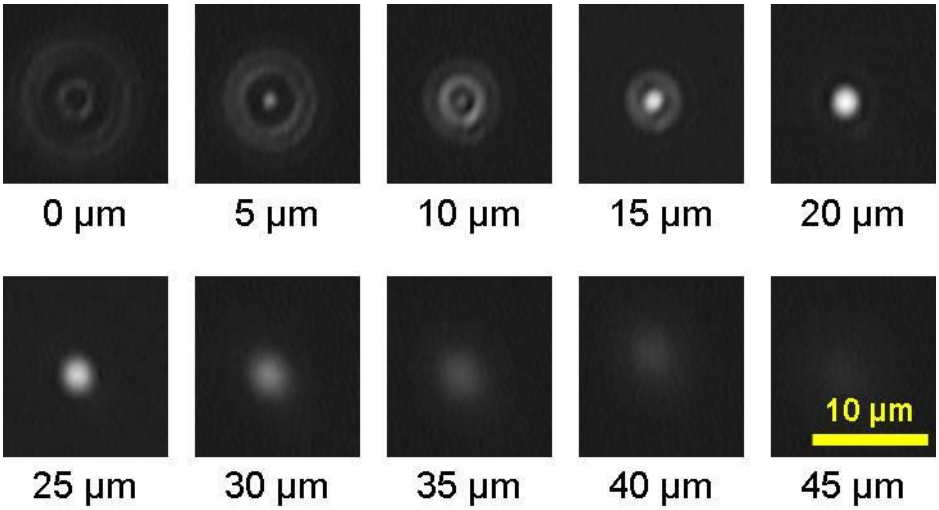

Fig. 5.5. *Images of the cross sections of the output beam from a microlens tipped fiber taken at different position from 0 µm (defined at the apex of the microlens) to 45 µm along the output beam.*

5.2.2 Cell Transfection Using the Microlens Fiber

CHO-K1 and HEK-293 cells were routinely cultured according to the protocol described in Section 3.4.2. Cells were grown to sub-confluence in 30 mm diameter glass-bottomed Petri dishes (World Precision Instruments, Stevenage, UK) in 2 ml of culturing medium. Prior to experimentation, the cell monolayer was washed twice with OptiMEM (Invitrogen) and for the microlensed fiber based transfection, the sample was bathed in 1 ml solution of OptiMEM containing 9 µg/ml mitoDsRED. For the transfection performed using the integrated system, the solution was delivered microfluidically.

Cell transfection was instigated by a femtosecond Ti: Sapphire laser emitting at 800 nm, with an output pulse duration of ~100 fs and a pulse repetition frequency of 80 MHz (Coherent, MIRA). At the output end of the microlens tipped fiber, the pulse undergoes stretching due to non-linear phenomena occurring inside the fiber - SPM and GVD - giving an overall pulse duration of approximately 800 fs, as measured using a home built auto-correlator [249]. A home built optical transfection setup was used for the optical transfection experiment as shown in Fig. 5.6.

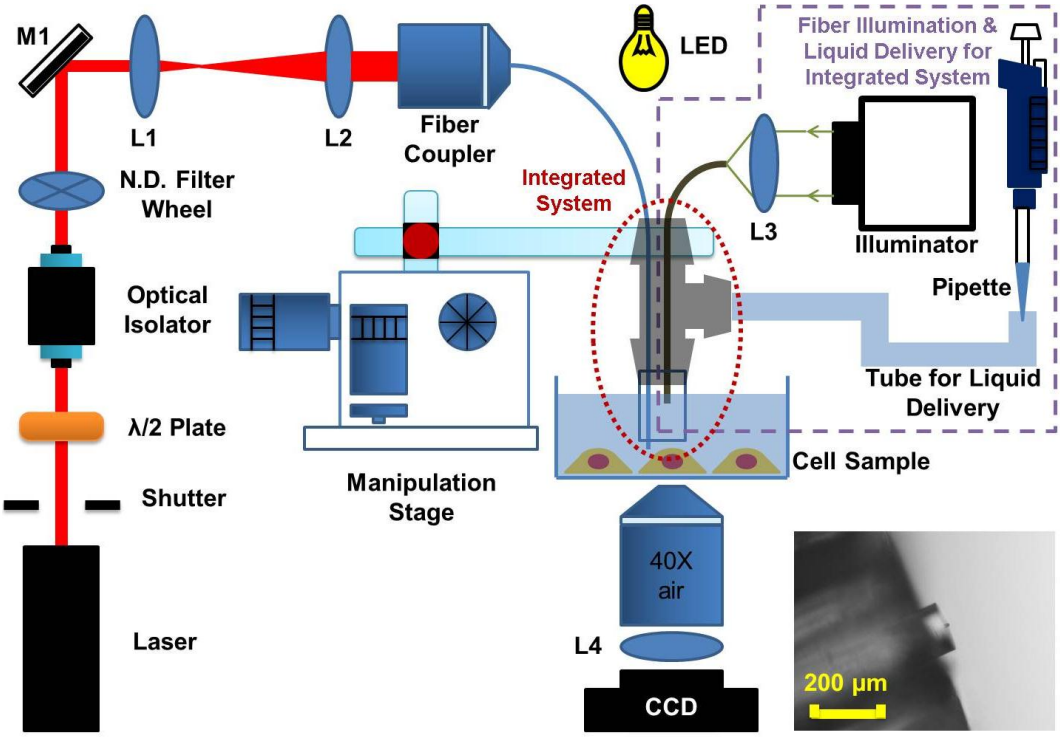

Fig. 5.6. *Schematic of the experimental setup for fiber based optical transfection. A collimated laser beam generated by Ti: Sapphire laser is directed onto a half wave plate and an optical isolator. Lens L1 and L2 expands the incoming laser beam by 1.6 times and subsequently couples the beam into the 35 cm long optical fiber, through a fiber collimator. For microlens tipped fiber transfection, an LED light source is used for illumination. For integrated system, the illumination fiber is connected to a home built fiber illuminator and a micropipette is connected to liquid delivery tube. The inset picture shows the side view of the tip of the integrated system.*

A collimated laser beam was directed into a combination of a half-wave plate and an optical isolator (Laser2000, UK, I-80-2), which were used to eliminate the back reflection from the beam path. A magnifying telescope of magnification 1.6X was used to expand the incoming laser beam which was subsequently coupled to the 35 cm long optical fiber, through a fiber collimator (Thorlabs, F810FC-780). The fiber output power was adjusted using a variable ND filter wheel appropriately placed in the beam path. During optical transfection, the average power of the beam

was kept at 20 mW, with a peak power per pulse of 0.31 kW. The fiber was mounted on a xyz translation stage and was carefully inserted into the medium. A mechanical shutter (Newport, UK, model 845HP-02) controlled the time duration of the laser dosage on the cell membrane. Each cell was irradiated with 3 - 5 laser doses. The duration of each dose was experimentally optimized to be 100 ms. The peak intensity of the pulse was estimated to be 4.4×10^9 W/cm^2 and the total energy per dose was estimated to be 2 mJ.

For microlens tipped fiber transfection, due to the restrictions imposed by the geometry of the fiber and the imaging path, the fiber was tilted at a ~5 – 10° angle with respect to the vertical axis. With a white LED light source on top and an imaging system below the sample, the sample cells were observed during the transfection procedure as shown in Fig. 5.7(b). During laser irradiation no visual response was observed. After the laser treatment, the cell monolayer was washed three times by, and thereafter bathed in, 2 ml complete medium and returned to the incubator. The sample was viewed 48 hours later under a fluorescent microscope, where successfully transfected cells expressed the red fluorescent protein as shown in Fig. 5.11.

The microlens tipped fiber has a relatively long working distance (~20 µm) which made it easy to be positioned and focused on the cell membrane. In contrast to the axicon tipped fiber based transfection, transfection with a microlensed fiber does not need focusing and re-focusing for transfection of each cell and therefore greatly increase the transfection throughput. During the transfection, the beam focus was fixed at 5 µm above bottom of the Petri dish, which is the average height of these cells adhered to the bottom of the dish. Without any further axial positioning, the tip of the fiber could be laterally scanned in order to transfect different cells within one Petri dish.

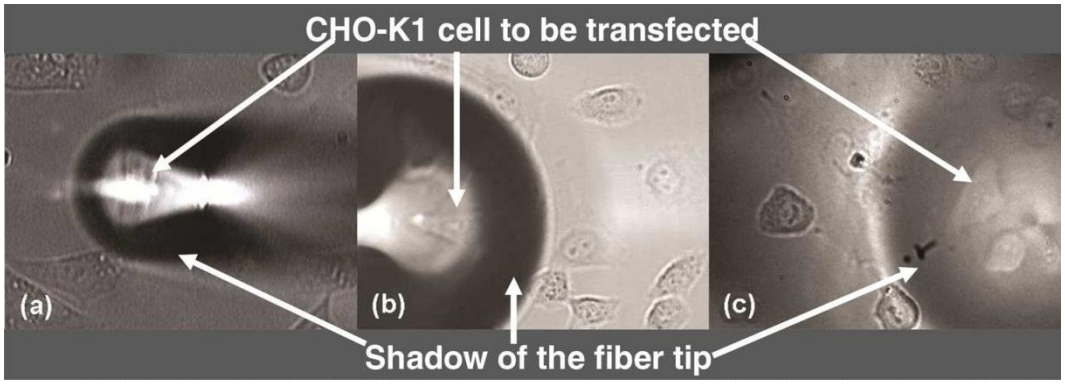

Fig. 5.7. *Illumination at the cell sample during optical transfection using (a) axicon tipped fiber; (b) microlens tipped fiber and (c) integrated system. It can be seen that, with the fiber based illumination, the cell boundaries are clearly visible during the transfection procedure, when transfected with the integrated system (c).*

5.2.3 Design of an Integrated System for Localized Drug Delivery

In order to achieve localized drug delivery during optical transfection, the microlensed fiber mentioned in the previous section was integrated with a micro-capillary tube (Harvard Apparatus, Inner Diameter = 0.58 mm, Outer Diameter = 1 mm). The implementation of this integrated drug delivery system in the optical transfection device is shown in Fig. 5.6. A barbed T junction (Harvard Apparatus, 72-1487) with three ports was used to build this integrated system as shown in Fig. 5.9(a). The micro-capillary was attached to port 1 of the T junction using flexible plastic tubing (Tygon T3601, I.D. = 0.8 mm, O.D. = 2.4 mm) as a connector. The microlensed fiber was inserted through port 2, into the microcapillary and the tip of the fiber was positioned close to the tip of the microcapillary, as shown in Fig. 5.9(a). A cleaved MMF of core diameter 200 µm (Thorlabs, BFL37-200) was also inserted similarly into the microcapillary in order to achieve uniform illumination in a liquid environment. The optimum distance of the tip of the MMF from the apex of the microlens was experimentally estimated to be ~1 cm so as to achieve the best contrast for the sample. A slide clamp (WPI, Luer Valve

Assortment, 14042) was used to seal the flexible tubing, attached to the fiber inlet port, in order to ensure that the system was air-tight during sample injection. The flexible tubing, attached to port 3 was used for DNA delivery, whilst the other end was connected to a micropipette. A photograph of the integrated system is shown in Fig. 5.9(b), where a gene delivery system and a fiber based illumination system are combined with the microlens tipped fiber.

For optical transfection, the sample was bathed in 1 ml OptiMEM, whilst 1 ml of OptiMEM containing 20 µg/ml mitoDsRED plasmid was loaded into the pipette for delivery. The pipette, loaded with the DNA was connected to the integrated system through a tube as shown in Fig. 5.6. Controlled injection of DNA locally into the medium, in the vicinity of the cell to be transfected, was achieved using the pipette during optical transfection. The injection was tested and practiced using food colouring (Fig. 5.8) to ensure that the cells were immersed in the genetic material during laser irradiation. By slight twisting (rather than pushing) the button on the pipette, the food colouring was slowly injected into the medium. From Fig. 5.8 it is can be seen that this is a highly controllable process and the resolution of the liquid delivering can be controlled using pipettes of different resolution. The flow rate of the buffer containing DNA, inside the microcapillary, was estimated to be 630 µm/s. Each cell was exposed to this flow for ~5 s, which results in a delivery of 0.02 µg of DNA per cell.

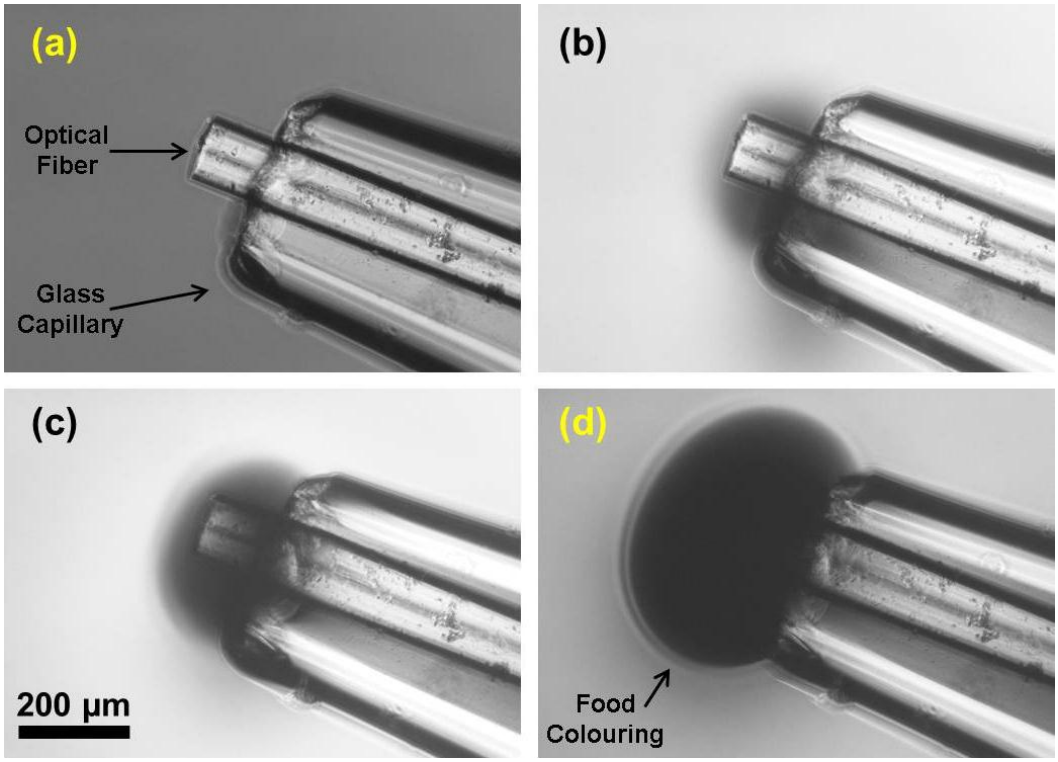

Fig. 5.8. *Test of the DNA delivery using food colouring. By twisting (rather than pushing) the button on the pipette, which is connected to the integrated system through a tube, the food colouring is slowly injected into the liquid environment. This is a highly controllable process and the resolution of the liquid delivery can be controlled by selecting pipettes of different resolution. From the scale of the graphs, it can be seen that a cell will be completely immersed in the DNA agent during transfection experiment.*

In order to demonstrate the ability of the system to optically transfect cell lines, CHO-K1 and HEK-293 cells were transfected using this integrated system. An image of cells recorded during optical transfection with the integrated illumination system, is shown in Fig. 5.7(c). Despite the poor image contrast due to a shadow cast by the optical transfection fiber, when targeted cells were imaged, the cell boundaries were clearly visible, which permitted them to be transfected. For the purpose of comparison, the imaging of cells during the axicon tipped fiber transfection experiment is also showed in Fig. 5.7(a).

In order to ensure the sterility of the drug delivery system, before each transfection experiment 2 ml of 70% ethanol was run through to sterilize the whole system and was subsequently dried using filtered air. The same capillary tube was used for multiple transfection experiments and the subsequent experiments showed that the system remains sterile with the above mentioned sterilization procedure.

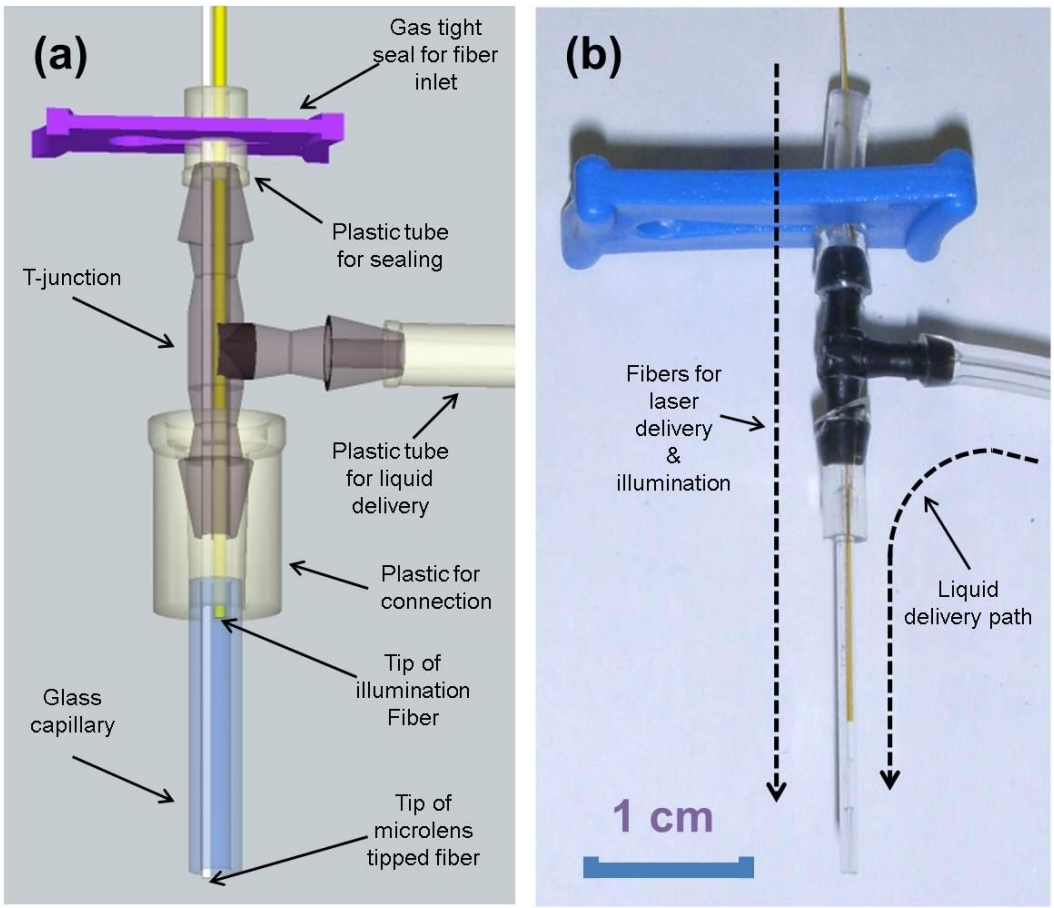

Fig. 5.9. *(a) Design of the integrated system. A glass capillary tube with 580 µm inner diameter is connected to port 1 of a barbed T junction through a piece of plastic tube. One optical fiber for laser delivery and another multimode fiber for illumination are inserted into the glass capillary through port 2. A piece of plastic tube and a slide clamp are used to hold two fibers and seal the fiber inlet at the same time. Another piece of plastic tube for liquid delivery is connected to port 3 of T junction. (b) Photograph of the integrated system.*

5.3. Results and Discussion

Figure 5.10 shows the comparison of the transfection efficiency of CHO-K1 cells achieved using an axicon tipped fiber (obtained from Section 3.5), microlens tipped fiber and my integrated system respectively, and in addition the transfection efficiency of HEK-293, transfected with the integrated system. The transfection efficiency is calculated in a same way to those presented in previously reported studies. It is defined as the number of cells expressing the targeted red fluorescent protein after 48 hours after laser treatment, divided by the total number of cells that were laser treated in a particular area of interest [30, 246]. An example of successfully transfected fluorescent cells is shown in Fig. 5.11. In order to monitor for potentially spontaneous transfected cells, each photoporated sample dish was accompanied by a control sample dish in which cells were cultured, bathed in plasmid DNA solution and then experienced the fiber presence in the absence of laser radiation. The number of treated cells and the results are summarized in Table 5.1. The number of spontaneously transfected cells varied between 0 – 2 cells for each sample dish.

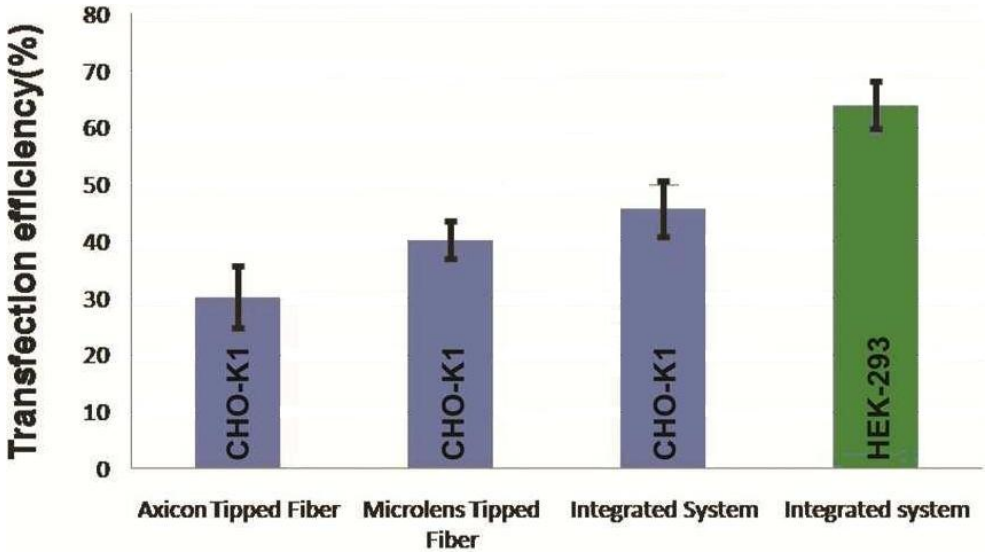

Fig. 5.10. *The transfection results of CHO-K1 and HEK-293 cells using 3 different methods. The error bar shown is standard error of the mean.*

	Cell type	*No. of Dish Treated*	*Total No. of Treated cells*	*Transfection Efficiency (±SM) (%)*
Axicon tipped fiber	CHO-K1	15	450	30.22 ± 5.36
Microlens tipped fiber	CHO-K1	20	800	40.25 ± 3.39
Integrated system	CHO-K1	15	525	45.71 ± 4.84
	HEK-293	5	175	64.00 ± 4.10

Table 5.1. *Transfection results. SM indicates the standard error of the mean.*

My results show that the efficiency of the fiber based optical transfection technique is comparable to that of the free-space transfection [30]. Also as shown in these results, the microlens tipped fiber provides significantly higher transfection efficiency with a smaller margin of transfection efficiency than the axicon tipped fiber method. This reflects the fact that due to the longer working distance, the manipulation of a microlens tipped fiber is easier and more stable when compared to an axicon tipped fiber. During the transfection procedure, the axial focal position needed to be found only at the beginning of the procedure and then multiple cells in the same sample dish could be photoporated by solely moving the fiber mount laterally. This results in reduced damage to both cells and the fiber tip, high transfection efficiency and more consistency.

The transfection efficiency for the integrated system with localized gene delivery is comparable to that of non-localized gene delivery systems. The slightly higher transfection efficiency might be attributed to the higher local concentration of DNA near the transfected cells. The average concentration of the DNA in the cell medium after treating 35 cells in a

dish is estimated to be 1.3 µg/ml, in contrast to the average DNA concentration of 9 µg/ml used for the non-integrated system. It was shown in previously reported studies that the transfection efficiency reduces dramatically below 9 µg/ml of DNA concentration [43, 51]. The resultant transfection efficiency obtained shows that our localized gene delivery is successful in creating a localized high concentration of plasmid in the vicinity of the cell to be transfected. This means that the total required amount of DNA for performing transfection procedure is significantly low for integrated system compared to that of non-integrated systems.

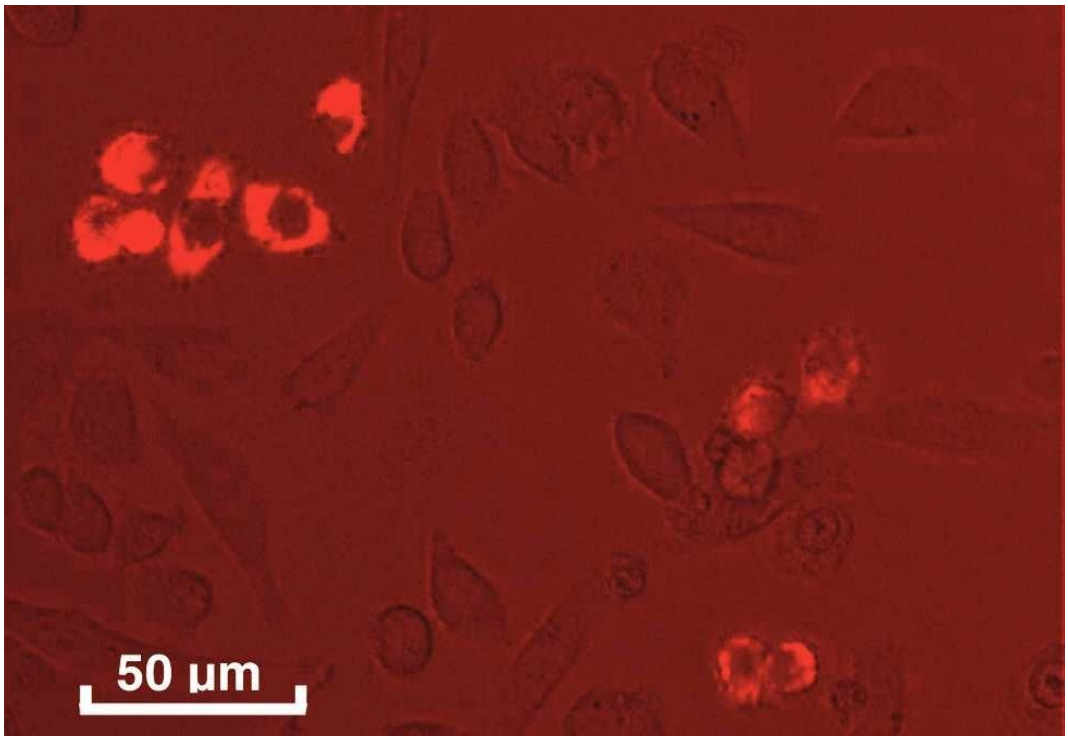

Fig. 5.11. *Fluorescent microscope image of optically transfected CHO-K1 cells, incubated for 48 hours after transfection. The bright cells are transfected successfully resulting in the uptake of the plasmid and thereby expressing the mitochondrially targeted red fluorescent protein.*

5.4. Summary and Conclusion

This chapter has reported the first realization of an optical transfection system which can deliver genes locally, near the vicinity of the cell to be transfected. In order to achieve this, a fiber based optical transfection system was developed which is viable and easy to implement compared to its previously reported counterpart – the traditional optical transfection system. A novel fabrication method is described to produce a polymer microlens at the tip of an optical fiber. This technique is cheap, less complex than most of the other lensed fiber fabrication techniques and has the flexibility of fabricating customized microlenses for specific applications compared to other existing microlens fabrication techniques. This fabrication technique was used to fabricate a 'microstick' which can produce a tightly focused beam (~3 μm focal diameter) with a comparatively large working distance (~20 μm), which is ideal for fiber based femtosecond optical transfection of cells. This microlens tipped fiber was used for optical transfection of CHO-K1 cells and the transfection efficiency achieved is comparable to that of conventional free-space optical transfection setups and significantly better than the previously reported axicon tipped fiber based optical transfection. By combining the microlens tipped fiber with a microcapillary system, an integrated system that achieves localized drug (gene) delivery during transfection was realized. A MMF based illumination system was also combined with this integrated system to allow the efficient visual identification of the cell boundaries during optical transfection. This integrated system was used for optical transfection of CHO-K1 and HEK-293 cells and the obtained transfection efficiency was better than that of the non-integrated system. Also with the integrated system, the total amount of DNA required for transfection could be lowered significantly. This new technique opens up prospects for a portable "hand-held" system that can locally deliver therapeutic agents and transfect cells within a fiber geometry placing minimal requirements upon any microscope system. However, an

objective lens was still needed in the configuration of this experiment, which prevents the integrated system to be used in *in vivo* applications. The next chapter will introduce a fiber based optical transfection system on a microscope free platform which would be compatible with an endoscopic system to achieve *in vivo* optical transfection.

Chapter 6:

6. Optical Transfection Using an Endoscope-like System

6.1. Introduction

Laser-mediated optical nanosurgery has been developing rapidly in recent years [246]. Pulsed lasers [28, 30, 31] and CW lasers [29] spanning the infrared [28] to UV range of the electromagnetic spectrum [29] have found applications in this area. Two-photon microscopy [252], cellular microsurgery [253], neuron regeneration [45], tissue ablation [254], optical injection [64], and optical transfection [28, 30], have all been studied. However, traditionally these forms of experiments have involved a free-space optical setup, and a high NA objective lens, which is required to focus the laser beam onto the cellular sample. In addition, the short working distance and bulky size of microscope objectives have severely restricted the application of optical nanosurgery at depth. Therefore, researchers are now paying more attention to the potential use of optical fibers in order to advance such optical nanosurgery toward clinical applications. For example, Hoy et al. recently reported a miniaturized portable device for femtosecond laser microsurgery combined with two-photon imaging [46]. Another design based on a scanning double-clad fiber (DCF) was also used as a microendoscope for two-photon fluorescence imaging and cell nanosurgery [255, 256]. Both of their fiber probes had a working distance of over 200 µm, which could be used for deep skin treatment. In chapter 5, an integrated optical transfection system, using a microlens-tipped SMF combined with a localized microfluidic gene delivery and illumination has been reported [71]. Using this setup, a transfection efficiency comparable to that obtained with traditional free-space systems was achieved. However, the necessity of an objective lens for imaging prevents this system being used for *in vivo* applications at present. On the other hand, imaging fiber-based systems

with subcellular resolution have been developed [119, 257, 258] and applied in tissue imaging [259] and disease detection [260]. Optical fiber-based Raman spectroscopy [261] and fiber-based OCT [144] have all been developed. Generally, the use of optical fiber-based systems for the miniaturization of traditional optics tools is gaining more importance in the field of biophotonics.

Here report the first endoscope-like cell transfection system based on one single commercially available imaging fiber (coherent fiber bundle). Epifluorescence imaging with subcellular resolution, femtosecond laser light delivery, and microfluidic localized drug delivery were combined simultaneously. In order to achieve this, the exit face of an imaging fiber was chemically modified to create an ordered axicon array in order to increase the intensity and decrease the waist size (~3.75 µm) of the output laser beam at a relatively remote distance (~5 µm). A membrane permeable green fluorescent dye was used for epifluorescence cell imaging. Optical transfection experiments were then successfully carried out with this system on CHO-K1 cells. This system could be readily adapted for a number of laser mediated *in vivo* or *ex vivo* optical microsurgery experiments.

6.2. Experiment

6.2.1 Imaging Fiber Preparation

An imaging fiber (coherent optical fiber bundle) usually consists of a large number of cores (pixels), and each core can independently transmit light like a conventional SFM. The cores are normally laid in parallel in a honeycomb-like structure throughout the whole length (coherent configuration) of the fiber. Therefore, an image projected on to one end of the imaging fiber can be divided into pixels and transferred to the other end. The imaging fiber not only inherits most of the features of a conventional optical fiber, but it can also be used to image in traditionally

unattainable invasive endoscopic environments (e.g. the stomach, intestines, bladder, lymph nodes, brain, reproductive organs in females, and the prostate). In addition, it can substitute for an expensive articulated arm-based image acquisition setup, hence allowing its potential application into many new areas. However, the naturally divergent properties of the output beam from each core prevents imaging of objects (for example, biological cells) at a relative remote distance, which is necessary for the protection of both the fiber tip and cell from inadvertent damaging contact. Also, for optical transfection to occur, a high-intensity, micron-sized laser spot irradiated on the cell membrane is essential to initiate the required multiphoton process to permeabilize the cell membrane and minimize cell damage. Therefore a lens like microstructure at the end face of fiber tip is needed to focus or collimate the output beams. Specifically, a microlens has to be fabricated at the tip of each core of the imaging fiber in order to achieve optical transfection and imaging simultaneously.

The microlens tipped fiber fabrication technique was described and reviewed in Chapter 3. However, most of these procedures cannot readily fulfil the requirements of optical transfection mentioned above. As such, most methods are only suitable for a conventional single-core fiber and have disadvantages such as complexity, high cost, or lack of flexibility. However, chemical etching of the polished face of an imaging fiber using HF can create structures at the end facet of the imaging fiber, which is favourable to our application. An ordered array of conical lenses (axicon) made from each core of the imaging fiber are created at the end face of the imaging fiber tip [181, 186, 262]. Each axicon can focus the output beam from each core at a relative remote position, thereby increasing the intensity of produced light and, in addition, protect both the imaging fiber tip and cells.

The imaging fiber used in this work was a commercially available product (FIGH-06-300S, Fujikura, UK), where 6000 ± 600 cores (pixels) are embedded in a fiber cladding of 300 ± 25 μm in diameter, producing

an image circle of 270 ± 20 µm in diameter. The fiber was first soaked in acetone for a few seconds before the resin coating outside of the fiber cladding was wiped off using a lens-cleaning tissue. The conventional optical fiber cleaver and wedge-shaped diamond scribe were unable to perform a clean cleaving for our imaging fiber. Therefore, the fiber end face was manually polished using a method modified from a conventional fiber-polishing procedure [263]. A home-built holder based on a MMF connector (30126G2-340, Thorlabs, UK) was used to facilitate this process. Once a flat end face was obtained [Fig. 6.1(a) and 1(b)], the fiber tip was chemically etched with an etchant comprising of HF (48–51%) and ammonium fluoride (NH_4F, 40%). Different mixing proportions of these two solutions can create axicons of differing apex angles. With a decrease in the axicon apex angle, transmittance from the imaging fiber decreased substantially, which can be attributed to an increase in the total internal reflection within the axicon [181]. On the other hand, an increase in the axicon apex angle will increase the diameter of the focal spot and reduce the working distance, which is detrimental to optical transfection. In addition, because of the honeycomb-like structure and closeness of the cores, the axicon evolves into a pyramidal shape while the apex angle becomes larger (Fig. 6.2). This shape is not a preferred geometry for optical transfection and it limits the maximum apex angle of an axicon that can be created using a chemical etching method. Therefore, a compromised volume ratio of NH_4F to HF, 1.6:1, was chosen which creates an axicon cone angle of ~55º [Fig. 6.1(c) and 1(d)]. The fiber tip was immersed in the etchant for 10 minutes at 23 ºC room temperature. This procedure allows the axicon to be fully created before the cladding material was totally removed, thus keeping the imaging area uncompromised. The fiber tip was subsequently rinsed with both water and isopropanol, both for 30 s, to remove the residual etchant.

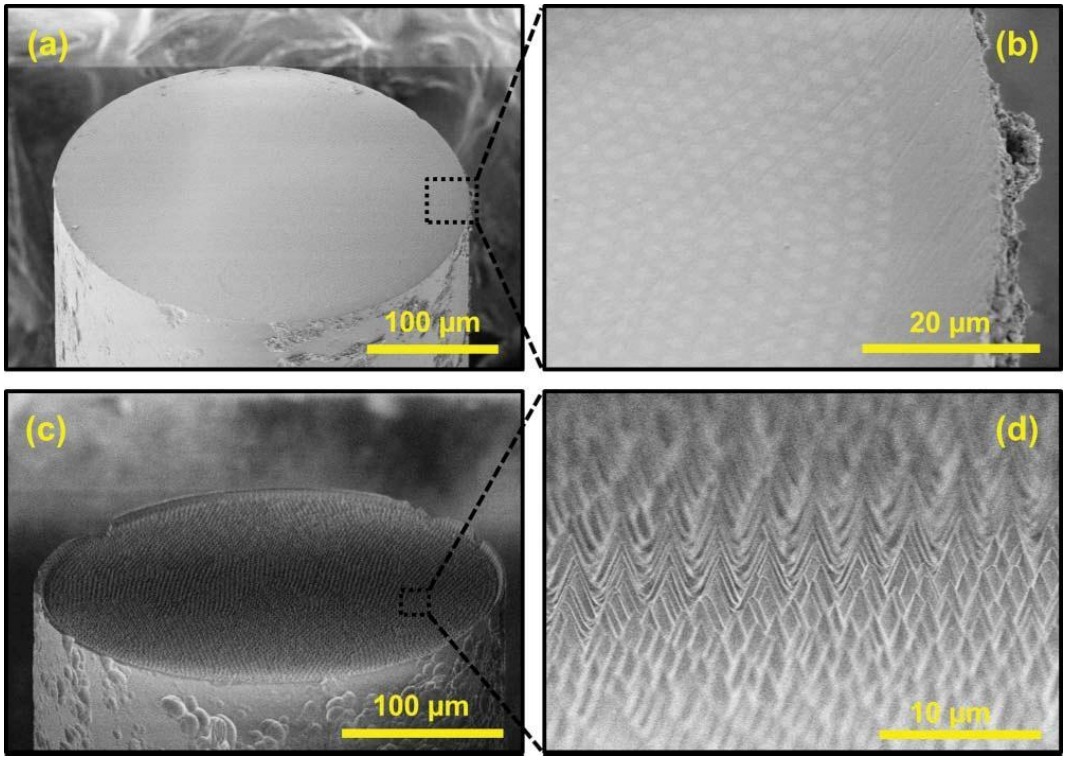

Fig. 6.1. *(a, b) SEM image of the polished imaging fiber end face, from which (c, d) an ordered axicon array was created using a chemical etching method.*

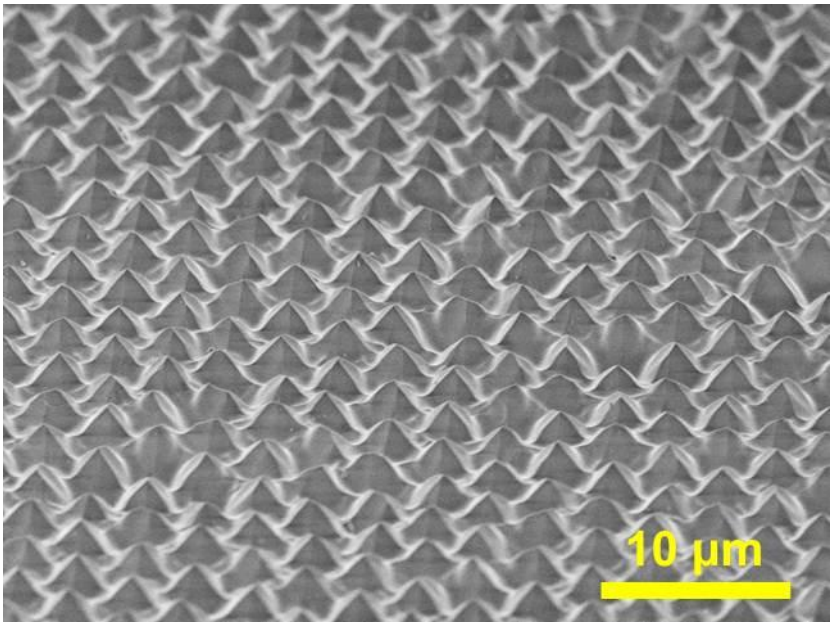

Fig. 6.2. *The axicons [Fig. 6.1(d)] evolve into a pyramidal shape while the apex angle of the axicon increases during chemical etching. This geometry is not suitable for optical transfection and therefore it limits the*

maximum apex angle of the axicons that can be created using chemical etching method.

6.2.2 Laser Output Characterization and Modeling

The imaging fiber output beam from a single core was analysed using a computer model modified from the literature [247] which has been proven to be precise for a wide range of different angles of the axicon tip including the work of axicon tipped fiber transfection reported in chapter 4. The same model was applied to the imaging fiber for the output beam analysis (Fig. 6.3). The detail of this theoretical model is shown in section 3.3.2.

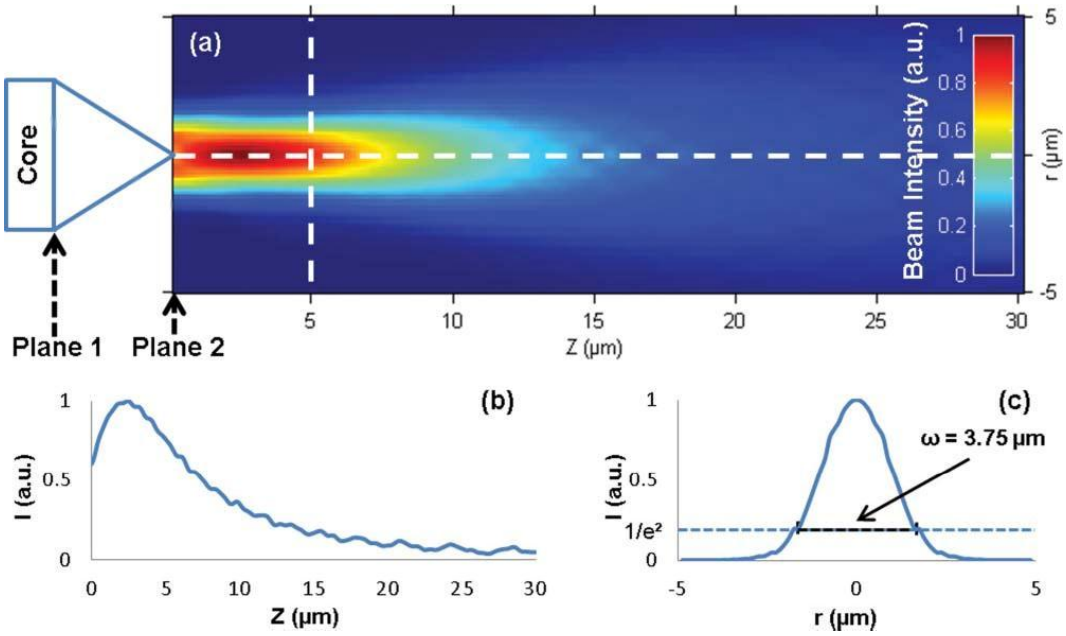

Fig. 6.3. *(a) The simulated axial intensity profiles of the fiber output beam in water; r and Z are the cylindrical coordinates with the Z-axis pointing in the direction of the beam propagation. Planes 1 and 2 were defined at the base and apex of the axicon tip, respectively. (b) On-axis intensity distribution corresponding to the horizontal dashed line in (a). (c) Transverse intensity distribution corresponding to vertical dashed line in (a). A beam diameter of ω = 3.75 µm can be obtained from it.*

Fig. 6.3(a) shows the theoretical results of the azimuthally averaged intensity profile of the beam as a function of the distance from the apex of the etched axicon in water. A 2.4 µm mode field diameter (average value from measurements) of the core, a 55º axicon angle and a wavelength of 800 nm were used in this modelling. The refractive index of the core and surrounding medium were assumed to be 1.5 and 1.33, respectively. Fig. 6.3(b) shows the on-axis intensity distribution corresponding to the horizontal dashed line in Fig. 6.3(a). From this can be seen that the peak intensity occurred at ~2.5 µm behind the axicon apex, which was considered too short to allow safe manipulation. Therefore, cells were targeted at 5 µm away from the axicon apex during the experiment. At this distance, a beam diameter (where the intensity falls to $1/e^2$ times the maximum value) of 3.75 µm was obtained [Fig. 6.3(c)]. The experimental measurements were in good agreement with the theoretical predictions.

6.2.3 Endoscope-like System

A system for the simultaneous epifluorescence imaging and optical transfection was constructed (Fig. 6.3). A half-wave plate was used to adjust the laser polarization direction before it was directed into a combination of a half-wave plate and an optical isolator (I-80-2, Laser2000, UK), which were then used to eliminate the back reflection from the optics. A dichroic mirror [(DM), DMLP425, Thorlabs, UK] was used to direct the incoming laser beam into the back aperture of a 10X objective lens, from which the laser beam was focused onto the input end face of the imaging fiber. The coupling efficiency of the objective imaging fiber system was ~40%. The fiber output power was adjusted using a variable ND filter wheel. The fiber was mounted on an xyz translation stage (not shown in Fig. 6.4) and was carefully inserted into the medium. A mechanical shutter (model 845HP-02, Newport, UK) controlled the laser exposure time on the cell membrane.

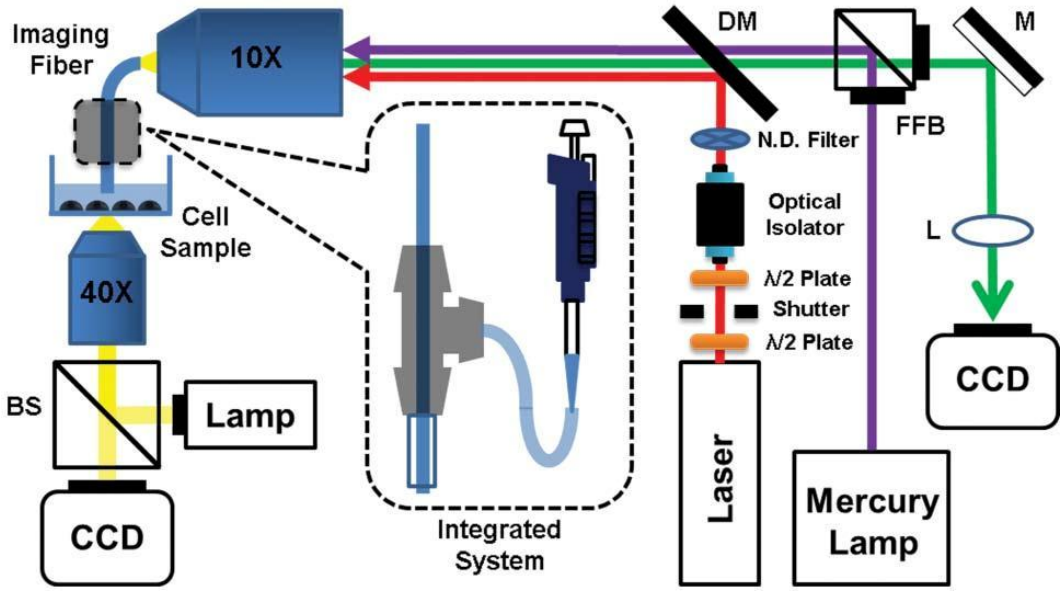

Fig. 6.4. *Schematic of the optical path for simultaneous epifluorescence imaging and optical transfection. The femtosecond laser beam passes through two half-wave plates, a shutter, an optical isolator, and a ND filter wheel before being directed into the back aperture of the 10 × objective lens by a DM. The epifluorescence excitation emitted from mercury lamp is simultaneously directed into the back aperture of the same objective lens by a fluorescence filter block (FFB). The output beam is subsequently focused onto the entrance face of a piece of imaging fiber targeting at the cell sample. The inset shows the imaging fiber is coupled through an "integrated system" for the localized drug delivery. The fluorescence emission collected by the same beam path is imaged by a lens (L) and CCD camera. The arrows indicate the direction of the light beams. Another imaging system with illumination underneath the cell sample was used for the ease of alignment of the whole system. Notation: beam splitter (BS), mirror (M).*

For epifluorescence imaging, a FFB (Nikon, B-2A) was used. The excitation light from 450–490 nm, indicated by the blue line (Fig. 6.4), was selected by the filter block and directed into the back aperture of the 10X objective by the filter block. The output beam was subsequently focused onto the entrance face of an imaging fiber targeting at the cell sample. The

fluorescence emission collected by the same beam path, indicated by the green line in Fig. 6.4, was imaged by a lens and CCD camera. The integrated system installed on the imaging fiber was described in Chapter 5. In this chapter, an upgraded version of this system replaced the microlens-tipped fiber and illumination fiber from the previous setup with a single imaging fiber. Epifluorescence imaging and illumination were both achieved through this imaging fiber. Another imaging system with illumination underneath the cell sample was used for the alignment of the whole system.

6.2.4 Cell Culture and Imaging

CHO-K1 cells were cultured according to the protocol described in Section 3.4.2. Prior to experimentation, the cell monolayer was washed twice with 2 ml of OptiMEM (Invitrogen, UK) then 2 μM of Calcein AM (Invitrogen, UK) in 1 ml of OptiMEM was added and the cells were further incubated for 15 min. Calcein AM is a cell-membrane permeable dye. In live cells, after acetoxymethyl ester hydrolysis by intracellular esterases, the non-fluorescent Calcein AM is converted to green fluorescent calcein. The power of the beam for the fluorescent excitation (450–490 nm) of the whole imaging field was <1 mW, and the average time of exposure for each cell was <5 s. Control dishes were prepared in the same manner without the treatment by laser.

A typical image taken during an experiment through the imaging fiber is shown in Fig. 6.5(a). Individual cores (pixels) can be clearly seen. The arrow in Fig. 6.5(a) indicates a cell that has been irradiated by a laser beam. Two relative brighter pixels in the centre of the cell are the back reflection from the cell. However, notably the laser beam was coupled into one core of the imaging fiber, which was confirmed by the imaging system underneath cell sample (Fig. 6.4), and the cell was irradiated by one beam spot at a time. According to the Nyquist-Shannon sampling theorem, the highest spatial frequency that can be resolved is given by 1/(2d), where d

is the core spacing in this case. Given a core spacing of ~3.8 µm, the lateral resolution of the current version of imaging fiber is ~7.6 µm, which is enough to identify individual cells. However, the contrast of the image could be enhanced through image-processing techniques. Fig. 6.5(b) shows the processed version of Fig. 6.5(a) after a fast Fourier transform (FFT) band-pass filter (filter large, small structures down, up to 480, 8 pixels) has been applied to filter out the honeycomb-like structure and increase the intensity while subtracting background noise. A real-time image processing at 25 Hz could be realized for on-line visualization of the sample. Also by using this method, the amount of Calcein AM and the power of the excitation beam, could be reduced, therefore decreasing the amount of potential disturbance to the cells caused by the imaging.

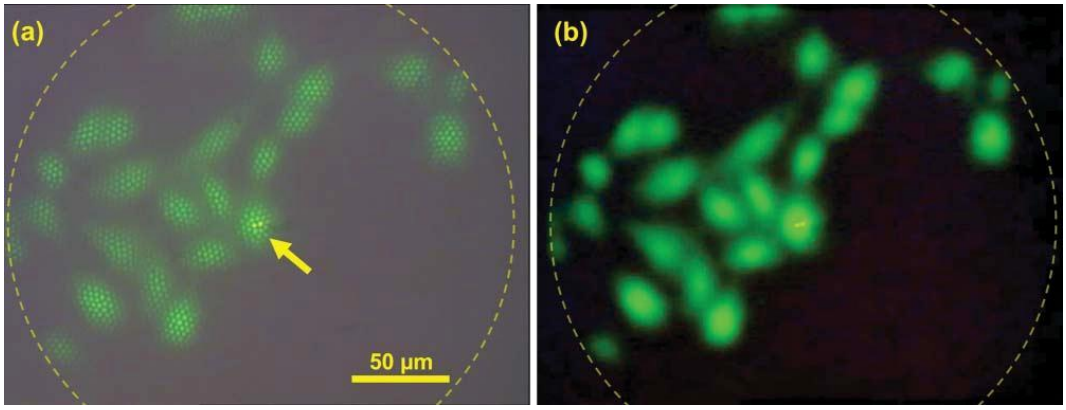

Fig. 6.5. *(a) Fluorescent image of cells, imaged through the imaging fiber captured by the CCD camera, on the right in Fig. 6.4. Individual pixels can be clearly resolved. The arrow indicates a cell that is being irradiated by a laser beam. Two relatively brighter pixels in the centre of the cell are the back reflection from the cell. (b) By adding a FFT bandpass filter, increasing the image intensity and then adding a background noise filter to (a), a more convenient view can be obtained. The dashed circle indicates the field of the view (image circle).*

6.2.5 Cell Transfection Using an Endoscope-like System

Cell transfection was achieved by using an 800 nm femtosecond Ti:sapphire laser with an output pulse duration of ~100 fs and a pulse repetition rate of 80 MHz (2 W average power, Coherent, MIRA). At the output end of the imaging fiber, the pulses undergo stretching mainly due to nonlinear phenomena occurring inside the fiber — SPM and GVD — giving an overall pulse duration of approximately from ~0.8 to 1.6 ps for the imaging fiber of the length from ~18 to 35 cm at the laser power used during the experiment, as measured using a home-built autocorrelator [249]. Laser light was coupled into one core of the imaging fiber, and the output from the axicon on the other side of the imaging fiber was targeted on the cell membrane, which was located 5 µm away from the axicon apex on the centre of the cell (Fig. 6.5). The 5 µm working distance is less than the normal thickness of a biological cell. Therefore, although the cell shape can be resolved, the centre (peak) rather than the edge of the cell was selected for targeting by the laser. Multiple cells can be treated within one field of view by steerring the laser beam from one core to the other that targets on the relative cells (Fig. 6.5). However, the thin layer of cladding between adjacent fiber bundle cores sometimes leads to optical cross talk in which light from neighbouring image pixels (cores) can leak into one another, reducing the beam power and creating multiple spots on cell membrane [119]. For example, by focusing the input beam at one end of the imaging fiber, 1 to 3 cores can be illuminated simultaneously (Fig. 6.6). Thus, the consistency of the transfection could be affected; therefore, during the whole experiment the laser beam was kept within one core to ensure that only one laser spot was targeted on the cell membrane at a time. Targeting different cells was achieved by either moving the imaging fiber or cell sample dish using an xyz translation stage. In the future, computer assisted cell tracking [264] and raster-scanning techniques [69] could be adapted to increase the cell selectivity and transfection throughput. A SLM can also be used to illuminate pixels (cores)

sequentially without sweeping the input beam so as to decrease the cross talk effect [265]. During experiments, the average power of the beam was 30–70 mW. Each cell was irradiated with 3–5 laser doses. About 20 cells from each sample dish were treated in <15 min. The duration of each dose was experimentally decided to be ~70 ms.

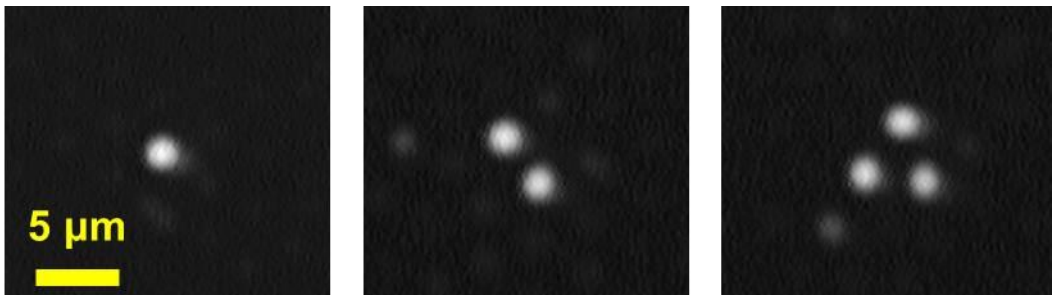

Fig. 6.6. *1 to 3 cores of the fiber bundle can be illuminated simultaneously due to the cross talk between adjacent cores. This affects the resolution of the imaging fiber and may create multiples spots on cell membrane during optical transfection. Therefore, during the whole experiment the laser beam was kept within one core to ensure that only one laser spot was targeted on the cell membrane at a time.*

The genetic material to be transfected consisted of a 1 ml solution of OptiMEM containing 20 µg/ml mitoDsRED plasmid. This solution was delivered microfluidically through integrated system during optical transfection (Chapter 5) [71]. After the laser treatment, the cell monolayer was washed twice with 2 ml of culturing medium before it was bathed in 2 ml of culturing medium and returned in the incubator. Then, 48 hours later, the sample was viewed under a fluorescent microscope, where successfully transfected cells expressed the red fluorescent protein.

6.3. Results and Discussions

In the course of this experiment, a total number of 566 CHO-K1 cells from 30 dishes were laser treated. The transfection efficiency did not show a strong correlation with differing powers, exposure times, or pulse

duration (which depends on the length of the fiber and output power). The number of spontaneously transfected cells was zero for all five control dishes. An optical transfection efficiency of up to ~72% and an overall 32% efficiency with this system was obtained (Table 6.1). These transfection efficiencies compare favourably with traditional free-space microscope-based transfection [30] and previous fiber-based optical transfection techniques [71]. However, a few dishes showed poorer results. This may be due to the difficulty in manipulating the short working distance (~5 μm) imaging fiber. Even though a highly stabilized setup was used, a cell or a fiber end can still get damaged, resulting in a reduced transfection efficiency. To minimize this damage during an experiment, once a potential contact between the fiber and a cell was observed, further treatment of that particular sample dish was abandoned. Also in such cases, the imaging fiber was re-etched to create an ordered axicon array at the end face before further experiments. Another factor that may affect transfection efficiency is that, due to the short working distance, the laser may have targeted the nucleus of a cell, which would reduce the cell viability, when compared to targeting at the edge of a cell [266]. In addition, due to SPM and GVD, the pulse duration of the laser pulses targeted on the cell was affected by the length of the imaging fiber, which was varied during the experiment due to the accident damage. However, on the other hand, the fluorescent imaging, cell staining, and gene delivery flow did not compromise the cell viability from observation.

Dish	*Laser Power (mW)*	*No. of Transfected Cell*	*Total No. of Treated Cells*	*Transfection Efficiency (%)*
1	30	12	25	48
2		9	25	36
3		3	20	15
4		2	12	17
5		4	19	21
6		7	20	35
7	40	6	20	30
8		1	10	10
9		9	20	45
10		3	19	16
11		8	20	40
12		14	20	70
13	50	7	20	35
14		7	20	35
15		6	20	30
16		4	20	20
17		13	20	65
18		9	20	45
19	60	2	20	10
20		1	18	6
21		4	20	20
22		6	20	30
23		7	20	35
24		2	19	11
25	70	6	13	46
26		3	20	15
27		9	20	45
28		13	18	72
29		3	8	38
30		2	20	10
Total		182	566	32

Table 6.1. *Transfection results. An optical transfection efficiency of up to ~72% and an overall 32% efficiency were obtained.*

In conclusion, the first endoscope-like, fiber-based optical transfection system combined with localized microfluidic drug delivery and fluorescent imaging capability was demonstrated. In order to achieve this, an imaging fiber was used for fluorescent imaging, laser delivery, and illumination. A circular field of view of ~300 μm in diameter and a resolution of ~7.6 μm was achieved through this imaging fiber. Multiple cells within one field of view and the shapes of each fluorescent cell can be clearly resolved. An ordered array of micro-axicons with an apex angle of 55º was chemically created at the polished exit surface of the imaging fiber in order to increase the light intensity at a relative remote distance. A beam spot of 3.75 μm in diameter was targeted on the cell membrane, which is located 5 μm away from the apex of the micro-axicon lens for the protection of both fiber tip and biological cells. This device is a step forward toward achieving an endoscopic system for *in vivo* optical transfection applications because it is possible to achieve imaging with subcellular resolution with this device. New engineering methods have to be developed to achieve an imaging fiber with a longer working distance, which would enhance the reproducibility of this device. However, this new system opens up prospects for a miniaturized, objective free probe that could greatly reduce the cost and might be applied in tissue slices or clinical *in vivo* optical transfection applications. In future, other popular tools, such as two-photon microscopy, microfluidic chips and Raman spectroscopy, could also be integrated with this system to make it a versatile biophotonics tool.

In the next chapter, in order to explore the possibility of increasing the working distance of optical transfection device, the development of miniaturized microscope technique is briefly reviewed. A GRIN lens based imaging probe is also developed and used in an optical transfection experiment. This new design not only shows a longer working distance, but also has less pulse stretching due to the adoption of a LMA-PCF for the laser delivery. This imaging probe allows more freedom of the optical transfection technique to be realized in the *in vivo* environment.

Chapter 7:

7. An GRIN Lens Based Imaging Probe For Optical Transfection

7.1. Introduction

In previous chapters, several optical fiber based optical transfection techniques have been presented. All of these techniques achieve a transfection efficiency that is comparable to the traditional free-space optical transfection technique. However, none of these would fulfill the requirements of an ideal optical transfection tool that should have the potential to be used in medical applications. In a clinical environment, an ideal optical transfection tool would have the ability to image individual cells embedded in biological tissue and to manipulate them simultaneously whilst ensuring the damage to the patient is kept to a minimum. With regard to the mechanism of optical transfection, an ideal tool must also focus the perturbation beam to a tiny spot and maintain a safe distance between the optical probe and the cell under treatment. The fiber bundle based endoscope-like optical transfection system presented in Chapter 6 is very close to meeting these requirements with the exception that the working distance is too short, thus extra care must be taken to keep both the fiber tip and the targeted cell intact. In Chapter 6 a miniaturized microscopy technique that has been developed in the last two decades was introduced, and many ideas from this technique can be adopted into the design of an ideal optical transfection system. This chapter begins with a brief review of the development of this miniaturized microscope technique and is followed by the presentation of a GRIN lens based imaging probe used for epifluorescence imaging and optical transfection. Preliminary optical transfection results have been obtained using this imaging probe on CHO-K1 cells. However, epifluorescence imaging and drug delivery have not yet been attempted on this imaging probe. Future work in these areas is due to be undertaken.

7.2. Review of the Miniaturized Microscope Technique

7.2.1 Introduction

Miniaturized microscopy has been developed for around two decades [267, 268]. Differing from traditional bulk microscopes, miniaturized microscopes are mainly used in the area of biology. Miniaturized microscopy permits cellular imaging under conditions where conventional microscopy cannot be used. A miniaturized microscope can image cells residing within hollow tissue tracts [269]. It can also provide imaging access to cells buried deep within organs by implanting or inserting the imaging probe into the relevant organ in a minimally invasive manner, which allows long-term *in vivo* imaging to be realized [270, 271]. With the implanted miniaturized microscope, the development of cells under the treatment of therapeutics or simply from aging can be studied *in vivo* at the subcellular level [271]. It has been shown that some low-weight flexible miniaturized microscopes can even be installed on certain parts of the body of a moving animal [272-274]. The link between certain cells and disease symptoms or animal behaviours can therefore be studied directly over time. Recently, miniaturized microscopy has been increasingly applied in clinical diagnostics [132, 275] and cell surgeries [46, 256]. Its potential in the clinical area is just starting to show.

The challenges of building a miniaturized microscopy system involve miniaturization of optical and mechanical components, ingenious design of the system, and dealing with the other issues that arise from miniaturization. Imaging using the miniaturized microscopy technique has mainly been limited to epifluorescence, fluorescence confocal and two-photon modalities [119, 133]. Other imaging methods using reflective fiber-optic confocal [267, 276-278], second and third harmonic generation [279, 280] and Coherent Anti-Stokes Raman Scattering (CARS) [281] techniques have also been adopted in miniaturized microscopy and are currently undergoing rapid development.

There are various different embodiments of the miniaturized microscope [119, 133]. Some are enclosed in a small compact package and can be used as a hand-held microscope for imaging at depth beneath the sample surface. Some utilize a scanning fiber or fiber bundle for miniaturization and are used as a microendoscope. GRIN and miniature lenses are also commonly used to fabricate compact imaging probes. A miniaturized microscope typically consists of one or more excitation sources, a light delivery mechanism, an x-y scanning mechanism, a focusing mechanism, a light collecting system, an optical detector, and a computer for monitoring, controlling and coordinating the whole system. Many of them also have customized accessories to realize specialized functions, such as side viewing, rotation, liquid delivery, and auto-focus adjustment. This chapter will focus on the introduction of components commonly used in a miniaturized microscope and selected basic embodiments that have been developed previously. Only miniaturized microscopes with a subcellular resolution will be covered in this section.

7.2.2 Components

7.2.2.1. Optical fiber

Optical fibers were originally used as a diagnostic tools or sensors by measuring the collected fluorescent emission from a point or an area *in vivo* [127-129]. Due to its size and flexibility, optical fibers have now been used in many types of miniaturized microscope for light delivery and collection with the new additional capability of transferring an image. To realize this new capability, a scanning mechanism is involved to reconstruct an image point by point. Fiber bundles have also been used in the miniaturized microscopy technique to transfer all the points of an image simultaneously. Several types of optical fiber have been commonly used in the miniaturized microscopy technique to effectively deliver and collect signals from the specimen.

SMF for visible light usually have a core diameter from 3-7 µm and guide only one spatial mode of light, which can be focused to a near diffraction-limited spot in order to achieve high resolution imaging. Therefore, the low-cost SMF is widely used in confocal type scanning miniaturized microscopes [267, 282]. The core of the SMF also works as a pinhole, simultaneously rejecting the out of focus fluorescence emissions.

Step-index MMF guide more than one spatial mode in the fiber core. MMFs not only have larger cores, typically from ~50 µm up to a few millimetres, but also generally have large NA values. These fibers therefore are more effective at collecting light when compared to SMFs and therefore they are used for signal collection in many types of miniaturized microscope.

Two-photon microscopy is a powerful technique that allows cellular imaging at several hundred microns deep within biological tissues. A femtosecond laser with pulses of ~80-250 fs duration and nanojoule energies is normally used in a traditional microscope to induce two photon-excited fluorescence *in vivo* [32]. However, due to GVD and SPM (see Chapter 2.4), the temporal profile of ultrashort optical pulses delivered through an SMF are severely stretched and thus the efficiency of two-photon excitation is compromised. Therefore, alternative means of delivering ultrashort pulses must be adopted.

Photonic crystal or microstructured fibers are a newly developed class of optical fiber made from pure silica. Their name derives from the regular periodic pattern of air holes and silica glass these fibers exhibit within their internal structure (Fig. 7.1). By careful design of the air hole array, a core of a large mode area (LMA) with single-mode operation over a broad range of wavelengths (from UV to infrared) can be made. This property is called endless single mode guidance and this kind of fiber is called a large mode area photonic crystal fiber (LMA-PCF) [Fig. 7.1(a), (d)]. The air hole array decreases the effective refractive index of the material and acts as the fiber cladding. The light travels within the silica core by a modified form of total internal reflection. The LMA-PCF for 800 nm light,

which is the typical wavelength for two-photon microscopy, has a mode field diameter of ~15 µm compared to ~5-6 µm mode field diameter of SMF for the same wavelength. The light intensity in the fiber core area and the subsequent pulse stretching is thus significantly reduced.

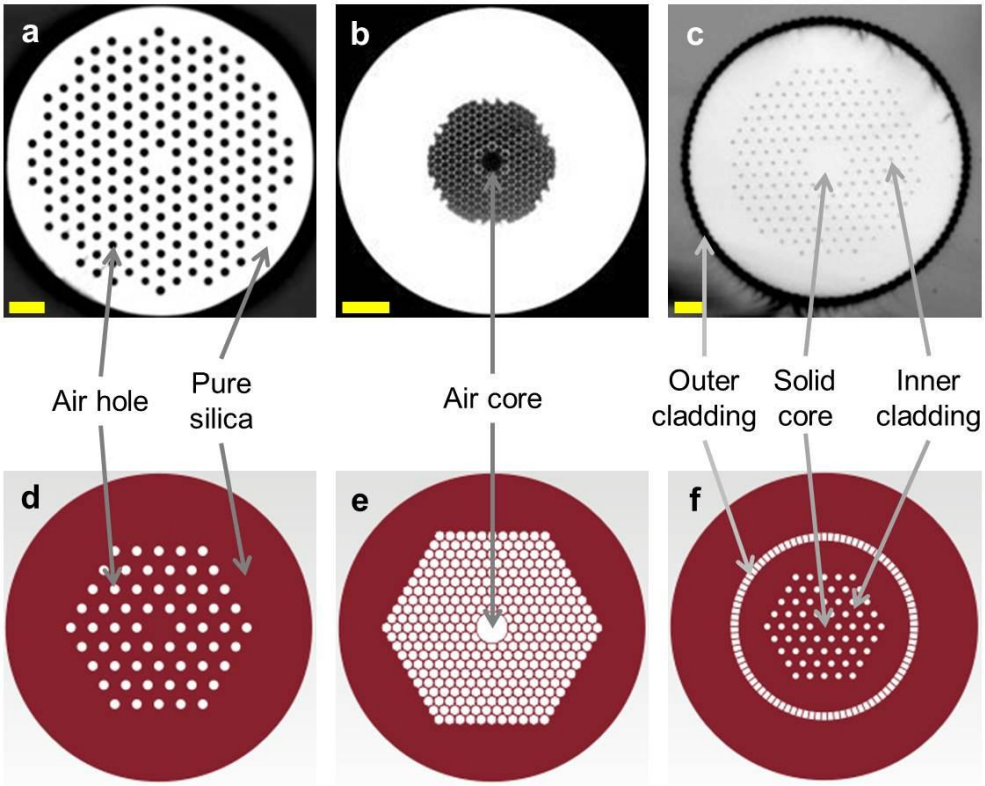

Fig. 7.1. *Photographs and schematics of photonic crystal fibers. (a) LMA-PCF has a bigger core and wider transmission range for single mode delivery compare with a SMF. (b) Hollow-core* photonic bandgap fiber *(PBF). Ultrashort optical pulses are localized to the air core, effectively eliminating SPM. (c) Double-clad photonic crystal fiber (DCF). The inner cladding and solid core work as an LMA-PCF for guiding single mode excitation light and the outer air cladding creates a higher-NA fiber that can collect fluorescence emission efficiently. Scale bars, 20 µm. Photographs are obtained from [119]. (d), (e) and (f) obtained from NKT Photonics A/S are the relative schematic graphs of (a), (b) and (c). The white area indicates the air hole and the grey area indicates the silica material.*

Pulse stretching can be further reduced using a hollow-core PCF [283]. This kind of photonic bandgap fiber (PBF) does not rely on total internal reflection for light guiding [Fig. 7.1 (b), (e)]. The cladding of a hollow-core PCF may be regarded as a 2D photonic crystal, which is similar to an electronic bandgap in crystalline solids [118]. If the optical frequency lies within the photonic bandgap, the cladding becomes impermeable to the photons and the fiber serves as a photonic-crystal waveguide. The air core can increase the transmission efficiency with reduced nonlinear effects. Hollow-core PCF have been used in many embodiments of two-photon miniaturized microscopes and other nonlinear optical imaging modalities, because even high-energy pulses do not undergo SPM in an air core [274, 284, 285]. Normally the working wavelength for a hollow-core PCF covers a spectral range of several tens to over a hundred nanometres. Within this range there is usually a zero dispersion point at which the pulse stretching vanishes, making the hollow-core PCF a perfect means for ultrashort pulse delivery.

Another type of fiber commonly adopted in the miniaturized microscopy technique is double-clad photonic crystal fiber (DCF) [256, 286, 287]. DCF is basically an LMA-PCF surrounded by an outer cladding composed almost entirely of air [Fig. 7.1 (c), (f)]. The LMA-PCF works for the delivery of single mode high power excitation light. The outer cladding makes the entire LMA-PCF (solid core and air hole cladding) the core of a MMF with very high NA up to ~0.6. This arrangement allows excitation light to be delivered through the LMA-PCF in the centre and the excited signal is collected through the outer MMF simultaneously, all within one DCF. Using one fiber for both delivery and excitation can decrease the size of the miniaturized microscope imaging probe and aid in miniaturization.

In contrast to the optical fibers mentioned above, that only have one core for light delivery and therefore require scanning mechanisms to reconstruct an image point by point, an imaging fiber (coherent optical fiber bundle) can deliver an image on its own (Chapter 6). An imaging fiber

usually consists of a large number (up to ~100,000) of cores (pixels), and each core can independently transmit light like a conventional optical fiber. The cores are normally laid in parallel along the fiber axis in a honeycomb-like structure throughout the whole length (coherent configuration) of the fiber. Therefore, an image projected on to one end of the imaging fiber can be divided into pixels and then transferred to the other end. The total diameter of an imaging fiber ranges from hundreds of micrometres to a few millimetres depending on the number and size of each core. Epifluorescence imaging can be easily realized using such an imaging fiber (Chapter 6) [114, 275, 288]. Scanning confocal [265] or two-photon [257] imaging modalities can also be realized by scanning the excitation beam on the proximal (relative to the light source) end of an imaging fiber while keep the distal end targeted at the sample. However the size of the core in a fiber bundle, which is normally ~2-3 μm, is smaller than the core in a SMF. This means ultrashort pulses passing through these cores suffer severe pulse stretching and this decreases the two-photon excitation efficiency. Pre-compensation of the pulse stretching may be required when using an imaging fiber. One advantage of using an imaging fiber is that its small size facilitates miniaturization. The imaging fiber can be pushed against the sample during imaging, removing the need for other focusing optics, if damage is not a concern. The main disadvantage of an imaging fiber is that the image is transferred in a pixelated fashion, which reduces the lateral optical resolution in the specimen plane to about twice the average core-to-core distance. A focusing lens can be attached to the distal end of imaging fiber to increase the resolution and keep the imaging probe apart from the sample.

7.2.2.2. Focusing mechanism

With the exception of miniaturized microscopes which utilizes a coherent fiber bundle held against the tissue during imaging, a focusing mechanism is always needed in a miniaturized microscope. For some

types of hand-held microscopes where there is no space limitation, a traditional objective can be used [280, 289]. On the other hand, for applications where miniaturization is needed, various focusing mechanisms have been developed and successfully applied in miniaturized microscopy. Typically a customized miniature objective lens is used to focus the output beam from a scanning fiber or a fiber bundle to the sample. GRIN lenses and small spherical lenses (a few millimetres in diameter), or a combination of these, are commonly used focusing mechanisms.

GRIN lenses resemble a piece of glass rod ranging from 0.35 – 2 mm in diameter and are commonly used in miniaturized microscopy. Their refractive index profiles decline approximately quadratically with the radius, which can be described using the equation: $n(r) = n_0(1 - g^2r^2/2)$, where r is the radius from the fiber axis, n_0 is the refractive index on axis and g is a constant parameter [118]. This gradual variation of the refractive index makes the light traveling through the GRIN lens follow an approximately sinusoidal path where the length of one sinusoidal period is defined as one pitch of the GRIN lens (Fig. 7.2). An image can be transferred through a GRIN lens as shown in Fig. 7.2. Therefore a single GRIN lens of appropriate length can be used as an image conduit for deep tissue imaging [290]. Similar to a spherical lens, a GRIN lens of specific length can be used to focus, collimate and diverge light; different focal lengths can be made by cleaving the GRIN lens at relative pitch length [Fig. 7.2 (inset)]. With a flat end face, an imaging probe (objective lens) can be easily built by gluing a series of GRIN lenses with different focal lengths together. However, due to their optical aberrations and relatively low NA values, GRIN lenses do not provide optical resolutions comparable to those of conventional microscopy [291]. A normal GRIN lens based imaging probe measures about one centimetre or more in length and contains two or more GRIN lenses. Customized GRIN lenses and GRIN lens based imaging probes are available from multiple vendors. Three typical examples of GRIN lens based imaging probe are shown in Fig. 7.3.

These triplet imaging probes comprise three parts: A coupling lens with a lower NA, is used to receive the output beam from a scanning fiber; a relay lens transferring the beam to a remote distance; and an objective lens with high NA used to focus the beam at the sample plane [292].

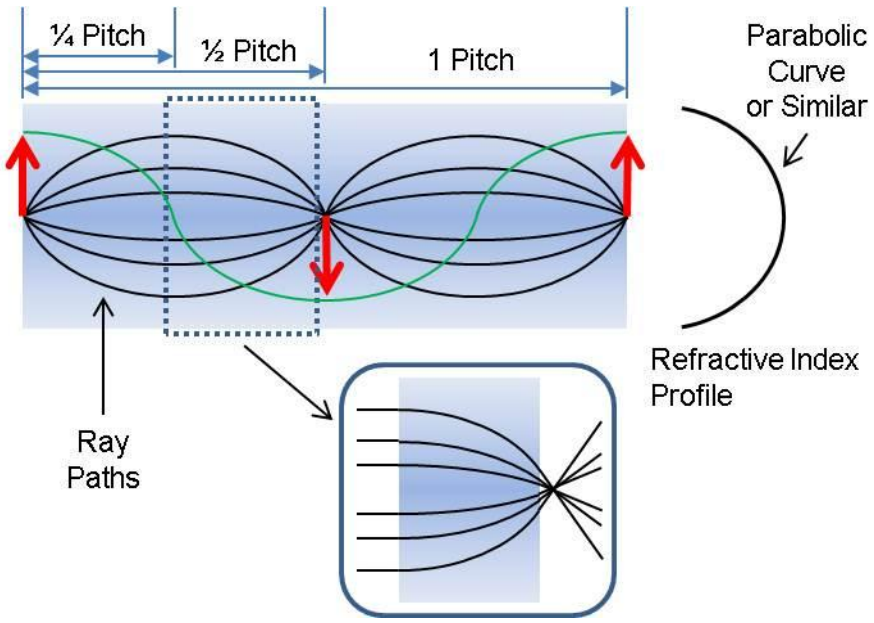

Fig. 7.2. *A GRIN lens with a parabolic variation of refractive index with radial distance. Light traveling through the GRIN lens follows an approximately sinusoidal path and therefore it can be used to transfer an image from one end to the other. The inset shows that a GRIN lens of specific length can be used to focus light like conventional spherical lens.*

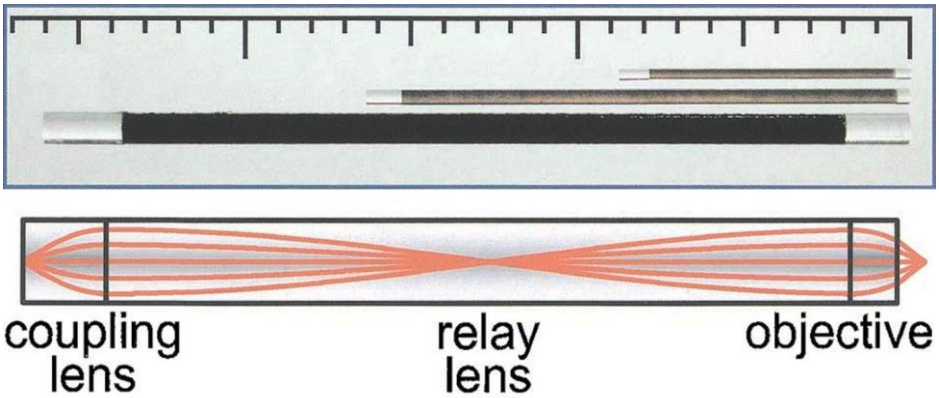

Fig. 7.3. *Top, photograph of three GRIN lens based imaging probes, of 1.0, 0.5 and 0.35 mm diameter, oriented with the coupling lens on the left, a relay lens in the middle and an objective lens on the right [292]. A minor tick on the scale equals 1.0 mm. Bottom, optical schematic of the beam path in the triplet imaging probe. A coupling lens is used to receive the output beam from a scanning fiber; a relay lens transfers the beam to a remote distance, and an objective lens is used to focus the beam at the sample plane.*

Similar to a traditional objective lens, miniature objective lenses can also be fabricated using spherical lenses normally from 0.8 - 5 mm in diameter. For some imaging modalities, such as scanning microscopy, a few spherical lenses are enough for the focusing requirement [293]. However, for other modalities, such as epifluorescence, where different colours of excitation and emission beams are involved, more complicated lens designs for image aberration correction are needed [255, 276, 294]. Two examples of objective lens designs are shown in Fig. 7.4 [276]: Fig. 7.4(a) is made of eight spherical lens elements; with the assistance of optical design software, smaller objective lenses composed of five injection-molded plastic lenses can be made [Fig. 7.4(b)]. This reduction in the number of lenses and overall size of the objective lens result from the use of aspheric lenses in the injection-molding process, which is extremely difficult and expensive to manufacture with glass lenses of this size.

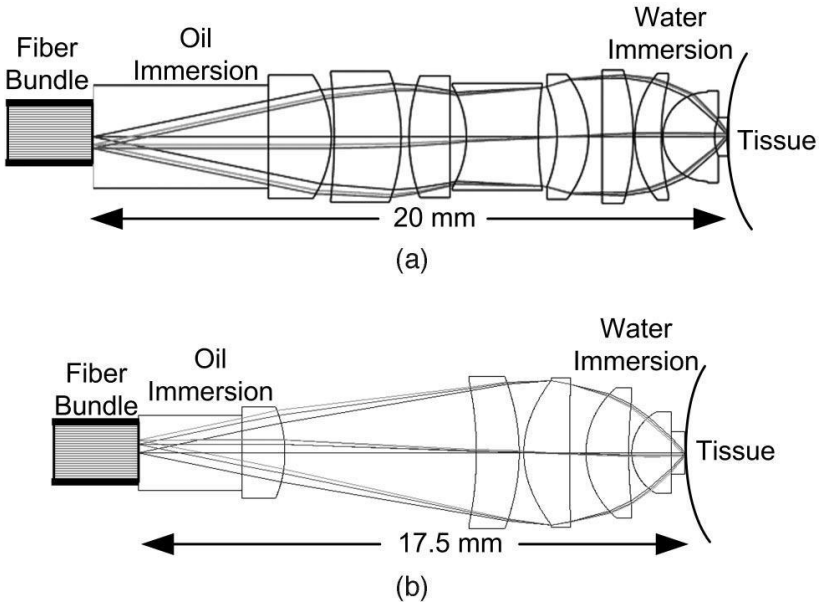

Fig. 7.4. *Two examples of optical designs for miniature objective lenses. The fiber bundle is located to the left of the objective lenses and the sample is placed to the right. (a) Glass lens design with eight spherical lens elements. (b) Plastic lens design with five lens elements utilizing aspheric surfaces. Diagrams obtained from [276].*

7.2.2.3. Scanning mechanism

In order to transfer an image using a single fiber in a miniaturized microscope, a scanning mechanism is usually involved to reconstruct the image point by point. However, not every miniaturized microscope system needs a scanning mechanism, examples include epifluorescence [114, 295] and reflective confocal modes [296]. Imaging modalities that do adopt scanning mechanisms can be divided into two categories: proximal and distal (relative to the light source) scanning. Proximal scanning indirectly scans the sample by scanning over one end-face of a fiber bundle or imaging probe, whilst keeping the other end targeted to the sample [Fig. 7.5(a)]. In this fashion, the scanning unit and the sample are separated. Thus miniaturization of the scanning unit is unnecessary and the size of the imaging probe can be reduced without affecting the scanning unit. Proximal scanning can be easily realized using a pair of galvo mirrors or

simply by attaching the fiber bundle or imaging probe to a conventional scanning microscope [279]. Line scanning over the end-face of a fiber bundle or imaging probe can greatly increase the image acquisition rate [297]. A SLM can also be used to couple selectively the scanning beam into individual cores of a fiber bundle rather than sweeping across the entire end-face and so decrease the cross-talk between adjacent cores and increases the resolution [265].

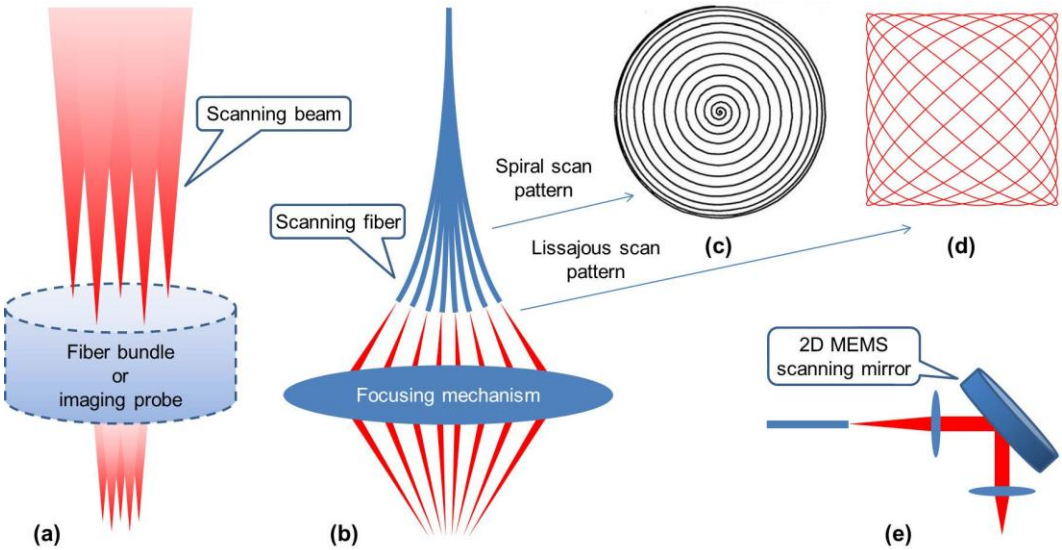

Fig. 7.5. *Scanning mechanisms. (a) Proximal scanning can image the sample by scanning at one end-face of a fiber bundle or an imaging probe while keeping the other end targeted to the sample. (b) Distal scanning. The fiber tip is vibrated at the mechanical resonant frequency driven by a piezoelectric actuator and the output excitation beam is then focused at the sample. Two scan patterns are commonly used: spiral (d) and Lissajous (d). (e) Distal scanning can also be realized by using an electrostatic driven MEMS torsion scanning mirror.*

Distal scanning can be realized by scanning a single optical fiber over the sample with a focusing mechanism in between [Fig. 7.5(b)]. A piezoelectric excited actuator is normally used to drive the fiber tip, vibrating it at the mechanical resonant frequency [255, 298]. Spiral [Fig. 7.5(c)] [285] and Lissajous [Fig. 7.5(d)] [272] scan patterns are commonly

used. Thanks to the development of MEMS in recent years, electrostatic driven torsion scanning mirrors at ~0.3 – 2 mm in diameter can be fabricated and used for distal scanning [46, 284] [Fig. 7.5(e)]. MEMS mirrors are fabricated through sequential material etching and deposition processes and can be batch fabricated. One and two dimensional MEMS mirrors are both available. This is a more robust scanning mechanism to scan the beam delivered from an optical fiber. MEMS mirrors change the incoming beam by 90º, therefore these are normally used in slightly larger hand-held miniaturized microscopes (rather than the pencil-shape implanted type) [46] or they can be used to provide a side-viewing functionality [284] [Fig. 7.5(e)].

7.2.3 Embodiments

Using the previously detailed components, various types of miniaturized microscope can be built. There are no set standards for fabricating a miniaturized microscope and the modality of each miniaturized microscope is always strongly driven by the relative application and limited by the available technologies. On the other hand, the same imaging modality can be realized through different types of miniaturized microscope. In this section a few basic and common types of miniaturized microscope will be introduced (Fig. 7.6) and it will be shown that other types with special features can be easily modified from these examples.

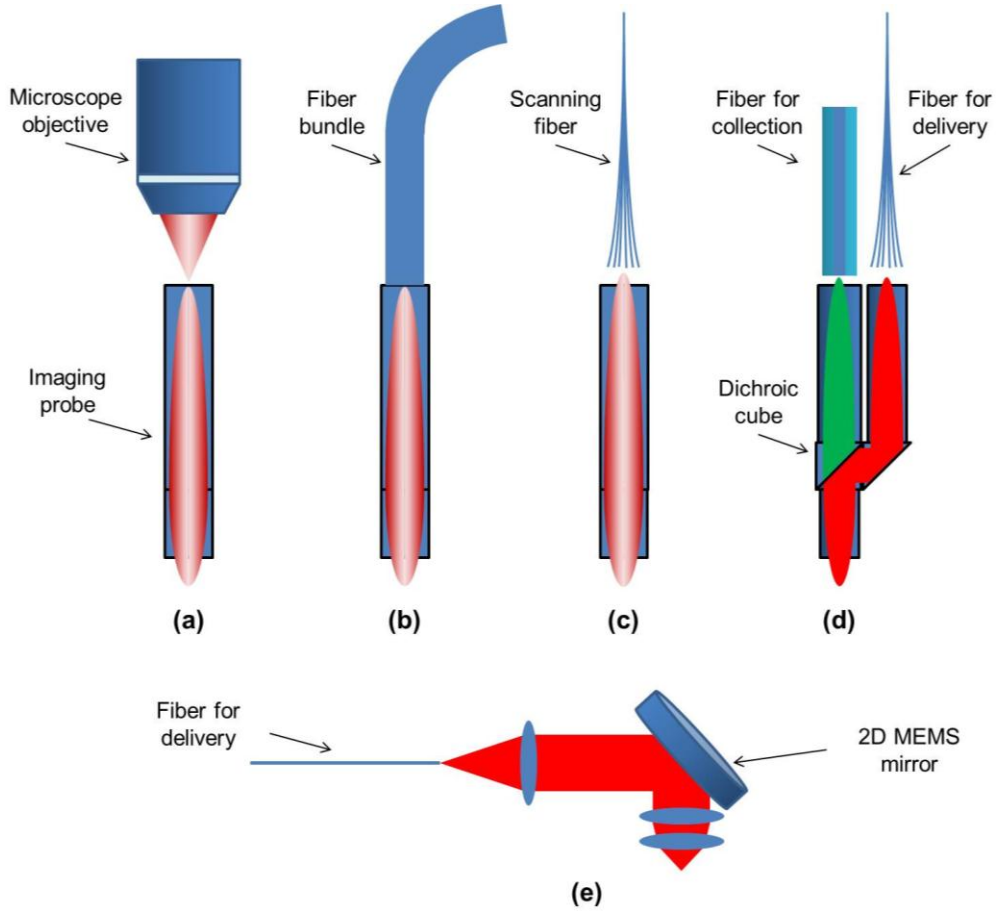

Fig. 7.6. *Different miniaturized microscope embodiments. (a) An imaging probe is attached to a conventional scanning microscope. The imaging probe acts as an extension of the microscope objective and can be used to direct and focus the scanning beam on the sample. (b) By attaching the imaging probe to a flexible fiber bundle (imaging fiber), remote and conventionally unattainable places can be imaged. (c) Using a single scanning fiber in addition to an imaging probe, an image can be reconstructed point by point and a pencil-like compact miniaturized microscope can be made. (d) By splitting the excitation beam delivery and emission beam collection, the chromatic aberrations commonly seen in GRIN lens based imaging probes can be circumvented. Using different special fibers for delivery and collection can also enhance the efficiencies of delivery and collection. (e) Using a MEMS mirror to scan the beam delivered by a fixed fiber, one can not only realize a system with a side-viewing ability, but can also create a more robust* miniaturized microscope *than other embodiments.*

The first and also perhaps simplest type of miniaturized microscope is shown in Fig. 7.6(a). An imaging probe is attached to a conventional scanning microscope [290, 299]. The microscope objective lens scans over the proximal end of an imaging probe which transfers and focuses the scanning beam to the distal end on the sample plane. The imaging probe acts as an extension of the bulk objective and allows imaging of a conventionally unattainable area. The imaging modality then depends on the relative modality of the scanning microscope. Scanning imaging modalities are readily compatible with this type miniaturized microscope. However, it is worth mentioning that epifluorescence imaging is not easily achieved using GRIN lens based imaging probes due to the large chromatic aberrations from the GRIN lens.

The second type of miniaturized microscope is shown in Fig. 7.6(b), where a fiber bundle is attached to the proximal end (relative to the light source) of an imaging probe [131, 132, 257, 259, 273, 278, 288, 295, 300]. Epifluorescence [273, 288, 295], confocal [132, 278] and multiphoton [257] microscopes can all be realized using this type of miniaturized microscope. The fiber bundle transfers the excitation beam from the proximal to the distal end and then the imaging probe focuses the excitation beam onto the sample. The reversed beam path is also used for emission beam collection. In the application of miniaturized microscope to confocal microscopy (both fluorescent and back reflection microscopy), a pinhole is needed at an appropriate plane [not shown in Fig. 7.6(b)] to eliminate out-of-focus fluorescence and produce the sectioning ability. In its application to multiphoton microscopy, the length of the fiber bundle is limited by the pulse stretching occurring within the core of the fiber bundle [257].

In some applications of confocal and epifluorescence microscopy, a focusing mechanism is not necessary when the end-face of the fiber bundle is in direct contact with the sample during imaging [259, 288, 295]. Without the focusing mechanism, the imaging probe (tip of fiber bundle) can be made as small as ~300 μm [114] and there are commercialized products of this type of miniaturized microscope on the market already

(Mauna Kea Technologies). The drawback of this design comes from the image pixilation, which is due to the nature of the fiber bundle and which decreases the image resolution. However, this might be overcome by using a high magnification (NA) imaging probe.

Replacing the microscope objective in Fig. 7.6(a) with a single scanning optical fiber, another type of miniaturized microscope can be fabricated [Fig. 7.6(c)] [272, 285, 293, 298, 301, 302]. The scanning mechanism in a conventional scanning microscope is realized by the fiber tip scanning. SMFs can be used in this design and the fiber core itself acts as a pinhole making this design a confocal system [298, 301]. However, for the SMF the collection efficiency is low. Therefore, DCF and a modified fiber tip have been used to increase the collection efficiency [287, 293, 302, 303]. Many types of multiphoton systems based on this design have also been developed with hollow core PCF [46, 272, 285] or LMA-PCF [120] for pulsed excitation beam delivery. Additional means for pulse broadening compensation are used in some cases to increase two-photon excitation. This design can be easily included in a compact pencil-like housing with a diameter of only a few millimetres.

Another common design is made by splitting the beam paths of excitation beam delivery and emission beam collection using a micro-dichroic cube, [Fig. 7.6(d)] [250, 272, 274, 285]. Using relevant fibers for different beam paths has two major advantages: firstly, in the multiphoton imaging mode, the fibers for beam delivery and collection are separated, a large core MMF used for emission collection can promote the collection efficiency and a hollow core PCF used for pulsed light delivery can promote the multiphoton excitation. Secondly, when using this design in the epifluorescence mode, the axial position of the fiber (fiber bundle or objective) used for collection, can be adjusted therefore avoiding the problem of chromatic aberration (which will be discussed later in this chapter).

Fig. 7.6(e) shows a miniaturized microscope with a side-viewing ability which is produced through a MEMS scanning mirror [284, 304, 305].

A side-viewing miniaturized microscope is very useful especially when imaging a tunnel-like structure, where a normal miniaturized microscope cannot reach. With a rotational motor a 3D (3 dimensional) model of a tunnel-like structure can be reconstructed [269]. By keeping the position of the fiber for excitation beam delivery fixed and using a 2D MEMS scanning mirror, a very robust system can be built. Many imaging modalities have been realized using this geometry.

7.2.4 Summary and Future

In this section the miniaturized microscope technique has been briefly reviewed. Common components for building a miniaturized microscope have been discussed: including various types of optical fiber, focusing and scanning mechanisms. Based on these components, different embodiments of a miniaturized microscope each with their own merits and problems can be built. The optical principles for realizing different imaging modalities on a miniaturized microscope are theoretically the same as their equivalents in conventional bulk microscopy. Thus miniaturization is more of an engineering challenge than a theoretical problem. There are also many related issues that are very important in miniaturized microscopy, such as a micro-motor for axial positioning or rotational control, a micro-camera, liquid delivery system, device housing, ray-tracing and computer-aided design software. Further information on these aspects can be found in numerous literatures [119, 133, 306]. Other embodiments with customized properties can be modified from the ones discussed here. For example, a miniaturized dual-optical-zone (dual fields of view and resolution) endoscope objective lens using a new lens was developed in Watt Webb's group [307]. Another *in vivo* epifluorescence miniaturized microscope was achieved by connecting it to a digital camera making this system a portable real time diagnostic tool [295]. With the aid of a guiding tube, a miniaturized microscope can reach and image deep within the living mammalian brain with the ability to return and observe the

same location over a period of weeks [271].

The capabilities of a miniaturized microscope can be promoted greatly through appropriate and ingenious accessories. Although the miniaturized microscopy technique has been developed for two decades, it is only relatively recently that this technique has begun to be widely applied in animal models to study tissue structure [269, 308], disease diagnostics [259], and has even been used in clinical trials [131, 132, 275]. In the near future, more clinical trials will be carried out and the trend for further miniaturization will continue. There is a drive to develop this technique towards a portable, economical device and this technique may be integrated with the modern endoscopy technique.

7.3. Design and Characterization of GRIN Lens Based Microendoscope Optical Transfection System

In the last chapter an endoscope-like integrated optical transfection system was presented. Fluorescence imaging was realized on that system as well as a drug delivery module. Successful optical transfection results were obtained using cultured cell lines. However, the short working distance (~5 μm) of this system prevents its application in *in vivo* experiments. A longer working distance, to keep the biological tissue and imaging probe separated and intact, is essential for the success of an *in vivo* optical transfection experiment. Therefore, based on ideas from miniaturized microscopy techniques, a GRIN lens based optical transfection probe was developed (Fig. 7.7).

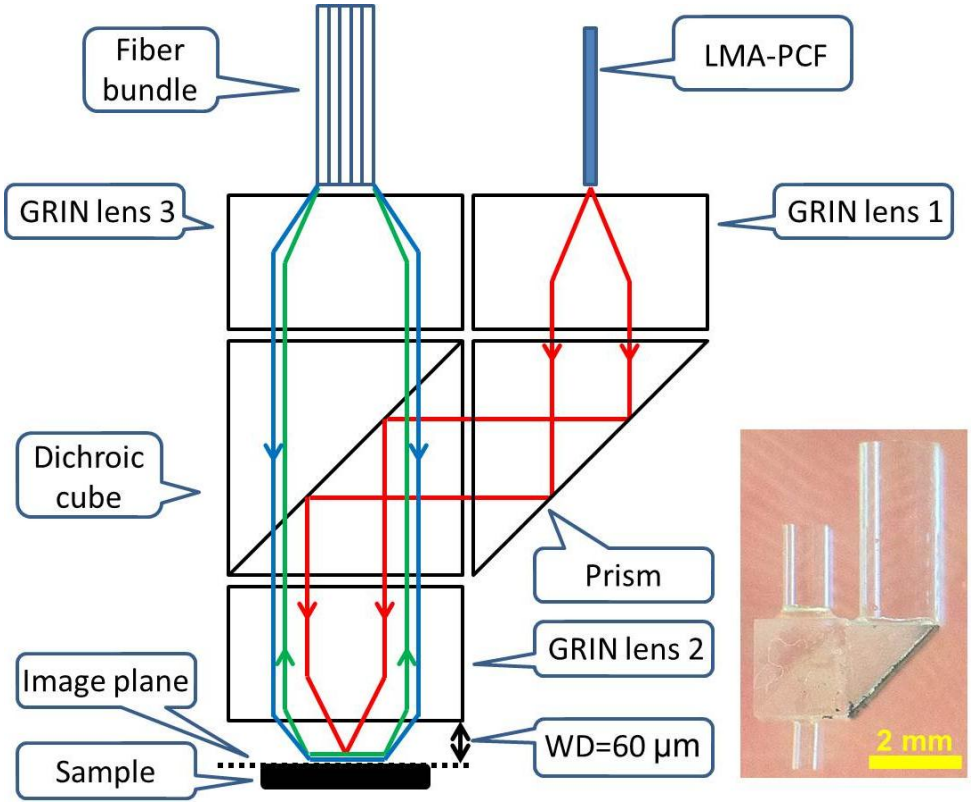

Fig. 7.7. *The schematic graph on the left shows the design of the GRIN lens based imaging probe. The 800 nm femtosecond beam (red) and visible light (green and blue) for fluorescence imaging are separated in order to avoid the chromatic aberration from GRIN lenses. The femtosecond laser for optical transfection is delivered by a LMA-PCF fiber and the output beam is coupled and collimated by GRIN lens 1 before it is reflected by a prism and a custom-made dichroic cube. The beam was then focused on the image plane by GRIN lens 2. Fluorescence imaging is achieved in a similar way as in section 6.2.4 through a fiber bundle with an imaging probe, made of GRIN lens 3, a dichroic cube and GRIN lens 2, on top. A working distance (WD) of 60 µm is achieved. A photograph of the imaging probe is shown on the lower right.*

Fig. 7.7 shows a GRIN lens based imaging probe adopting a design which splits the 800 nm femtosecond beam for cell transfection and visible light for fluorescence imaging. Beam splitting was realized through a custom-tailored dichroic cube which was fabricated by the Tower Optical Corporation. The cube was made by gluing two 2 mm BK7 right angle

prisms together (Fig. 7.7). The hypotenuse of one prism was coated to reflect the 800 nm femtosecond beam with a reflectance of over 95% and to allow the 450 – 600 nm light to pass with a transmission over 95% at an incident angle of 45º. A 35 cm long LMA-PCF (Thorlabs, LMA-20) controlled by a xyz translation stage, was used for femtosecond laser delivery. The output beam from LMA-PCF was coupled and collimated by GRIN lens 1 (Edmund Optics, NT64-544) before it was reflected by a prism with an aluminized hypotenuse (Edmund Optics, NT47-922) and the dichroic cube. The femtosecond beam was then focused on the sample by GRIN lens 2. The imaging was realized in a similar way as in Chapter 6 (section 6.2.4) except that the imaging probe was placed between the fiber bundle (FIGH-06-300S, Fujikura, UK) and the sample to increase the working distance for the protection of both imaging probe and biological cells. Briefly, a fiber bundle with the imaging probe (GRIN lens 3, dichroic cube and GRIN lens 2) was used to deliver the excitation beam to the sample and collect the green fluorescent emission. The position of the fiber bundle can be adjusted in order to compensate the chromatic aberrations from the GRIN lenses. The optical components were glued together using Norland Optical Adhesive.

The specifications of GRIN lens 1, 2 and 3 are shown in table 7.1. A GRIN lens can be treated as a thick spherical lens in terms of its focusing properties. Therefore, the magnification of the GRIN lens based imaging probe is determined by the focal length ratio of GRIN lens 1 to GRIN lens 2, which in this case is 1.72/0.46 = 3.73. The mode field diameter of the LMA-PCF is 15 µm, which gives a beam spot diameter at the image plane equal to 15/3.73 ≈ 4 µm. By adjusting the distance between LMA-PCF and GRIN lens 1, the spot size (and also the working distance) can be adjusted within a small range. The focal length ratio of the GRIN lens 3 to GRIN lens 2 is equal to 0.94/0.46 ≈ 2, which gives a 2 times magnification of the fluorescent imaging. The theoretical resolution that can be achieved by a fiber bundle and imaging probe combination is equal to the resolution of the fiber bundle divided by the magnification of the imaging probe,

which for this design (Fig. 7.7) is 7.6 µm (section 6.2.4) / 2 = 3.8 µm. The working distance of the imaging probe is decided by the working distance of GRIN lens 2, which is 60 µm (table 7.1). The longer working distance compared with the previously discussed fiber based techniques gives this new GRIN lens based imaging probe more flexibility.

	Pitch	*Diameter (mm)*	*Length (mm)*	*Focal Length (mm)*	*NA*	*Working Distance (mm)*	*Design Wavelength (nm)*
GRIN lens 1	0.23	1.80	3.96	1.72	0.55	0.23	810
GRIN lens 2	0.23	0.50	1.06	0.46	0.55	0.06	810
GRIN lens 3	0.23	1.00	2.18	0.94	0.55	0.12	810

Table 7.1. *Specifications of the GRIN lenses used to build an imaging probe.*

The output beam profile of the imaging probe was characterized in a similar way as described in section 5.2.1. Briefly, an 800 nm femtosecond laser beam was coupled to the imaging probe (through GRIN lens 1 in Fig. 7.7) and the output beam from the imaging probe (through GRIN lens 2 in Fig. 7.7) was profiled in water using a series of lateral cross-sections with a 5 µm step change and using a water immersion objective (X60 Olympus UPlanSApo). The axial position of the LMA-PCF in Fig. 7.7 was adjusted in order to form a smallest spot on the image plane. The reconstructed output beam intensity profile around the focus area using beam lateral cross-sections is shown in Fig. 7.8. The working distance of the imaging probe, as defined in Fig. 7.7, was estimated from the beam profiling and the diameter of the focal spot and was ~50 µm and ~2 µm respectively.

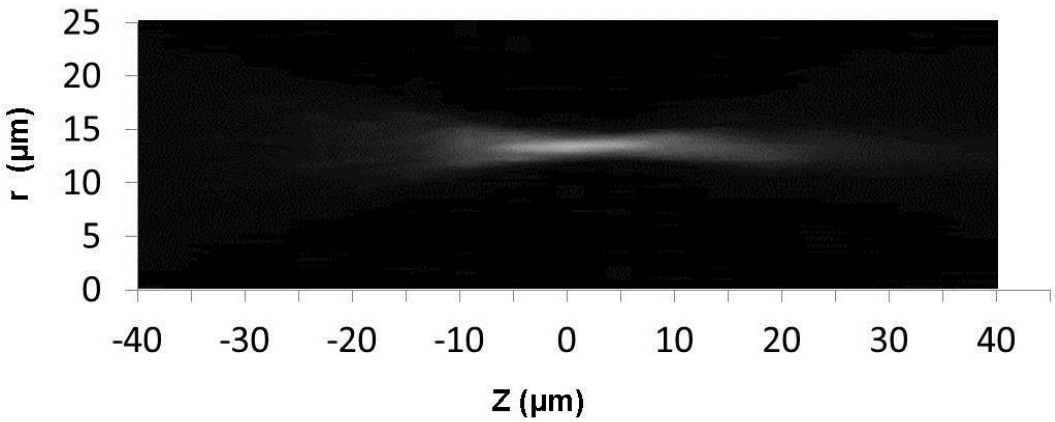

Fig. 7.8. *The measured output beam intensity profile of the imaging probe in water where r and Z are cylindrical coordinates with the Z axis pointing in the direction of beam propagation.*

7.4. Cell Transfection

The experimental setup was largely the same as is shown in Fig. 3.12 with the exception that the axicon tipped single mode fiber was replaced by a 35 cm long LMA-PCF with an imaging probe attached on the output end (Fig. 7.7). The overall transmission efficiency of the LMA-PCF and imaging probe for femtosecond laser beam delivery is about 25%. Due to time limitations, fluorescence imaging has not been tested on this device and the pulse duration has not as yet been measured. However, based on other studies it is expected that the pulse broadening of the femtosecond pulses passing through a LMA-PCF should be significantly decreased compared to using a single mode optical fiber at the same length [119, 120]. Therefore, the pulse duration of the output beam in this setup should be much lower than 800 fs as it is in Chapter 4 using an axicon tipped single mode fiber of the same length.

Optical transfection of CHO-K1 cells was preliminary attempted without optimization of the experiment parameters. The experimental procedures were the same as in Chapter 4. For each dose an output beam of 30 mW average power and 100 ms duration were used throughout the optical transfection experiments. Due to the longer working

distance, ~50 µm, compared with previously presented fiber based optical transfection devices, the imaging probe can be transversely scanned across the sample dish without the risk of contact between biological cells and the imaging probe. The efficiency of cell laser treatment was greatly increased. A total of 250 cells were manipulated, 50 cells per dish for 5 dishes. The transfection efficiency for each dish varied from 0% to 44% with an average efficiency of 13.6% (with a standard error of the mean of 4.25%) (Table 7.2). The number of spontaneously transfected cells varied between 0 – 2 cells for each sample dish.

Dish	*No. of Transfected Cell*	*Total No. of Treated Cells*	*Transfection Efficiency (%)*
1	22	50	44
2	0	50	0
3	0	50	0
4	5	50	10
5	7	50	14
Total	34	250	13.6 ± 4.25 (SM)

Table 7.2. *Transfection results. SM indicates the standard error of the mean.*

7.5. Summary and Conclusion

At the beginning of this chapter the development of miniaturized microscope technique was briefly reviewed. Taking inspiration from miniaturized microscopy techniques, a 2X4X7.02 mm GRIN lens based imaging probe was designed and built. A LMA-PCF with a larger core (~20 µm in diameter) was used for femtosecond laser beam delivery to decrease the pulse broadening effect. This probe utilizes a design that has a separated beam paths for delivery of the 800 nm femtosecond laser beam and for fluorescence imaging (450 nm – 600 nm). A longer working

distance of ~50 µm (which can be increased to 60 µm with a larger spot size) and a smaller beam spot of ~2 µm diameter, compared with the previously presented fiber based optical transfection technique have been achieved. Therefore a higher transfection efficiency and a more user friendly device can be expected. Due to time limitations, fluorescence imaging has not as yet been tested on this probe.

This device has great potential to be used as a hand-held microscope for skin treatment and could also be inserted directly into biological tissue through a tube or needle for long term imaging and/or treatment. A pencil-like or matchbox shaped housing for the imaging probe will be developed in the future along with a liquid delivery module. A hollow core PCF will be used to replace LMA-PCF to further decrease the femtosecond pulse broadening in the next phase of the experiment. Further miniaturization of the imaging probe will also be investigated. In addition to broadening this study to include different cell lines, spinal cord and hippocampus tissue slices will also be experimented with for optical manipulation. The aim is to develop versatile, inexpensive, portable devices that can be used for *in vivo* optical manipulation at a sub-cellular level. This would open exciting potential for commercialization of this device.

Chapter 8:

8. Conclusion & Future Outlook

8.1. Summary of Thesis

This thesis began with a brief introduction to the basic principles of gene transfer, which include the brief introduction of the definition of cell transfection and three basic objectives for any successful transfections; the reporter genes commonly used to assess different transfection methods and how to measure these transfection efficiencies were also introduced.

Chapter 1 continued to briefly introduce most of the popular non-viral (chemical and physical) gene transfection technologies. By comparison with these traditional gene transfection methods, it is easier to understand the strength and weakness of laser based optical transfection techniques.

Chapter 2 focused on the introduction of mechanisms of femtosecond laser mediated cell membrane permeabilization and briefly mentioned other laser transfection techniques. Instead of biological tissue, pure water was used as a model to illustrate the plasma formation in bulk material since the optical breakdown threshold in water is similar to that in biological tissue and optical transfection is performed in liquid environment. Plasma formation through a highly focused femtosecond laser beam in pure water was discussed thoroughly. The time evolution of the free electron at the focus was studied and the simulation showed that the electron density can be very well controlled through the tuning of the relative laser irradiance value, wide density range below optical breakdown threshold can be created. The relationship between pulse duration and optical breakdown thresholds were also investigated.

Low density plasma induced chemical effects (ROS and free electron mediated fragmentation of biomolecules) were also discussed and believed to be the main mechanism of the membrane

permeabilization during femtosecond optical transfection. Temperature evolution within the laser focus is also explored through numerical simulation and it excludes the highly localized moderate heat accumulation effects being a major effect for cell membrane permeabilization. The simulation shows that long-lasting bubbles created under the parameters used for optical transfection cause much more damage to biological tissue and better to be avoided. Chapter 2 then moved on to review the development of femtosecond laser mediated optical transfection technique and discuss the propagation of femtosecond pulses through the core of an optical fiber since fiber based optical transfection is the main topic of this thesis. Two ultrashort pulse dispersion mechanisms, GVD and SPM, were introduced. Chapters 1 and 2 serve as a theoretical background to fiber based optical transfection work in Chapter 4, 5, 6 and 7. An understanding of the mechanisms from biology and physics aspects can help to understand better and optimize this technique.

Chapter 3 reviewed various microlensed fiber fabrication methods, including arc discharge, laser micro-machining, polishing, chemical etching, single- and two-photon polymerization and FIB milling technique. While choosing a suitable microlensed fabrication method for a specific application there are several factors to be considered such as the operating wavelength, output beam profile, optical break down threshold, fabrication cost, instrumentation and throughput. The design requirements for microlensed fibers are diverse due to the diversity of the fields in which they are used; there is no single fabrication technique which can be chosen as the best. Each fabrication method has its own merits and each of them caters some specific requirements depending on the field of application. Therefore, based on the specific applications, among various techniques, chemical etching method in Chapter 4 and 6, single-photon polymerization method in Chapter 5 were used to fabricate microlensed fiber with tailored parameters that fulfill the requirements of my experiments.

Chapter 4 showed successful axicon tipped fiber based optical transfection of CHO-K1 cells. An axicon tipped single mode optical fiber was used to direct and target the femtosecond laser pulses on the cell membrane to perform optical transfection. A selective chemical etching method was adopted for fabrication of axicon tipped optical fibers. This method provides many advantages over the alternatives in this particular application of fiber based optical transfection. The fabrication and characterization of axicon tipped fibers and properties of the output beam in water have been discussed in detail. A theoretical model has been developed, which provides a good simulation and prediction of the output beam from an axicon tipped fiber. Finally, based on experimental characterization, theoretical modeling and some physical limitations, a fiber with an axicon of ~110º was chosen to perform optical transfection. A new experimental configuration, to include accommodation of the fiber into a microscope based optical transfection setup, positioning of the fiber relative to CHO-K1 cells and imaging of the cells has also been developed. The transfection efficiencies achieved using axicon tipped fiber compare favorably with the traditional free-space transfection technique.

Chapter 5 reported the first realization of an optical transfection system which can deliver genes locally, near the vicinity of the cell to be transfected. In order to achieve this, a fiber based optical transfection system was developed which is viable and easy to implement compared to its previously reported counterpart – the traditional optical transfection system. A novel fabrication method, mentioned in section 4.6.1 (single-photon polymerization technique), was described in detail in this chapter in order to produce a polymer microlens at the tip of an optical fiber. This method is cheap, less complex than most of the lensed fiber fabrication techniques and has the flexibility of fabricating customized microlenses for specific applications compared to other existing microlens fabrication techniques. This fabrication technique was used to fabricate a ‘microstick’ which can produce a tightly focused beam (~3 µm focal diameter) with a comparatively large working distance (~20 µm), which is ideal for fiber

based femtosecond optical transfection of cells. This microlens tipped fiber was used for optical transfection of CHO-K1 cells and the transfection efficiency achieved is comparable to that of conventional free-space optical transfection setups and significantly better than the previously reported axicon tipped fiber based optical transfection (Chapter 4). By combining the microlens tipped fiber with a microcapillary system, an integrated system that achieves localized drug (gene) delivery during transfection was produced. A MMF based illumination system was also combined with this integrated system to allow the efficient visual identification of the cell boundaries during optical transfection. This integrated system was used for optical transfection of CHO-K1 and HEK-293 cells and the obtained transfection efficiency was better than that of the non-integrated system. Also with the integrated system, the total amount of DNA required for transfection could be lowered significantly. This new technique opens up prospects for a portable “hand-held” system that can locally deliver therapeutic agents and transfect cells within a fiber geometry placing minimal requirements upon any microscope system. However, an objective lens was still needed in the configuration of this experiment, which prevents the integrated system to be used in *in vivo* applications. This problem was tackled in Chapter 6.

Chapter 6 demonstrated the first endoscope-like, fiber-based optical transfection system combined with localized microfluidic drug delivery and fluorescent imaging. This system, without the need of an objective lens for imaging, is an upgraded version of the integrated system presented in Chapter 5. A single imaging fiber was used for fluorescent imaging, laser delivery, and illumination. A circular field of view of ~300 µm in diameter and a resolution of ~7.6 µm were achieved through this imaging fiber. Multiple cells within one field of view and the shapes of each fluorescent cell can be clearly resolved. An ordered array of micro-axicons with an apex angle of 55º was chemically created at the polished exit surface of the imaging fiber in order to increase the light intensity at a relative remote distance. A beam spot of 3.75 µm in diameter was targeted on the cell

membrane, which is located 5 µm away from the apex of the micro-axicon lens for the protection of both fiber tip and biological cells. This device is a step forward toward achieving an endoscopic system for *in vivo* optical transfection applications because it is possible to achieve imaging with subcellular resolution with this device.

One weakness of the endoscope-like system presented in Chapter 6 is the short working distance. In order to overcome this, miniaturized microscopy technique was adopted in Chapter 7 to build a miniaturized microscope that can perform fluorescence imaging and optical transfection simultaneously. At the beginning of this chapter the development of miniaturized microscope technique was briefly reviewed. The common components, including various types of optical fiber, focusing mechanism and scanning mechanism, for building a miniaturized microscope have been discussed. Based on these components, different embodiments of a miniaturized microscope with their own merit and demerit can be built. A few common type miniaturized microscopes were also presented. Taking inspiration from miniaturized microscopy techniques, a 2X4X7.02 mm GRIN lens based imaging probe was designed and built. A LMA-PCF with a larger core (~20 µm in diameter) was used for femtosecond laser beam delivery to decrease the pulse broadening effect. This probe utilizes a design that has a separated beam paths for delivery of the 800 nm femtosecond laser beam and for fluorescence imaging (450 nm – 600 nm). A longer working distance of ~50 µm (which can be increased to 60 µm with a larger spot size) and a smaller beam spot of ~2 µm diameter, compared with the previously presented fiber based optical transfection technique have been achieved. Therefore a higher transfection efficiency and a more user friendly device can be expected. Due to time limitations, fluorescence imaging has not as yet been tested on this probe.

8.2. Future Work

8.2.1 Engineering Aspects

Optical transfection techniques would greatly benefit from advancements in engineering aspects. For example, the work presented in Chapter 7 can be readily improved in two aspects. First, pulse stretching can be further reduced using a hollow-core PCF instead of the LMA-PCF used for femtosecond laser pulses delivery. By doing this, a smaller laser focus spot is also expected due to the smaller mode field diameter of the hollow-core PCF (~7.5 μm in diameter, about 1/3 of the LMA-PCF). Therefore, theoretically, less damage to cells and the resulted higher transfection efficiency can be achieved. Second, a pencil-like or matchbox shaped housing for the imaging probe will be developed along with a liquid delivery module. The housing acting as a protection cover can be easily fabricated using a micro-milling machine.

To further improve the imaging probe, apart from adopting a micro-motor for axial positioning or rotational control, a micro-camera to avoid using long and thick imaging fiber for image delivery. This imaging probe can also be connected to a scanning microscope to become a miniaturized scanning microscope to achieve better imaging resolution and acquire sectioning ability [Fig. 7.6(a)]. This can also be realized using a scanning SMF [Fig. 7.6(c, d)] and by fabricating a microlens at the tip of the fiber (using chemical etching or single-photon polymerization technique discussed in Chapter 3), better resolution can be achieved. Bessel beams have been produced on fiber based imaging probes [209] and can be used for fiber based optical transfection to eliminate the requirement for precise cell membrane targeting.

Recently, an electrically tunable lens was used to realize fast axial focus shifts within 15ms [309]. This type of lens has a great potential to be used in miniaturized microscopy technique to adjust the focus without the involvement of any moving parts. In the near future, as soon as the

miniaturized version of this lens comes available, the flexibility, miniaturization and imaging (sectioning) speed of the miniaturized microscope can all be greatly improved.

Other avenues for further developing miniaturized optical transfection technique could be to integrate this technique with other popular tools, such as microfluidic chips, two-photon microscopy, OCT, Raman spectroscopy and optical trapping. The long-term aim is to develop a versatile, inexpensive, portable biophotonics workstation, which can be used for *in vivo* and *ex vivo* optical manipulation, at a sub-cellular level. This would open exciting potential for various applications and commercialization of this device.

8.2.2 Biology

Apart from further improvement from physics and engineering aspects, the fundamental breakthroughs stem from biology or biochemistry are essential for optical transfection to achieve and finally reach the clinical level.

One of the problems of optical transfection technique is that the parameters (including laser power, pulse duration, DNA concentration and cell passage number) for transfection of different cell lines are often different [70, 246]. Therefore broadening this technique to include various model cell lines and build up a data base with sets of optimized transfection parameters for each cell lines (similar to nucleofection technique introduced in section 1.2.3.1) are essential for optical transfection technique to become standardized and eventually commercialized. Other cell types including primary neuronal cells, stem cells, fungi (such as yeast), bacteria, plant cells and small living organisms, such as *C. elegans* roundworm could all potentially be optically transfected.

Optical transfection, especially miniaturized transfection techniques, could be potentially proved particularly useful for studying neuronal cells *in vivo* or *ex vivo*, by selectively manipulating individual neurons within a

large cell population. Cultured cell lines, isolated neuronal cells, tissue (spinal cord or hippocampus) slices and finally *in vivo* trials (with animal brains) are some of the possible paths for the development of optical transfection towards the clinical arena. The current research of optical transfection is moving from transfection of cultured cell lines towards isolated neuron cells. This brings another challenge as neurons are non-dividing cells and in order for the DNA to be transcribed it has to be delivered into the nucleus of the cell, which is mainly relies on the mitotic division of the cells. Some synthetic peptides (NeuroFECT Reagent, Genlantis, Inc.) have been designed for transfection of neuronal cells, but are not effective when used in optical transfection scenario. This challenge might be solved by using mRNA instead of DNA, because mRNA can be directly transcribed in the cytoplasm. Other possibilities such as using different carrier solutions (rather than OptiMEM), modulation of the extracellular space and plasmid construction, might be keys for this optical transfection technique to reach clinical level.

Appendix A

A. The Simulated Output Beam Intensity Profiles of an Axicon Tipped Fiber

The MATLAB source code:

```
%%%%%%%%%%%%%%%%%%%%%%%%%%%%%%%%%%%%%%%%%%%%%%%%%%
%% An example of free space propagation of the output beam from an axicon tipped single %%
mode optical fiber using Hankel transform
%% Nan Ma 2011
%%%%%%%%%%%%%%%%%%%%%%%%%%%%%%%%%%%%%%%%%%%%%%%%%%
%% Input parameters; length unit is 1µm
lambda=.8;                      %% wavelength
rmax=5;                         %% the field boundary
w=2.8;                          %% width of incoming Gausian beam = half of core diameter
nf=1.5;                         %% refractive index of fiber core
nw=1.33;                        %% refractive index of water
axang=55/180*pi;                %% axang is half axicon angle
axang2=axang+asin(nf/nw*cos(axang))-pi/2;
                                %% axang2 is the angle between output beam and Z axis
zmax=30;                        %% end of beam propagation
st=0.125;                       %% step for propagation
%%%%%%%%%%%%%%%%%%%%%%%%%%%%%%%%%%%%%%%%%%%%%%%%%%
k=2*pi/lambda;                  %% k-vector length
N=rmax*k;                       %% sampling condition
r=rmax*[0:1/N:1].^2;            %% declaration of radius coordinate
R=[0:1/N:1].^2;                 %% spatial spectrum coordinate
dr=2*rmax*[0:N]/N.^2;
dR=2*[0:N]/N.^2;
rlin=rmax*[0:1/N:1];            %% equidistant sampled coordinate
for j=1:size(r,2)               %% to evaluate indices for r -> rlin transform
        [null,ind(round(j))]=min(abs(r-rlin(j)));
end
in=1;
H=k*besselj(0,k*r'*R);          %% the Hankel transform matrix
f=exp(-(r/w).^2);               %% Input field declaration
```

```
fc=f.*exp(i*k*((w-
(r*(1+sin(axang2)/tan(axang)/cos(axang2))))/tan(axang)*nf+(r*(1+sin(axang2)/tan(axang)/co
s(axang2)))/tan(axang)/cos(axang2)*nw));
                                 %% Axicon modification
                                 %% Initial plane is transformed from Plane 1 to Plane2
F=(fc.*r.*dr)*H;                 %% Hankel transform
%%%%%%%%%%%%%%%%%%%%%%%%%%%%%%%%%%%%%%%%%%%%%%%%%%%%%%%%%%%%%%%%%%%%%%%%%%%%%%%%%%%%%%%%%%%%%%%%%%%
%% Free space propagation
v=zeros(size(r,2),zmax/st+1);    % % memory allocation for the intensity distribution
for z=0:st:zmax
Fz=F.*exp(i*k*z*nw*(sqrt(1-(R).^2)));
ff=(Fz.*R.*dR)*H;                 %% Inverse Hankel transform
fr=ff(ind);                      %% r -> rlin transform
plot(r,abs(ff).^2);
drawnow;
v(:,in)=abs(fr').^2;             %% the field intensity
in=in+1;
end
%%%%%%%%%%%%%%%%%%%%%%%%%%%%%%%%%%%%%%%%%%%%%%%%%%%%%%%%%%%%%%%%%%%%%%%%%%%%%%%%%%%%%%%%%%%%%%%%%%%
imshow(log10([flipud(v(2:size(v,1),:));v]+1)/max(max(log10(v+1))))
```

Bibliography

1. A. E. Siegman, *Lasers* (University Science Books, 1986).
2. F. Träger, *Springer handbook of lasers and optics* (Springer, New York, 2007).
3. R. M. Twyman, *Gene transfer to animal cells* (BIOS Scientific, Abingdon, 2005).
4. W. C. Heiser, *Gene delivery to mammalian cells. Vol. 2, Viral gene transfer techniques* (Humana ; Oxford : Blackwell, Totowa, N.J., 2003).
5. W. C. Heiser, *Gene delivery to mammalian cells. Vol. 1, Nonviral gene transfer techniques* (Humana ; Oxford : Blackwell, Totowa, N.J., 2003).
6. K. Appasani, *MicroRNAs : from basic science to disease biology* (Cambridge University Press, Cambridge, 2008).
7. J. Lippincott-Schwartz, and G. H. Patterson, "Development and use of fluorescent protein markers in living cells," Science **300**, 87-91 (2003).
8. G. Lipps, *Plasmids : current research and future trends* (Caister Academic, Wymondham, 2008).
9. S. D. Dib-Hajj, J. S. Choi, L. J. Macala, L. Tyrrell, J. A. Black, T. R. Cummins, and S. G. Waxman, "Transfection of rat or mouse neurons by biolistics or electroporation," Nat Protoc **4**, 1118-1126 (2009).
10. T. Imaoka, I. Date, T. Ohmoto, T. Yasuda, and M. Tsuda, "In vivo gene transfer into the adult mammalian central nervous system by continuous injection of plasmid DNA-cationic liposome complex," Brain Res **780**, 119-128 (1998).
11. D. C. Chang, and T. S. Reese, "Changes in membrane structure induced by electroporation as revealed by rapid-freezing electron microscopy," Biophys J **58**, 1-12 (1990).
12. T. A. Yang, W. C. Heiser, and J. M. Sedivy, "Efficient in situ electroporation of mammalian cells grown on microporous membranes," Nucleic Acids Res **23**, 2803-2810 (1995).
13. H. Potter, "Transfection by electroporation," Curr Protoc Immunol **Chapter 10**, Unit 10 15 (2001).
14. M. Zeitelhofer, J. P. Vessey, Y. Xie, F. Tubing, S. Thomas, M. Kiebler, and R. Dahm, "High-efficiency transfection of mammalian neurons via nucleofection," Nat Protoc **2**, 1692-1704 (2007).
15. J. Rathenberg, T. Nevian, and V. Witzemann, "High-efficiency transfection of individual neurons using modified electrophysiology techniques," J Neurosci Methods **126**, 91-98 (2003).
16. M. Graessmann, and A. Graessmann, "Microinjection of tissue culture cells," Methods Enzymol **101**, 482-492 (1983).
17. W. Ansorge, and R. Pepperkok, "Performance of an automated system for capillary microinjection into living cells," J Biochem Biophys Methods **16**, 283-292 (1988).
18. M. Uchida, X. W. Li, P. Mertens, and H. O. Alpar, "Transfection by particle bombardment: delivery of plasmid DNA into mammalian cells using gene gun," Biochim Biophys Acta **1790**, 754-764 (2009).

19. R. S. Williams, S. A. Johnston, M. Riedy, M. J. DeVit, S. G. McElligott, and J. C. Sanford, "Introduction of foreign genes into tissues of living mice by DNA-coated microprojectiles," Proc Natl Acad Sci U S A **88**, 2726-2730 (1991).
20. J. E. Biewenga, O. H. Destree, and L. H. Schrama, "Plasmid-mediated gene transfer in neurons using the biolistics technique," J Neurosci Methods **71**, 67-75 (1997).
21. P. Campbell, and M. R. Prausnitz, "Future directions for therapeutic ultrasound," Ultrasound Med Biol **33**, 657 (2007).
22. R. K. Schlicher, H. Radhakrishna, T. P. Tolentino, R. P. Apkarian, V. Zarnitsyn, and M. R. Prausnitz, "Mechanism of intracellular delivery by acoustic cavitation," Ultrasound Med Biol **32**, 915-924 (2006).
23. V. G. Zarnitsyn, and M. R. Prausnitz, "Physical parameters influencing optimization of ultrasound-mediated DNA transfection," Ultrasound Med Biol **30**, 527-538 (2004).
24. P. Prentice, A. Cuschierp, K. Dholakia, M. Prausnitz, and P. Campbell, "Membrane disruption by optically controlled microbubble cavitation," Nature Physics **1**, 107-110 (2005).
25. J. Wu, and W. L. M. Nyborg, *Emerging therapeutic ultrasound* (World Scientific, 2006).
26. R. Rao, and S. Nanda, "Sonophoresis: recent advancements and future trends," J Pharm Pharmacol **61**, 689-705 (2009).
27. S. Kurata, M. Tsukakoshi, T. Kasuya, and Y. Ikawa, "The laser method for efficient introduction of foreign DNA into cultured cells," Exp Cell Res **162**, 372-378 (1986).
28. U. K. Tirlapur, and K. Konig, "Cell biology - Targeted transfection by femtosecond laser," Nature **418**, 290-291 (2002).
29. M. L. Torres-Mapa, L. Angus, M. Ploschner, K. Dholakia, and F. J. Gunn-Moore, "Transient transfection of mammalian cells using a violet diode laser," J Biomed Opt **15**, 041506 (2010).
30. D. Stevenson, B. Agate, X. Tsampoula, P. Fischer, C. T. A. Brown, W. Sibbett, A. Riches, F. Gunn-Moore, and K. Dholakia, "Femtosecond optical transfection of cells: viability and efficiency," Optics Express **14**, 7125-7133 (2006).
31. V. Venugopalan, A. Guerra, K. Nahen, and A. Vogel, "Role of Laser-Induced Plasma Formation in Pulsed Cellular Microsurgery and Micromanipulation," Physical Review Letters **88**, 078103 (2002).
32. F. Helmchen, and W. Denk, "Deep tissue two-photon microscopy," Nature Methods **2**, 932-940 (2005).
33. J. Guck, R. Ananthakrishnan, H. Mahmood, T. J. Moon, C. C. Cunningham, and J. Kas, "The optical stretcher: a novel laser tool to micromanipulate cells," Biophys J **81**, 767-784 (2001).
34. V. Kohli, A. Y. Elezzabi, and J. P. Acker, "Cell nanosurgery using ultrashort (femtosecond) laser pulses: Applications to membrane surgery and cell isolation," Laser Surg Med **37**, 227-230 (2005).
35. P. Fischer, A. McWilliam, L. Paterson, C. T. A. Brown, W. Sibbett, K. Dholakia, and M. P. MacDonald, "Two-photon ablation with 1278 nm laser radiation," Journal of Optics a-Pure and Applied Optics **9**, S19-S23 (2007).

36. C. T. A. Brown, D. J. Stevenson, X. Tsampoula, C. McDougall, A. A. Lagatsky, W. Sibbett, F. Gunn-Moore, and K. Dholakia, "Enhanced operation of femtosecond lasers and applications in cell transfection," Journal of Biophotonics **1**, 183-199 (2008).
37. A. Uchugonova, A. Isemann, E. Gorjup, G. Tempea, R. Buckle, W. Watanabe, and K. Konig, "Optical knock out of stem cells with extremely ultrashort femtosecond laser pulses," J Biophotonics **1**, 463-469 (2008).
38. D. J. Stevenson, F. J. Gunn-Moore, P. Campbell, and K. Dholakia, "Single cell optical transfection," J R Soc Interface **7**, 863-871 (2010).
39. G. Palumbo, M. Caruso, E. Crescenzi, M. F. Tecce, G. Roberti, and A. Colasanti, "Targeted gene transfer in eucaryotic cells by dye-assisted laser optoporation," Journal of Photochemistry and Photobiology B-Biology **36**, 41-46 (1996).
40. H. Schneckenburger, A. Hendinger, R. Sailer, W. S. Strauss, and M. Schmitt, "Laser-assisted optoporation of single cells," J Biomed Opt **7**, 410-416 (2002).
41. A. V. Nikolskaya, V. P. Nikolski, and I. R. Efimov, "Gene printer: laser-scanning targeted transfection of cultured cardiac neonatal rat cells," Cell Commun Adhes **13**, 217-222 (2006).
42. A. Vogel, J. Noack, G. Huttman, and G. Paltauf, "Mechanisms of femtosecond laser nanosurgery of cells and tissues," Appl Phys B-Lasers O **81**, 1015-1047 (2005).
43. M. Tsukakoshi, S. Kurata, Y. Nomiya, Y. Ikawa, and T. Kasuya, "A Novel Method of DNA Transfection by Laser Microbeam Cell Surgery," Appl Phys B-Photo **35**, 135-140 (1984).
44. R. F. Marchington, Y. Arita, X. Tsampoula, F. J. Gunn-Moore, and K. Dholakia, "Optical injection of mammalian cells using a microfluidic platform," Biomed Opt Express **1**, 527-536 (2010).
45. M. F. Yanik, H. Cinar, H. N. Cinar, A. D. Chisholm, Y. S. Jin, and A. Ben-Yakar, "Neurosurgery - Functional regeneration after laser axotomy," Nature **432**, 822-822 (2004).
46. C. L. Hoy, N. J. Durr, P. Y. Chen, W. Piyawattanametha, H. Ra, O. Solgaard, and A. Ben-Yakar, "Miniaturized probe for femtosecond laser microsurgery and two-photon imaging," Optics Express **16**, 9996-10005 (2008).
47. C. McDougall, D. J. Stevenson, C. T. Brown, F. Gunn-Moore, and K. Dholakia, "Targeted optical injection of gold nanoparticles into single mammalian cells," J Biophotonics **2**, 736-743 (2009).
48. Y. A. Badr, M. A. Kereim, M. A. Yehia, O. O. Fouad, and A. Bahieldin, "Production of fertile transgenic wheat plants by laser micropuncture," Photochem Photobiol Sci **4**, 803-807 (2005).
49. W. Tao, J. Wilkinson, E. J. Stanbridge, and M. W. Berns, "Direct gene transfer into human cultured cells facilitated by laser micropuncture of the cell membrane," Proc Natl Acad Sci U S A **84**, 4180-4184 (1987).
50. Y. Guo, H. Liang, and M. W. Berns, "Laser-mediated gene transfer in rice," Physiologia Plantarum **93**, 19-24 (1995).
51. Y. Shirahata, N. Ohkohchi, H. Itagak, and S. Satomi, "New technique for gene transfection using laser irradiation," J Invest Med **49**, 184-190 (2001).

52. L. Paterson, B. Agate, M. Comrie, R. Ferguson, T. K. Lake, J. E. Morris, A. E. Carruthers, C. T. A. Brown, W. Sibbett, P. E. Bryant, F. Gunn-Moore, A. C. Riches, and K. Dholakia, "Photoporation and cell transfection using a violet diode laser," Optics Express **13**, 595-600 (2005).
53. J. S. Soughayer, T. Krasieva, S. C. Jacobson, J. M. Ramsey, B. J. Tromberg, and N. L. Allbritton, "Characterization of cellular optoporation with distance," Analytical Chemistry **72**, 1342-1347 (2000).
54. I. B. Clark, E. G. Hanania, J. Stevens, M. Gallina, A. Fieck, R. Brandes, B. O. Palsson, and M. R. Koller, "Optoinjection for efficient targeted delivery of a broad range of compounds and macromolecules into diverse cell types," J Biomed Opt **11**, 014034 (2006).
55. Y. Arita, M. L. Torres-Mapa, W. M. Lee, T. ?i?már, P. Campbell, F. J. Gunn-Moore, and K. Dholakia, *Spatially optimized gene transfection by laser-induced breakdown of optically trapped nanoparticles* (AIP, 2011).
56. U. K. Tirlapur, K. Konig, C. Peuckert, R. Krieg, and K. J. Halbhuber, "Femtosecond near-infrared laser pulses elicit generation of reactive oxygen species in mammalian cells leading to apoptosis-like death," Exp Cell Res **263**, 88-97 (2001).
57. E. Zeira, A. Manevitch, A. Khatchatouriants, O. Pappo, E. Hyam, M. Darash-Yahana, E. Tavor, A. Honigman, A. Lewis, and E. Galun, "Femtosecond infrared laser-an efficient and safe in vivo gene delivery system for prolonged expression," Mol Ther **8**, 342-350 (2003).
58. V. Kohli, J. P. Acker, and A. Y. Elezzabi, "Reversible permeabilization using high-intensity femtosecond laser pulses: applications to biopreservation," Biotechnol Bioeng **92**, 889-899 (2005).
59. F. Stracke, I. Rieman, and K. Konig, "Optical nanoinjection of macromolecules into vital cells," J Photochem Photobiol B **81**, 136-142 (2005).
60. L. E. Barrett, J. Y. Sul, H. Takano, E. J. Van Bockstaele, P. G. Haydon, and J. H. Eberwine, "Region-directed phototransfection reveals the functional significance of a dendritically synthesized transcription factor," Nat Methods **3**, 455-460 (2006).
61. M. J. Zohdy, C. Tse, J. Y. Ye, and M. O'Donnell, "Optical and acoustic detection of laser-generated microbubbles in single cells," IEEE Trans Ultrason Ferroelectr Freq Control **53**, 117-125 (2006).
62. C. Peng, R. E. Palazzo, and I. Wilke, "Laser intensity dependence of femtosecond near-infrared optoinjection," Phys Rev E Stat Nonlin Soft Matter Phys **75**, 041903 (2007).
63. X. Tsampoula, K. Taguchi, T. Cizmar, V. Garces-Chavez, N. Ma, S. Mohanty, K. Mohanty, F. Gunn-Moore, and K. Dholakia, "Fibre based cellular transfection," Optics Express **16**, 17007-17013 (2008).
64. J. Baumgart, W. Bintig, A. Ngezahayo, S. Willenbrock, H. M. Escobar, W. Ertmer, H. Lubatschowski, and A. Heisterkamp, "Quantified femtosecond laser based opto-perforation of living GFSHR-17 and MTH53a cells," Optics Express **16**, 3021-3031 (2008).
65. M. Lei, H. Xu, H. Yang, and B. Yao, "Femtosecond laser-assisted microinjection into living neurons," J Neurosci Methods **174**, 215-218 (2008).

66. X. Tsampoula, V. Garcés-Chávez, M. Comrie, D. J. Stevenson, B. Agate, C. T. A. Brown, F. Gunn-Moore, and K. Dholakia, *Femtosecond cellular transfection using a nondiffracting light beam* (AIP, 2007).
67. A. Uchugonova, K. Konig, R. Bueckle, A. Isemann, and G. Tempea, "Targeted transfection of stem cells with sub-20 femtosecond laser pulses," Optics Express **16**, 9357-9364 (2008).
68. A. Yamaguchi, Y. Hosokawa, G. Louit, T. Asahi, C. Shukunami, Y. Hiraki, and H. Masuhara, "Nanoparticle injection to single animal cells using femtosecond laser-induced impulsive force," Applied Physics A: Materials Science & Processing **93**, 39-43 (2008).
69. M. Antkowiak, M. L. Torres-Mapa, F. Gunn-Moore, and K. Dholakia, "Application of dynamic diffractive optics for enhanced femtosecond laser based cell transfection," Journal of Biophotonics **3**, 696-705 (2010).
70. P. Mthunzi, K. Dholakia, and F. Gunn-Moore, "Phototransfection of mammalian cells using femtosecond laser pulses: optimization and applicability to stem cell differentiation," J Biomed Opt **15**, 041507 (2010).
71. N. Ma, P. C. Ashok, D. J. Stevenson, F. J. Gunn-Moore, and K. Dholakia, "Integrated optical transfection system using a microlens fiber combined with microfluidic gene delivery," Biomed. Opt. Express **1**, 694-705 (2010).
72. B. B. Praveen, D. J. Stevenson, M. Antkowiak, K. Dholakia, and F. J. Gunn-Moore, "Enhancement and optimization of plasmid expression in femtosecond optical transfection," J Biophotonics **4**, 229-235 (2011).
73. P. Soman, W. Zhang, A. Umeda, Z. J. Zhang, and S. Chen, "Femtosecond laser-assisted optoporation for drug and gene delivery into single mammalian cells," J Biomed Nanotechnol **7**, 334-341 (2011).
74. S. K. Mohanty, M. Sharma, and P. K. Gupta, "Laser-assisted microinjection into targeted animal cells," Biotechnol Lett **25**, 895-899 (2003).
75. T. Knoll, L. Trojan, S. Langbein, S. Sagi, P. Alken, and M. S. Michel, "Impact of holmium:YAG and neodymium:YAG lasers on the efficacy of DNA delivery in transitional cell carcinoma," Lasers Med Sci **19**, 33-36 (2004).
76. H. He, S. K. Kong, R. K. Lee, Y. K. Suen, and K. T. Chan, "Targeted photoporation and transfection in human HepG2 cells by a fiber femtosecond laser at 1554 nm," Opt Lett **33**, 2961-2963 (2008).
77. S. Sagi, T. Knoll, L. Trojan, A. Schaaf, P. Alken, and M. S. Michel, "Gene delivery into prostate cancer cells by holmium laser application," Prostate Cancer Prostatic Dis **6**, 127-130 (2003).
78. F. Docchio, C. A. Sacchi, and J. Marshall, "Experimental investigation of optical breakdown thresholds in ocular media under single pulse irradiation with different pulse durations," Lasers Light Ophthalmol **1**, 10 (1986).
79. C. A. Sacchi, "Laser-induced electric breakdown in water," J. Opt. Soc. Am. B **8**, 337-345 (1991).
80. L. V. Keldysh, "Ionization in the field of a strong electromagnetic wave," Soviet Physics JETP **20**, 1307-1314 (1965).
81. G. Mainfray, and C. Manus, "Multiphoton Ionization of Atoms," Rep Prog Phys **54**, 1333-1372 (1991).
82. C. L. Arnold, A. Heisterkamp, W. Ertmer, and H. Lubatschowski, "Streak formation as side effect of optical breakdown during processing the bulk of

transparent Kerr media with ultra-short laser pulses," Applied Physics B: Lasers and Optics **80**, 247-253 (2005).
83. A.-C. Tien, S. Backus, H. Kapteyn, M. Murnane, and G. Mourou, "Short-Pulse Laser Damage in Transparent Materials as a Function of Pulse Duration," Physical Review Letters **82**, 3883-3886 (1999).
84. A. Kaiser, B. Rethfeld, M. Vicanek, and G. Simon, "Microscopic processes in dielectrics under irradiation by subpicosecond laser pulses," Physical Review B **61**, 11437-11450 (2000).
85. A. Vogel, J. Noack, K. Nahen, D. Theisen, S. Busch, U. Parlitz, D. X. Hammer, G. D. Noojin, B. A. Rockwell, and R. Birngruber, "Energy balance of optical breakdown in water at nanosecond to femtosecond time scales," Applied Physics B: Lasers and Optics **68**, 271-280 (1999).
86. J. F. Ready, *Effects of high-power laser radiation* (Academic Press, New York ; London, 1971).
87. K. Thornber, "Applications of scaling to problems in high-field electronic transport," J. Appl. Phys. **52**, 279 (1981).
88. D. Arnold, and E. Cartier, "Theory of laser-induced free-electron heating and impact ionization in wide-band-gap solids," Physical Review B **46**, 15102-15115 (1992).
89. B. Rethfeld, "Unified model for the free-electron avalanche in laser-irradiated dielectrics," Phys Rev Lett **92**, 187401 (2004).
90. B. C. Stuart, M. D. Feit, S. Herman, A. M. Rubenchik, B. W. Shore, and M. D. Perry, "Nanosecond-to-femtosecond laser-induced breakdown in dielectrics," Physical Review B **53**, 1749-1761 (1996).
91. L. V. Keldysh, "Kinetic theory of impact ionization in semiconductors," Sov. Phys. JETP **37**, 509 (1960).
92. S. S. Mao, F. Quéré, S. Guizard, X. Mao, R. E. Russo, G. Petite, and P. Martin, "Dynamics of femtosecond laser interactions with dielectrics," Applied Physics A: Materials Science & Processing **79**, 1695-1709 (2004).
93. M. Lenzner, J. Krüger, S. Sartania, Z. Cheng, C. Spielmann, G. Mourou, W. Kautek, and F. Krausz, "Femtosecond Optical Breakdown in Dielectrics," Physical Review Letters **80**, 4076-4079 (1998).
94. J. Noack, and A. Vogel, "Laser-induced plasma formation in water at nanosecond to femtosecond time scales: calculation of thresholds, absorption coefficients, and energy density," Quantum Electronics, IEEE Journal of **35**, 1156 (1999).
95. D. N. Nikogosyan, A. A. Oraevsky, and V. I. Rupasov, "Two-photon ionization and dissociation of liquid water by powerful laser UV radiation," Chemical Physics **77**, 131-143 (1983).
96. B. C. Garrett, D. A. Dixon, D. M. Camaioni, D. M. Chipman, M. A. Johnson, C. D. Jonah, G. A. Kimmel, J. H. Miller, T. N. Rescigno, P. J. Rossky, S. S. Xantheas, S. D. Colson, A. H. Laufer, D. Ray, P. F. Barbara, D. M. Bartels, K. H. Becker, K. H. Bowen, S. E. Bradforth, I. Carmichael, J. V. Coe, L. R. Corrales, J. P. Cowin, M. Dupuis, K. B. Eisenthal, J. A. Franz, M. S. Gutowski, K. D. Jordan, B. D. Kay, J. A. LaVerne, S. V. Lymar, T. E. Madey, C. W. McCurdy, D. Meisel, S. Mukamel, A. R. Nilsson, T. M. Orlando, N. G. Petrik, S. M. Pimblott, J. R. Rustad, G. K. Schenter, S. J. Singer, A. Tokmakoff, L.-S. Wang, and T. S.

Zwier, "Role of Water in Electron-Initiated Processes and Radical Chemistry: Issues and Scientific Advances," Chemical Reviews **105**, 355-390 (2004).
97. A. Heisterkamp, T. Ripken, T. Mamom, W. Drommer, H. Welling, W. Ertmer, and H. Lubatschowski, "Nonlinear side effects of fs pulses inside corneal tissue during photodisruption," Applied Physics B: Lasers and Optics **74**, 419-425 (2002).
98. B. Boudaiffa, P. Cloutier, D. Hunting, M. A. Huels, and L. Sanche, "Resonant formation of DNA strand breaks by low-energy (3 to 20 eV) electrons," Science **287**, 1658-1660 (2000).
99. S. Gohlke, and E. Illenberger, "Probing biomolecules: Gas phase experiments and biological relevance," Europhysics News **33**, 207-209 (2002).
100. M. A. Huels, B. Boudaïffa, P. Cloutier, D. Hunting, and L. Sanche, "Single, Double, and Multiple Double Strand Breaks Induced in DNA by 3−100 eV Electrons," J Am Chem Soc **125**, 4467-4477 (2003).
101. W. Steiner, P. Ambrosch, and R. T. Gregor, *Endoscopic laser surgery of the upper aerodigestive tract : with special emphasis on cancer surgery* (Thieme, Stuttgart, 2000).
102. A. Vogel, and V. Venugopalan, "Mechanisms of Pulsed Laser Ablation of Biological Tissues," Chemical Reviews **103**, 577-644 (2003).
103. G. Paltauf, and H. Schmidt-Kloiber, "Photoacoustic cavitation in spherical and cylindrical absorbers," Applied Physics A: Materials Science & Processing **68**, 525-531 (1999).
104. G. Paltauf, and P. E. Dyer, "Photomechanical Processes and Effects in Ablation," Chemical Reviews **103**, 487-518 (2003).
105. W. Supatto, D. Debarre, B. Moulia, E. Brouzes, J. L. Martin, E. Farge, and E. Beaurepaire, "In vivo modulation of morphogenetic movements in Drosophila embryos with femtosecond laser pulses," Proc Natl Acad Sci U S A **102**, 1047-1052 (2005).
106. K. Koenig, O. Krauss, and I. Riemann, "Intratissue surgery with 80 MHz nanojoule femtosecond laser pulses in the near infrared," Opt Express **10**, 171-176 (2002).
107. B. Masters, "Mitigating thermal mechanical damage potential during two-photon dermal imaging," J. Biomed. Opt. **9**, 1265 (2004).
108. K. Konig, I. Riemann, P. Fischer, and K. J. Halbhuber, "Intracellular nanosurgery with near infrared femtosecond laser pulses," Cell Mol Biol (Noisy-le-grand) **45**, 195-201 (1999).
109. K. Konig, I. Riemann, and W. Fritzsche, "Nanodissection of human chromosomes with near-infrared femtosecond laser pulses," Opt Lett **26**, 819-821 (2001).
110. L. Sacconi, I. M. Tolic-Norrelykke, R. Antolini, and F. S. Pavone, "Combined intracellular three-dimensional imaging and selective nanosurgery by a nonlinear microscope," J Biomed Opt **10**, 14002 (2005).
111. N. Smith, "Generation of calcium waves in living cells by pulsed-laser-induced photodisruption," Appl. Phys. Lett. **79**, 1208 (2001).
112. H. Oehring, I. Riemann, P. Fischer, K. J. Halbhuber, and K. Konig, "Ultrastructure and reproduction behaviour of single CHO-K1 cells exposed to near infrared femtosecond laser pulses," Scanning **22**, 263-270 (2000).

113. H. Niioka, N. I. Smith, K. Fujita, Y. Inouye, and S. Kawata, "Femtosecond laser nano-ablation in fixed andnon-fixed cultured cells," Opt. Express **16**, 14476-14495 (2008).
114. N. Ma, F. Gunn-Moore, and K. Dholakia, "Optical transfection using an endoscope-like system," J Biomed Opt **16**, 028002-028007 (2011).
115. J.-Y. Sul, C.-w. K. Wu, F. Zeng, J. Jochems, M. T. Lee, T. K. Kim, T. Peritz, P. Buckley, D. J. Cappelleri, M. Maronski, M. Kim, V. Kumar, D. Meaney, J. Kim, and J. Eberwine, "Transcriptome transfer produces a predictable cellular phenotype," Proceedings of the National Academy of Sciences **106**, 7624-7629 (2009).
116. J. Durnin, "Exact-Solutions for Nondiffracting Beams .1. The Scalar Theory," Journal of the Optical Society of America a-Optics Image Science and Vision **4**, 651-654 (1987).
117. V. Kohli, V. Robles, M. L. Cancela, J. P. Acker, A. J. Waskiewicz, and A. Y. Elezzabi, "An alternative method for delivering exogenous material into developing zebrafish embryos," Biotechnology and Bioengineering **98**, 1230-1241 (2007).
118. B. E. A. Saleh, and M. C. Teich, *Fundamentals of photonics* (Wiley ; [Chichester : John Wiley, distributor], Hoboken, N.J., 2007).
119. B. A. Flusberg, E. D. Cocker, W. Piyawattanametha, J. C. Jung, E. L. M. Cheung, and M. J. Schnitzer, "Fiber-optic fluorescence imaging," Nature Methods **2**, 941-950 (2005).
120. F. Helmchen, D. W. Tank, and W. Denk, "Enhanced two-photon excitation through optical fiber by single-mode propagation in a large core," Appl Opt **41**, 2930-2934 (2002).
121. D. G. Ouzounov, K. D. Moll, M. A. Foster, W. R. Zipfel, W. W. Webb, and A. L. Gaeta, "Delivery of nanojoule femtosecond pulses through large-core microstructured fibers," Opt. Lett. **27**, 1513-1515 (2002).
122. S. W. Clark, F. Ö. Ilday, and F. W. Wise, "Fiber delivery of femtosecond pulses from a Ti:sapphire laser," Opt. Lett. **26**, 1320-1322 (2001).
123. A. Méndez, and T. F. Morse, *Specialty optical fibers handbook* (Academic Press, Oxford, 2007).
124. J. I. Yamada, Y. Murakami, J. I. Sakai, and T. Kimura, "Characteristics of a Hemispherical Microlens for Coupling between a Semiconductor-Laser and Single-Mode Fiber," Ieee J Quantum Elect **16**, 1067-1072 (1980).
125. G. D. Khoe, J. Poulissen, and H. M. de Vrieze, "Efficient coupling of laser diodes to tapered monomode fibres with high-index end," Electronics Letters **19**, 205-207 (1983).
126. H. M. Presby, A. F. Benner, and C. A. Edwards, "Laser micromachining of efficient fiber microlenses," Appl Opt **29**, 2692-2695 (1990).
127. C. L. Bashford, C. H. Barlow, B. Chance, J. Haselgrove, and J. Sorge, "Optical Measurements of Oxygen Delivery and Consumption in Gerbil Cerebral-Cortex," Am J Physiol **242**, C265-C271 (1982).
128. A. Mayevsky, and B. Chance, "Intracellular oxidation-reduction state measured in situ by a multichannel fiber-optic surface fluorometer," Science **217**, 537-540 (1982).
129. R. M. Cothren, M. V. Sivak, J. VanDam, R. E. Petras, M. Fitzmaurice, J. M. Crawford, J. Wu, J. F. Brennan, R. P. Rava, R. Manoharan, and M. S. Feld,

"Detection of dysplasia at colonoscopy using laser-induced fluorescence: A blinded study," Gastrointest Endosc **44**, 168-176 (1996).
130. C. J. Frank, R. L. McCreery, and D. C. B. Redd, "Raman Spectroscopy of Normal and Diseased Human Breast Tissues," Anal. Chem. **67**, 777-783 (1995).
131. A. F. Gmitro, A. A. Tanbakuchi, J. A. Udovich, A. R. Rouse, and K. D. Hatch, "In vivo imaging of ovarian tissue using a novel confocal microlaparoscope," Am J Obstet Gynecol **202** (2010).
132. A. F. Gmitro, A. A. Tanbakuchi, A. R. Rouse, J. A. Udovich, and K. D. Hatch, "Clinical confocal microlaparoscope for real-time in vivo optical biopsies," J Biomed Opt **14** (2009).
133. L. Fu, and M. Gu, "Fibre-optic nonlinear optical microscopy and endoscopy," J Microsc **226**, 195-206 (2007).
134. B. Park, M. C. Pierce, B. Cense, S.-H. Yun, M. Mujat, G. Tearney, B. Bouma, and J. de Boer, "Real-time fiber-based multi-functional spectral-domain optical coherence tomography at 1.3 μm," Opt. Express **13**, 3931-3944 (2005).
135. B. J. Vakoc, R. M. Lanning, J. A. Tyrrell, T. P. Padera, L. A. Bartlett, T. Stylianopoulos, L. L. Munn, G. J. Tearney, D. Fukumura, R. K. Jain, and B. E. Bouma, "Three-dimensional microscopy of the tumor microenvironment in vivo using optical frequency domain imaging," Nat Med **15**, 1219-1223 (2009).
136. S. Mononobe, M. Naya, T. Saiki, and M. Ohtsu, "Reproducible fabrication of a fiber probe with a nanometric protrusion for near-field optics," Applied Optics **36**, 1496-1500 (1997).
137. M. Naya, R. Micheletto, S. Mononobe, R. U. Maheswari, and M. Ohtsu, "Near-field optical imaging of flagellar filaments of Salmonella in water with optical feedback control," Applied Optics **36**, 1681-1683 (1997).
138. A. V. Zvyagin, J. D. White, and M. Ohtsu, "Near-field optical microscope image formation: A theoretical and experimental study," Optics Letters **22**, 955-957 (1997).
139. T. Yatsui, M. Kourogi, and M. Ohtsu, "Increasing throughput of a near-field optical fiber probe over 1000 times by the use of a triple-tapered structure," Applied Physics Letters **73**, 2090-2092 (1998).
140. T. Saiki, and K. Matsuda, "Near-field optical fiber probe optimized for illumination-collection hybrid mode operation," Applied Physics Letters **74**, 2773-2775 (1999).
141. M. Chaigneau, G. Louarn, and T. M. Minea, "Nanoaperture formation at metal covered tips by microspark optimized for near-field optical probes," Applied Physics Letters **92** (2008).
142. S. Y. Ryu, H. Y. Chow, J. Na, E. S. Choi, and B. H. Lee, "Combined system of optical coherence tomography and fluorescence spectroscopy based on double-cladding fiber," Optics Letters **33**, 2347-2349 (2008).
143. S. Y. Ryu, H. Y. Choi, J. Na, W. J. Choi, and B. H. Lee, "Lensed fiber probes designed as an alternative to bulk probes in optical coherence tomography," Applied Optics **47**, 1510-1516 (2008).
144. K. M. Tan, M. Mazilu, T. H. Chow, W. M. Lee, K. Taguchi, B. K. Ng, W. Sibbett, C. S. Herrington, C. T. A. Brown, and K. Dholakia, "In-fiber common-path optical coherence tomography using a conical-tip fiber," Optics Express **17**, 2375-2384 (2009).

145. H. Y. Choi, S. Y. Ryu, J. H. Na, B. H. Lee, I. B. Sohn, Y. C. Noh, and J. M. Lee, "Single-body lensed photonic crystal fibers as side-viewing probes for optical imaging systems," Optics Letters **33**, 34-36 (2008).
146. E. J. Min, J. Na, S. Y. Ryu, and B. H. Lee, "Single-body lensed-fiber scanning probe actuated by magnetic force for optical imaging," Optics Letters **34**, 1897-1899 (2009).
147. S. K. Mohanty, K. S. Mohanty, and M. W. Berns, "Manipulation of mammalian cells using a single-fiber optical microbeam," J Biomed Opt **13**, - (2008).
148. Z. Hu, J. Wang, and J. Liang, "Manipulation and arrangement of biological and dielectric particles by a lensed fiber probe," Opt. Express **12**, 4123-4128 (2004).
149. S. K. Mohanty, K. S. Mohanty, and M. W. Berns, "Organization of microscale objects using a microfabricated optical fiber," Optics Letters **33**, 2155-2157 (2008).
150. C. Liberale, S. K. Mohanty, K. S. Mohanty, V. Degiorgio, S. Cabrini, A. Carpentiero, E. Ferrari, D. Cojoc, and E. Di Fabrizio, "Optical micromanipulation of microscopic particles using axicon tipped fiber," A. N. Cartwright, and D. V. Nicolau, eds. (SPIE, San Jose, CA, USA, 2006), pp. 60950F-60910.
151. N. Ma, F. Gunn-Moore, and K. Dholakia, "Optical transfection using an endoscope-like system," J. Biomed. Opt. **16**, 028002 (2011).
152. G. J. Kong, L. Kim, H. Y. Choi, L. E. Im, B. H. Park, U. C. Paek, and B. H. Lee, "Lensed photonic crystal fiber obtained by use of an arc discharge," Optics Letters **31**, 894-896 (2006).
153. K. Shiraishi, H. Ohnuki, N. Hiraguri, K. Matsumura, I. Ohishi, H. Morichi, and H. Kazami, "A lensed-fiber coupling scheme utilizing a graded-index fiber and a hemispherically ended coreless fiber tip," J Lightwave Technol **15**, 356-363 (1997).
154. E. Li, "Characterization of a fiber lens," Opt Lett **31**, 169-171 (2006).
155. K. Shiraishi, N. Oyama, K. Matsumura, I. Ohishi, and S. Suga, "A Fiber Lens with a Long Working Distance for Integrated Coupling between Laser-Diodes and Single-Mode Fibers," J Lightwave Technol **13**, 1736-1744 (1995).
156. G. Rego, "Fibre optic devices produced by arc discharges," J Opt-Uk **12**, - (2010).
157. Y. Murakami, J.-i. Yamada, J.-i. Sakai, and T. Kimura, "Microlens tipped on a single-mode fibre end for InGaAsP laser coupling improvement," Electronics Letters **16**, 321-322 (1980).
158. H. Kuwahara, M. Sasaki, and N. Tokoyo, "Efficient coupling from semiconductor lasers into single-mode fibers with tapered hemispherical ends," Appl Opt **19**, 2578-2583 (1980).
159. G. A. Valaskovic, M. Holton, and G. H. Morrison, "Parameter control, characterization, and optimization in the fabrication of optical fiber near-field probes," Appl Opt **34**, 1215-1228 (1995).
160. E. Betzig, J. K. Trautman, T. D. Harris, J. S. Weiner, and R. L. Kostelak, "Breaking the diffraction barrier: optical microscopy on a nanometric scale," Science **251**, 1468-1470 (1991).

161. A. Malki, R. Bachelot, and F. Van Lauwe, "Two-step process for micro-lens-fibre fabrication using a continuous CO2 laser source," Journal of Optics a-Pure and Applied Optics **3**, 291-295 (2001).
162. P. Hoffmann, B. Dutoit, and R. P. Salathe, "Comparison of mechanically drawn and protection layer chemically etched optical fiber tips," Ultramicroscopy **61**, 165-170 (1995).
163. H. M. Presby, and C. R. Giles, "Asymmetric Fiber Microlenses for Efficient Coupling to Elliptic Laser-Beams," Ieee Photonics Technology Letters **5**, 184-186 (1993).
164. K. Shiraishi, N. Kawasaki, H. Yoda, K. Watanabe, M. Umetsu, T. Hitomi, and K. Muro, "High-Index-Layer Coating on a Lensed Fiber Endface for Enhanced Focusing Power," J Lightwave Technol **27**, 864-870 (2009).
165. C. A. Edwards, H. M. Presby, and C. Dragone, "Ideal Microlenses for Laser to Fiber Coupling," J Lightwave Technol **11**, 252-257 (1993).
166. H. M. Presby, and C. A. Edwards, "Near 100-Percent-Efficient Fiber Microlenses," Electronics Letters **28**, 582-584 (1992).
167. H. Sakaguchi, N. Seki, and S. Yamamoto, "Power Coupling from Laser-Diodes into Single-Mode Fibers with Quadrangular Pyramid-Shaped Hemi-Ellipsoidal Ends," Electronics Letters **17**, 425-426 (1981).
168. V. S. Shah, L. Curtis, R. S. Vodhanel, D. P. Bour, and W. C. Young, "Efficient Power Coupling from a 980-nm, Broad-Area Laser to a Single-Mode Fiber Using a Wedge-Shaped Fiber Endface," J Lightwave Technol **8**, 1313-1318 (1990).
169. R. A. Modavis, and T. W. Webb, "Anamorphic Microlens for Laser-Diode to Single-Mode Fiber Coupling," Ieee Photonics Technology Letters **7**, 798-800 (1995).
170. T. Held, S. Emonin, O. Marti, and O. Hollricher, "Method to produce high-resolution scanning near-field optical microscope probes by beveling optical fibers," Rev Sci Instrum **71**, 3118-3122 (2000).
171. Y. T. Tseng, J. H. Liu, T. Y. Hung, and F. P. Huang, "Automation of active quadrangular pyramid-shaped fiber endface polishing method," Ieee T Adv Packaging **29**, 599-606 (2006).
172. T. Grosjean, S. S. Saleh, M. A. Suarez, I. A. Ibrahim, V. Piquerey, D. Charraut, and P. Sandoz, "Fiber microaxicons fabricated by a polishing technique for the generation of Bessel-like beams," Applied Optics **46**, 8061-8067 (2007).
173. L. Y. K. Yeh S M, Huang S Y, Lin H H, Hsieh C H, and C. W. H, "A novel scheme of lensed fiber employing a quadrangular-pyramid-shaped fiber endface for coupling between high-power laser diodes and single-mode fibers," **22**, 1374 (2004).
174. H. S. Y. Yeh S M, and C. W. H, "A new scheme of conical-wedge-shaped fiber endface for coupling between high-power laser diodes and single-mode fibers," J Lightwave Technol **23**, 1781 (2005).
175. T. Y. C. Lu Y K, Liu Y D, Yeh S M, Lin C C, and C. W. H, "Asymmetric elliptic-cone-shaped microlens for efficient coupling to high-power laser diodes," Optics Express **15**, 1434 (2007).
176. Y. C. Tsai, Y. D. Liu, C. L. Cao, Y. K. Lu, and W. H. Cheng, "A new scheme of fiber end-face fabrication employing a variable torque technique," Journal of Micromechanics and Microengineering **18**, 1-7 (2008).

177. T. Y. C. Lu Y K, Liu Y D, Yeh S M, Lin C C, and C. W. H, "Asymmetric elliptic-cone-shaped microlens for efficient coupling to high-power laser diodes," **15**, 1434 (2007).
178. M. Ohtsu, *Near-field nano/atom optics and technology* (Springer, Tokyo; London, 1998).
179. G. Eisenstein, and D. Vitello, "Chemically Etched Conical Microlenses for Coupling Single-Mode Lasers into Single-Mode Fibers," Applied Optics **21**, 3470-3474 (1982).
180. A. Kotsas, H. Ghafourishiraz, and T. S. M. Maclean, "Microlens Fabrication on Single-Mode Fibers for Efficient Coupling from Laser-Diodes," Opt Quant Electron **23**, 367-378 (1991).
181. S. K. Eah, W. Jhe, and Y. Arakawa, "Nearly diffraction-limited focusing of a fiber axicon microlens," Rev Sci Instrum **74**, 4969-4971 (2003).
182. T. Okayama, and H. Seki, "Fabrication and evaluation of silica-based optical fiber probes by chemical etching method," Optical Review **12**, 25-28 (2005).
183. S. K. Eah, H. M. Jaeger, N. F. Scherer, G. P. Wiederrecht, and X. M. Lin, "Plasmon scattering from a single gold nanoparticle collected through an optical fiber," Applied Physics Letters **86**, - (2005).
184. K. Maruyama, H. Ohkawa, S. Ogawa, A. Ueda, O. Niwa, and K. Suzuki, "Fabrication and characterization of a nanometer-sized optical fiber electrode based on selective chemical etching for scanning electrochemical/optical microscopy," Analytical Chemistry **78**, 1904-1912 (2006).
185. Y. J. Yu, H. Noh, M. H. Hong, H. R. Noh, Y. Arakawa, and W. Jhe, "Focusing characteristics of optical fiber axicon microlens for near-field spectroscopy: Dependence of tip apex angle," Optics Communications **267**, 264-270 (2006).
186. A. Chovin, P. Garrigue, P. Vinatier, and N. Sojic, "Development of an ordered array of optoelectrochemical individually readable sensors with submicrometer dimensions: Application to remote electrochemiluminescence imaging," Analytical Chemistry **76**, 357-364 (2004).
187. A. Chovin, P. Garrigue, I. Manek-Honninger, and N. Sojic, "Fabrication, characterization, and far-field optical properties of an ordered array of nanoapertures," Nano Lett **4**, 1965-1968 (2004).
188. B. A. F. Puygranier, and P. Dawson, "Chemical etching of optical fibre tips - experiment and model," Ultramicroscopy **85**, 235-248 (2000).
189. M. Kawachi, T. Edahiro, and H. Toba, "Microlens Formation on Vad Single-Mode Fiber Ends," Electronics Letters **18**, 71-72 (1982).
190. T. Pangaribuan, S. D. Jiang, and M. Ohsu, "Highly Controllable Fabrication of Fiber Probe for Photon Scanning Tunneling Microscope," Scanning **16**, 362-367 (1994).
191. D. R. C. T. Turner, Morris County, NJ), "Etch procedure for optical fibers," (AT&T Bell Laboratories (Murray Hill, NJ), United States, 1984).
192. S. I. Hosain, Y. Lacroute, and J. P. Goudonnet, "A simple low-cost highly reproducible method of fabricating optical fiber tips for a photon scanning tunneling microscope," Microw Opt Techn Let **13**, 243-248 (1996).
193. D. Zeisel, S. Nettesheim, B. Dutoit, and R. Zenobi, "Pulsed laser-induced desorption and optical imaging on a nanometer scale with scanning near-field

microscopy using chemically etched fiber tips," Applied Physics Letters **68**, 2491-2492 (1996).
194. D. Zeisel, B. Dutoit, V. Deckert, T. Roth, and R. Zenobi, "Optical spectroscopy and laser desorption on a nanometer scale," Analytical Chemistry **69**, 749-754 (1997).
195. M. A. Unger, D. A. Kossakovski, R. Kongovi, J. L. Beauchamp, J. D. Baldeschwieler, and D. V. Palanker, "Etched chalcogenide fibers for near-field infrared scanning microscopy," Rev Sci Instrum **69**, 2988-2993 (1998).
196. M. M. Tao, Y. L. Jin, N. Gu, and L. Huang, "A method to control the fabrication of etched optical fiber probes with nanometric tips," J Opt-Uk **12**, - (2010).
197. R. C. Dunn, N. E. Dickenson, E. S. Erickson, and O. L. Mooren, "Characterization of power induced heating and damage in fiber optic probes for near-field scanning optical microscopy," Rev Sci Instrum **78** (2007).
198. A. Lazarev, N. Fang, Q. Luo, and X. Zhang, "Formation of fine near-field scanning optical microscopy tips. Part I. By static and dynamic chemical etching," Rev Sci Instrum **74**, 3679-3683 (2003).
199. P. Lambelet, A. Sayah, M. Pfeffer, C. Philipona, and F. Marquis-Weible, "Chemically etched fiber tips for near-field optical microscopy: a process for smoother tips," Applied Optics **37**, 7289-7292 (1998).
200. R. Stockle, C. Fokas, V. Deckert, R. Zenobi, B. Sick, B. Hecht, and U. P. Wild, "High-quality near-field optical probes by tube etching," Applied Physics Letters **75**, 160-162 (1999).
201. M. Chaigneau, G. Ollivier, T. Minea, and G. Louarn, "Nanoprobes for near-field optical microscopy manufactured by substitute-sheath etching and hollow cathode sputtering," Rev Sci Instrum **77** (2006).
202. K. S. Mohanty, C. Liberale, S. K. Mohanty, and V. Degiorgio, "In depth fiber optic trapping of low-index microscopic objects," Applied Physics Letters **92**, - (2008).
203. T. Pangribuan, S. Jaing, and M. Ohtsu, "2-Step Etching Method for Fabrication of Fiber Probe for Photon Scanning Tunneling Microscope," Electronics Letters **29**, 1978-1979 (1993).
204. R. U. Maheswari, S. J. Mononobe, and M. Ohtsu, "Control of apex shape of the fiber probe employed in photon scanning tunneling microscope by a multistep etching method," J Lightwave Technol **13**, 2308-2313 (1995).
205. T. Saiki, S. Mononobe, M. Ohtsu, N. Saito, and J. Kusano, "Tailoring a high-transmission fiber probe for photon scanning tunneling microscope," Applied Physics Letters **68**, 2612-2614 (1996).
206. S. Mononobe, and M. Ohtsu, "Fabrication of a pencil-shaped fiber probe for near-field optics by selective chemical etching," J Lightwave Technol **14**, 2231-2235 (1996).
207. S. Mononobe, R. U. Maheswari, and M. Ohtsu, "Fabrication of a pencil-shaped fiber probe with a nanometric protrusion from a metal film for near-field optical microscopy," Optics Express **1**, 229-233 (1997).
208. J. Kim, M. Han, S. Chang, J. W. Lee, and K. Oh, "Achievement of large spot size and long collimation length using UV curable self-assembled polymer lens on a beam expanding core-less silica fiber," Ieee Photonics Technology Letters **16**, 2499-2501 (2004).

209. J. K. Kim, J. Kim, Y. Jung, W. Ha, Y. S. Jeong, S. Lee, A. Tunnermann, and K. Oh, "Compact all-fiber Bessel beam generator based on hollow optical fiber combined with a hybrid polymer fiber lens," Optics Letters **34**, 2973-2975 (2009).
210. P. N. Minh, T. Ono, Y. Haga, K. Inoue, M. Sasaki, K. Hane, and M. Esashi, "Bach fabrication of microlens at the end of optical fiber using self-photolithgraphy and etching techniques," Optical Review **10**, 150-154 (2003).
211. L. G. Cohen, and Schneide.Mv, "Microlenses for Coupling Junction Lasers to Optical Fibers," Applied Optics **13**, 89-94 (1974).
212. J. K. Kim, D. U. Kim, B. H. Lee, and K. Oh, "Arrayed multimode fiber to VCSEL coupling for short reach communications using hybrid polymer-fiber lens," Ieee Photonics Technology Letters **19**, 951-953 (2007).
213. E. H. Park, M. J. Kim, and Y. S. Kwon, "Microlens for efficient coupling between LED and optical fiber," Ieee Photonics Technology Letters **11**, 439-441 (1999).
214. K. R. Kim, S. L. Chang, and K. Oh, "Refractive microlens on fiber using UV-curable fluorinated acrylate polymer by surface-tension," Ieee Photonics Technology Letters **15**, 1100-1102 (2003).
215. N. Ma, P. C. Ashok, F. J. Gunn-Moore, and K. Dholakia, "Fabrication of polymer microlens at the apex of optical fiber," in *Photonics 2010*(Guwahati, India, 2010).
216. P. D. Bear, "Microlenses for Coupling Single-Mode Fibers to Single-Mode Thin-Film Wave-Guides," Applied Optics **19**, 2906-2909 (1980).
217. M. Hocine, R. Bachelot, C. Ecoffet, N. Fressengeas, P. Royer, and G. Kugel, "End-of-fiber polymer tip: manufacturing and modeling," Synthetic Met **127**, 313-318 (2002).
218. X. H. Zeng, J. Plain, S. Jradi, P. R. Goud, R. Deturche, P. Royer, and R. Bachelot, "High speed sub-micrometric microscopy using optical polymer microlens," Chinese Optics Letters **7**, 901-903 (2009).
219. R. Bachelot, C. Ecoffet, D. Deloeil, P. Royer, and D. J. Lougnot, "Integration of micrometer-sized polymer elements at the end of optical fibers by free-radical photopolymerization," Applied Optics **40**, 5860-5871 (2001).
220. M. I. Fokina, I. Y. Denisyuk, Y. E. Burunkova, and L. N. Kaporskii, "Formation of microstructures based on UV-hardenable acrylates," J Opt Technol+ **75**, 664-669 (2008).
221. K. S. Lee, and F. S. Barnes, "Microlenses on the End of Single-Mode Optical Fibers for Laser Applications," Applied Optics **24**, 3134-3139 (1985).
222. M. Hocine, N. Fressengeas, G. Kugel, C. Carre, D. J. Lougnot, R. Bachelot, and P. Royer, "Modeling the growth of a polymer microtip on an optical fiber end," Journal of the Optical Society of America B-Optical Physics **23**, 611-620 (2006).
223. M. Sasaki, T. Ando, S. Nogawa, and K. Hane, "Direct photolithography on optical fiber end," Jpn J Appl Phys 1 **41**, 4350-4355 (2002).
224. H. Kodama, "Automatic Method for Fabricating a 3-Dimensional Plastic Model with Photo-Hardening Polymer," Rev Sci Instrum **52**, 1770-1773 (1981).
225. S. Maruo, and J. T. Fourkas, "Recent progress in multiphoton microfabrication," Laser Photonics Rev **2**, 100-111 (2008).

226. D. Y. Yang, S. H. Park, T. W. Lim, H. J. Kong, S. W. Yi, H. K. Yang, and K. S. Lee, "Ultraprecise microreproduction of a three-dimensional artistic sculpture by multipath scanning method in two-photon photopolymerization," Applied Physics Letters **90** (2007).
227. G. Cojoc, C. Liberale, P. Candeloro, F. Gentile, G. Das, F. De Angelis, and E. Di Fabrizio, "Optical micro-structures fabricated on top of optical fibers by means of two-photon photopolymerization," Microelectronic Engineering **87**, 876-879 (2010).
228. S. Maruo, O. Nakamura, and S. Kawata, "Three-dimensional microfabrication with two-photon-absorbed photopolymerization," Optics Letters **22**, 132-134 (1997).
229. H. B. Sun, and S. Kawata, "Two-photon photopolymerization and 3D lithographic microfabrication," Adv Polym Sci **170**, 169-273 (2004).
230. S. H. Wu, J. Serbin, and M. Gu, "Two-photon polymerisation for three-dimensional micro-fabrication," J Photoch Photobio A **181**, 1-11 (2006).
231. C. N. LaFratta, J. T. Fourkas, T. Baldacchini, and R. A. Farrer, "Multiphoton fabrication," Angew Chem Int Edit **46**, 6238-6258 (2007).
232. S. H. Park, D. Y. Yang, and K. S. Lee, "Two-photon stereolithography for realizing ultraprecise three-dimensional nano/microdevices," Laser Photonics Rev **3**, 1-11 (2009).
233. R. Guo, S. Z. Xiao, X. M. Zhai, J. W. Li, A. D. Xia, and W. H. Huang, "Micro lens fabrication by means of femtosecond two photon photopolymerization," Optics Express **14**, 810-816 (2006).
234. M. Malinauskas, A. Zukauskas, V. Purlys, K. Belazaras, A. Momot, D. Paipulas, R. Gadonas, A. Piskarskas, H. Gilbergs, A. Gaidukeviciute, I. Sakellari, M. Farsari, and S. Juodkazis, "Femtosecond laser polymerization of hybrid/integrated micro-optical elements and their characterization," J Opt-Uk **12**, - (2010).
235. C. Liberale, G. Cojoc, P. Candeloro, G. Das, F. Gentile, F. De Angelis, and E. Di Fabrizio, "Micro-Optics Fabrication on Top of Optical Fibers Using Two-Photon Lithography," Ieee Photonics Technology Letters **22**, 474-476 (2010).
236. R. Guo, Z. Y. Li, Z. W. Jiang, D. J. Yuan, W. H. Huang, and A. D. Xia, "Log-pile photonic crystal fabricated by two-photon photopolymerization," Journal of Optics a-Pure and Applied Optics **7**, 396-399 (2005).
237. H. B. Sun, S. Matsuo, and H. Misawa, "Three-dimensional photonic crystal structures achieved with two-photon-absorption photopolymerization of resin," Applied Physics Letters **74**, 786-788 (1999).
238. M. Deubel, G. Von Freymann, M. Wegener, S. Pereira, K. Busch, and C. M. Soukoulis, "Direct laser writing of three-dimensional photonic-crystal templates for telecommunications," Nat Mater **3**, 444-447 (2004).
239. J. Serbin, A. Ovsianikov, and B. Chichkov, "Fabrication of woodpile structures by two-photon polymerization and investigation of their optical properties," Optics Express **12**, 5221-5228 (2004).
240. M. Straub, M. Ventura, and M. Gu, "Multiple higher-order stop gaps in infrared polymer photonic crystals," Physical Review Letters **91**, - (2003).
241. N. Takeshima, Y. Narita, T. Nagata, S. Tanaka, and K. Hirao, "Fabrication of photonic crystals in ZnS-doped glass," Optics Letters **30**, 537-539 (2005).

242. F. Schiappelli, R. Kumar, M. Prasciolu, D. Cojoc, S. Cabrini, M. De Vittorio, G. Visimberga, A. Gerardino, V. Degiorgio, and E. Di Fabrizio, "Efficient fiber-to-waveguide coupling by a lens on the end of the optical fiber fabricated by focused ion beam milling," Microelectronic Engineering **73-74**, 397-404 (2004).
243. S. Cabrini, C. Liberale, D. Cojoc, A. Carpentiero, M. Prasciolu, S. Mora, V. Degiorgio, F. De Angelis, and E. Di Fabrizio, "Axicon lens on optical fiber forming optical tweezers, made by focused ion beam milling," Microelectronic Engineering **83**, 804-807 (2006).
244. V. Callegari, D. Iwaniuk, R. Bronnimann, E. Schmid, and U. Sennhauser, "Optimized fabrication of curved surfaces by a FIB for direct focusing with glass fibres," Journal of Micromechanics and Microengineering **19**, - (2009).
245. J. Orloff, M. W. Utlaut, and L. Swanson, *High resolution focused ion beams : FIB and its applications : the physics of liquid metal ion sources and ion optics and their application to focused ion beam technology* (Kluwer Academic/Plenum, New York ; London, 2003).
246. D. J. Stevenson, F. J. Gunn-Moore, P. A. Campbell, and K. Dholakia, *Transfection by optical injection in The Handbook of Photonics for Medical Science* (CRC Press, Taylor & Francis Group, London, 2010).
247. T. Cizmar, ""Optical traps generated by non-traditional beams" Ph.D. thesis," (Masaryk University in Brno, 2006), p. 24.
248. J. W. Goodman, *Introduction to Fourier Optics* (McGraw-Hill Companies, 1996).
249. F. Hache, T. J. Driscoll, M. Cavallari, and G. M. Gale, "Measurement of ultrashort pulse durations by interferometric autocorrelation: Influence of various parameters," Applied Optics **35**, 3230-3236 (1996).
250. R. Le Harzic, M. Weinigel, I. Riemann, K. Konig, and B. Messerschmidt, "Nonlinear optical endoscope based on a compact two axes piezo scanner and a miniature objective lens," Optics Express **16**, 20588-20596 (2008).
251. H. Aouani, F. Deiss, J. Wenger, P. Ferrand, N. Sojic, and H. Rigneault, "Optical-fiber-microsphere for remote fluorescence correlation spectroscopy," Optics Express **17**, 19085-19092 (2009).
252. W. Denk, J. H. Strickler, and W. W. Webb, "2-Photon Laser Scanning Fluorescence Microscopy," Science **248**, 73-76 (1990).
253. N. Shen, D. Datta, C. B. Schaffer, P. LeDuc, D. E. Ingber, and E. Mazur, "Ablation of cytoskeletal filaments and mitochondria in live cells using a femtosecond laser nanoscissor," Mechanics and Chemistry of Biosystems **2**, 17-25 (2005).
254. A. A. Oraevsky, L. B. DaSilva, A. M. Rubenchik, M. D. Feit, M. E. Glinsky, M. D. Perry, B. M. Mammini, W. Small, and B. C. Stuart, "Plasma mediated ablation of biological tissues with nanosecond-to-femtosecond laser pulses: Relative role of linear and nonlinear absorption," IEEE J. Sel. Top. Quantum Electron. **2**, 801-809 (1996).
255. H. C. Bao, J. Allen, R. Pattie, R. Vance, and M. Gu, "Fast handheld two-photon fluorescence microendoscope with a 475 mu m X 475 mu m field of view for in vivo imaging," Optics Letters **33**, 1333-1335 (2008).
256. M. Gu, H. C. Bao, and J. L. Li, "Cancer-cell microsurgery using nonlinear optical endomicroscopy," J Biomed Opt **15** (2010).

257. W. Gobel, J. N. D. Kerr, A. Nimmerjahn, and F. Helmchen, "Miniaturized two-photon microscope based on a flexible coherent fiber bundle and a gradient-index lens objective," Optics Letters **29**, 2521-2523 (2004).
258. C. J. Engelbrecht, F. Voigt, and F. Helmchen, "Miniaturized selective plane illumination microscopy for high-contrast in vivo fluorescence imaging," Optics Letters **35**, 1413-1415 (2010).
259. T. J. Muldoon, M. C. Pierce, D. L. Nida, M. D. Williams, A. Gillenwater, and R. Richards-Kortum, "Subcellular-resolution molecular imaging within living tissue by fiber microendoscopy," Optics Express **15**, 16413-16423 (2007).
260. T. J. Muldoon, N. Thekkek, D. Roblyer, D. Maru, N. Harpaz, J. Potack, S. Anandasabapathy, and R. Richards-Kortum, "Evaluation of quantitative image analysis criteria for the high-resolution microendoscopic detection of neoplasia in Barrett's esophagus," J Biomed Opt **15**, - (2010).
261. P. C. Ashok, G. P. Singh, K. M. Tan, and K. Dholakia, "Fiber probe based microfluidic raman spectroscopy," Optics Express **18**, 7642-7649 (2010).
262. S. Szunerits, P. Garrigue, J. L. Bruneel, L. Servant, and N. Sojic, "Fabrication of a sub-micrometer electrode array: Electrochemical characterization and mapping of an electroactive species by confocal Raman microspectroscopy," Electroanal **15**, 548-555 (2003).
263. THORLABS, "Guide to connectorization and polishing optical fibers," (THORLABS, 2006), http://www.thorlabs.de/Thorcat/1100/1166-D02.pdf.
264. D. J. Carnegie, T. Cizmar, J. Baumgartl, F. J. Gunn-Moore, and K. Dholakia, "Automated laser guidance of neuronal growth cones using a spatial light modulator," Journal of Biophotonics **2**, 682-692 (2009).
265. P. M. Lane, A. L. P. Dlugan, R. Richards-Kortum, and C. E. MacAulay, "Fiber-optic confocal microscopy using a spatial light modulator," Optics Letters **25**, 1780-1782 (2000).
266. K. Kuetemeyer, J. Baumgart, H. Lubatschowski, and A. Heisterkamp, "Repetition rate dependency of low-density plasma effects during femtosecond-laser-based surgery of biological tissue," Appl Phys B-Lasers O **97**, 695-699 (2009).
267. M. Gu, C. J. R. Sheppard, and X. Gan, "Image-Formation in a Fiberoptic Confocal Scanning Microscope," Journal of the Optical Society of America a-Optics Image Science and Vision **8**, 1755-1761 (1991).
268. A. F. Gmitro, and D. Aziz, "Confocal Microscopy through a Fiberoptic Imaging Bundle," Optics Letters **18**, 565-567 (1993).
269. S. H. Yun, P. Kim, E. Chung, H. Yamashita, K. E. Hung, A. Mizoguchi, R. Kucherlapati, D. Fukumura, and R. K. Jain, "In vivo wide-area cellular imaging by side-view endomicroscopy," Nature Methods **7**, 303-305 (2010).
270. W. M. Yu, and X. Li, "Deep tissue microscopic imaging of the kidney with a gradient-index lens system," Optics Communications **281**, 1833-1840 (2008).
271. R. P. Barretto, T. H. Ko, J. C. Jung, T. J. Wang, G. Capps, A. C. Waters, Y. Ziv, A. Attardo, L. Recht, and M. J. Schnitzer, "Time-lapse imaging of disease progression in deep brain areas using fluorescence microendoscopy," Nat Med **17**, 223-228 (2011).

272. B. A. Flusberg, J. C. Jung, E. D. Cocker, E. P. Anderson, and M. J. Schnitzer, "In vivo brain imaging using a portable 3.9 gram two-photon fluorescence microendoscope," Opt Lett **30**, 2272-2274 (2005).
273. M. J. Schnitzer, B. A. Flusberg, A. Nimmerjahn, E. D. Cocker, E. A. Mukamel, R. P. J. Barretto, T. H. Ko, L. D. Burns, and J. C. Jung, "High-speed, miniaturized fluorescence microscopy in freely moving mice," Nature Methods **5**, 935-938 (2008).
274. M. J. Schnitzer, W. Piyawattanametha, E. D. Cocker, L. D. Burns, R. P. J. Barretto, J. C. Jung, H. Ra, and O. Solgaard, "In vivo brain imaging using a portable 2.9 g two-photon microscope based on a microelectromechanical systems scanning mirror," Optics Letters **34**, 2309-2311 (2009).
275. K. J. Rosbach, D. Shin, T. J. Muldoon, M. A. Quraishi, L. P. Middleton, K. K. Hunt, F. Meric-Bernstam, T. K. Yu, R. R. Richards-Kortum, and W. Yang, "High-resolution fiber optic microscopy with fluorescent contrast enhancement for the identification of axillary lymph node metastases in breast cancer: a pilot study," Biomed Opt Express **1**, 911-922 (2010).
276. K. Carlson, M. Chidley, K. B. Sung, M. Descour, A. Gillenwater, M. Follen, and R. Richards-Kortum, "In vivo fiber-optic confocal reflectance microscope with an injection-molded plastic miniature objective lens," Applied Optics **44**, 1792-1797 (2005).
277. C. Liang, M. R. Descour, K. B. Sung, and R. Richards-Kortum, "Fiber confocal reflectance microscope (FCRM) for in-vivo imaging," Optics Express **9**, 821-830 (2001).
278. K. C. Maitland, A. M. Gillenwater, M. D. Williams, A. K. El-Naggar, M. R. Descour, and R. R. Richards-Kortum, "In vivo imaging of oral neoplasia using a miniaturized fiber optic confocal reflectance microscope," Oral Oncol **44**, 1059-1066 (2008).
279. S. Schenkl, A. Ehlers, R. Le Harzic, M. Stark, I. Riemann, B. Messerschmidt, M. Kaatz, and K. Konig, "Rigid and high NA multiphoton fluorescence GRIN-endoscopes - art. no. 66310Q," Novel Optical Instrumentation for Biomedical Applications Iii **6631**, Q6310-Q6310 (2007).
280. S. H. Chia, C. H. Yu, C. H. Lin, N. C. Cheng, T. M. Liu, M. C. Chan, I. H. Chen, and C. K. Sun, "Miniaturized video-rate epi-third-harmonic-generation fiber-microscope," Opt Express **18**, 17382-17391 (2010).
281. F. Legare, C. L. Evans, F. Ganikhanov, and X. S. Xie, "Towards CARS endoscopy," Optics Express **14**, 4427-4432 (2006).
282. L. Giniunas, R. Juskaitis, and S. V. Shatalin, "Endoscope with optical sectioning capability," Appl Opt **32**, 2888-2890 (1993).
283. W. Gobel, A. Nimmerjahn, and F. Helmchen, "Distortion-free delivery of nanojoule femtosecond pulses from a Ti:sapphire laser through a hollow-core photonic crystal fiber," Opt Lett **29**, 1285-1287 (2004).
284. S. Tang, W. Jung, D. McCormick, T. Xie, J. Su, Y. C. Ahn, B. J. Tromberg, and Z. Chen, "Design and implementation of fiber-based multiphoton endoscopy with microelectromechanical systems scanning," J Biomed Opt **14**, 034005 (2009).
285. C. J. Engelbrecht, R. S. Johnston, E. J. Seibel, and F. Helmchen, "Ultra-compact fiber-optic two-photon microscope for functional fluorescence imaging in vivo," Optics Express **16**, 5556-5564 (2008).

286. Y. Zhao, H. Nakamura, and R. J. Gordon, "Development of a versatile two-photon endoscope for biological imaging," Biomed Opt Express **1**, 1159-1172 (2010).
287. M. T. Myaing, D. J. MacDonald, and X. Li, "Fiber-optic scanning two-photon fluorescence endoscope," Opt Lett **31**, 1076-1078 (2006).
288. W. Zhong, J. P. Celli, I. Rizvi, Z. Mai, B. Q. Spring, S. H. Yun, and T. Hasan, "In vivo high-resolution fluorescence microendoscopy for ovarian cancer detection and treatment monitoring," Br J Cancer **101**, 2015-2022 (2009).
289. K. B. Sung, C. Liang, M. Descour, T. Collier, M. Follen, A. Malpica, and R. Richards-Kortum, "Near real time in vivo fibre optic confocal microscopy: sub-cellular structure resolved," J Microsc **207**, 137-145 (2002).
290. M. J. Levene, D. A. Dombeck, K. A. Kasischke, R. P. Molloy, and W. W. Webb, "In vivo multiphoton microscopy of deep brain tissue," J Neurophysiol **91**, 1908-1912 (2004).
291. R. P. Barretto, B. Messerschmidt, and M. J. Schnitzer, "In vivo fluorescence imaging with high-resolution microlenses," Nat Methods **6**, 511-512 (2009).
292. J. C. Jung, and M. J. Schnitzer, "Multiphoton endoscopy," Opt Lett **28**, 902-904 (2003).
293. E. J. Seibel, C. M. Lee, C. J. Engelbrecht, T. D. Soper, and F. Helmchen, "Scanning fiber endoscopy with highly flexible, 1 mm catheterscopes for wide-field, full-color imaging," Journal of Biophotonics **3**, 385-407 (2010).
294. A. R. Rouse, A. Kano, J. A. Udovich, S. M. Kroto, and A. F. Gmitro, "Design and demonstration of a miniature catheter for a confocal microendoscope," Applied Optics **43**, 5763-5771 (2004).
295. D. Shin, M. C. Pierce, A. M. Gillenwater, M. D. Williams, and R. R. Richards-Kortum, "A Fiber-Optic Fluorescence Microscope Using a Consumer-Grade Digital Camera for In Vivo Cellular Imaging," Plos One **5**, - (2010).
296. R. Drezek, J. T. Sun, C. H. Shu, and B. Appiah, "Needle-compatible single fiber bundle image guide reflectance endoscope," J Biomed Opt **15** (2010).
297. Y. S. Sabharwal, A. R. Rouse, L. Donaldson, M. F. Hopkins, and A. F. Gmitro, "Slit-scanning confocal microendoscope for high-resolution in vivo imaging," Applied Optics **38**, 7133-7144 (1999).
298. F. Helmchen, M. S. Fee, D. W. Tank, and W. Denk, "A miniature head-mounted two-photon microscope. high-resolution brain imaging in freely moving animals," Neuron **31**, 903-912 (2001).
299. K. Konig, A. Ehlers, I. Riemann, S. Schenkl, R. Buckle, and M. Kaatz, "Clinical two-photon microendoscopy," Microsc Res Tech **70**, 398-402 (2007).
300. F. Jean, G. Bourg-Heckly, and B. Viellerobe, "Fibered confocal spectroscopy and multicolor imaging system for in vivo fluorescence analysis," Opt Express **15**, 4008-4017 (2007).
301. E. J. Seibel, and Q. Y. Smithwick, "Unique features of optical scanning, single fiber endoscopy," Lasers Surg Med **30**, 177-183 (2002).
302. Y. Wu, Y. Leng, J. Xi, and X. Li, "Scanning all-fiber-optic endomicroscopy system for 3D nonlinear optical imaging of biological tissues," Opt Express **17**, 7907-7915 (2009).

303. Y. Wu, J. Xi, M. J. Cobb, and X. Li, "Scanning fiber-optic nonlinear endomicroscopy with miniature aspherical compound lens and multimode fiber collector," Opt Lett **34**, 953-955 (2009).
304. W. Jung, S. Tang, D. T. McCormic, T. Xie, Y. C. Ahn, J. Su, I. V. Tomov, T. B. Krasieva, B. J. Tromberg, and Z. Chen, "Miniaturized probe based on a microelectromechanical system mirror for multiphoton microscopy," Opt Lett **33**, 1324-1326 (2008).
305. G. Liu, T. Xie, I. V. Tomov, J. Su, L. Yu, J. Zhang, B. J. Tromberg, and Z. Chen, "Rotational multiphoton endoscopy with a 1 microm fiber laser system," Opt Lett **34**, 2249-2251 (2009).
306. R. Kiesslich, P. R. Galle, and M. Neurath, *Atlas of endomicroscopy* (Springer, Berlin ; London, 2008).
307. M. Chen, C. Xu, and W. W. Webb, "Endoscope lens with dual fields of view and resolutions for multiphoton imaging," Opt Lett **35**, 2735-2737 (2010).
308. M. E. Llewellyn, R. P. Barretto, S. L. Delp, and M. J. Schnitzer, "Minimally invasive high-speed imaging of sarcomere contractile dynamics in mice and humans," Nature **454**, 784-788 (2008).
309. B. F. Grewe, F. F. Voigt, M. van 't Hoff, and F. Helmchen, "Fast two-layer two-photon imaging of neuronal cell populations using an electrically tunable lens," Biomed Opt Express **2**, 2035-2046 (2011).